Doctoral Dissertations   Graduate School

12-2000

Application of occasional feedback trajectory correction to enhance lean combustion quality in a pulsed combustor

Kevin Dean Edwards

Follow this and additional works at: https://trace.tennessee.edu/utk_graddiss

To the Graduate Council:

I am submitting herewith a dissertation written by Kevin Dean Edwards entitled "Application of occasional feedback trajectory correction to enhance lean combustion quality in a pulsed combustor." I have examined the final electronic copy of this dissertation for form and content and recommend that it be accepted in partial fulfillment of the requirements for the degree of Doctor of Philosophy, with a major in Mechanical Engineering.

K. Nguyen, Major Professor

We have read this dissertation and recommend its acceptance:

D.D. Bruns, C.S Daw, W.S. Johnson
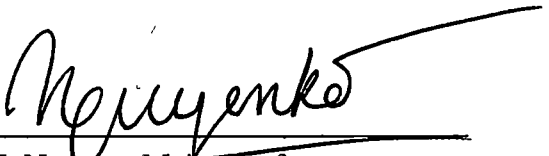
Accepted for the Council:

Carolyn R. Hodges

Vice Provost and Dean of the Graduate School

(Original signatures are on file with official student records.)
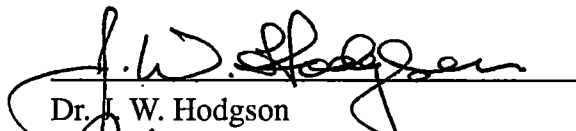
To the Graduate Council:

I am submitting herewith a dissertation written by Kevin Dean Edwards entitled *Application of occasional feedback trajectory correction to enhance lean combustion quality in a pulsed combustor*. I have examined the final copy of this dissertation for format and content and recommend that it be accepted in partial fulfillment of the requirements for the degree of Doctor of Philosophy, with a major in Mechanical Engineering.

_____
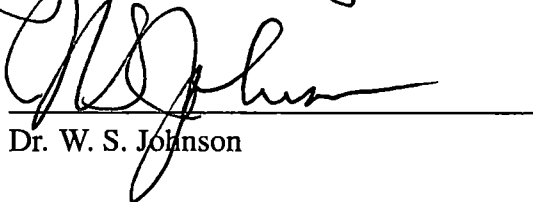
Dr. K. Nguyen, Major Professor

We have read this dissertation
and recommend its acceptance:

_____
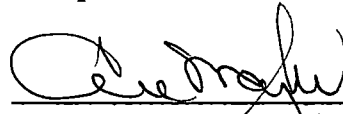
Dr. D. D. Bruns

_____

Dr. C. S. Daw

_____

Dr. J. W. Hodgson

_____

Dr. W. S. Johnson

Accepted for the Council:

_____

Dean of the Graduate School

Application of occasional feedback trajectory correction to enhance lean combustion quality in a pulsed combustor

A dissertation
presented for the degree of
Doctor of Philosophy
at The University of Tennessee, Knoxville

l

Kevin Dean Edwards

December 2000

Acknowledgements

This research would not have been possible without the assistance, support and patience of a great many people. First and foremost, I would like to recognize my major professor, Dr. Ke Nguyen, for his instruction, support and patience while I pursued my Master's and Doctorate under his fine stewardship. More than once, Ke has stood up for me and placed himself in the line of fire in my defense and, for this, I am extremely grateful. I would not have succeeded were it not for him. I would also like to thank the other members of my committee, Dr. Duane Bruns, Dr. Stuart Daw, Dr. Jeff Hodgson and Dr. Stan Johnson, for their instruction and patience throughout these years.

I would also like to thank all of my fellow members of the Chaos Research Group here at the University of Tennessee, Knoxville. Dr. Stuart Daw of the Oak Ridge National Laboratory was instrumental to the success of this project and deserves special thanks for his guidance. I would also like to thank Dr. Duane Bruns for his assistance throughout the years. Dr. Charles Finney, my fellow former graduate student, provided truly invaluable assistance in developing data analysis techniques for this project. In addition, I would like to thank Charles for his friendship, for always keeping the fridge well stocked and for all of the entertaining stories about alpacas. I would like to thank Dr. Nicolaas van Goor, another fellow former graduate student, for the use of his graphical routines which

I incorporated into my data-acquisition and control code. And thanks to all of the others with whom I have worked as part of the Chaos Research Group for helping to make the days a little more enjoyable.

I would like to thank all of our collaborators in this work beginning with Dr. Geo Richards of the National Energy Technology Laboratory where the original design and analytical model for the thermal pulse combustor were developed. I would like to thank our collaborators in the control studies of the METC analytical model. In addition, Dr. Mark Spano and Dr. Visarath In of the Naval Surface Warfare Center provided many of the instruments and equipment used in this study. Finally, I would like to thank Dr. John Storie of Oak Ridge National Laboratory for the use of the flame ionization detector and Dr. Butch Irick of UTK for the use of the oxygen analyzer.

I would be greatly remiss not to thank Dennis Higdon for all of the technical expertise that I have gained from him over the years and Steve Hunley, Danny Graham, and Gary Hatmaker for the construction of the pulsed combustor. Research in the Mechanical and Aerospace Engineering and Engineering Science Department at the University of Tennessee, Knoxville, could not continue without the services provided by these gentlemen.

Finally, I would like to thank my family and friends for all of their support throughout the years. My parents, Dewel and Muriel Edwards, have given me more love and support throughout my life than I can ever repay. A simple "thanks" is not enough to express my gratitude for all they have given me nor does "I love you" begin to explain how much they mean to me.

I would like to thank Amber Hensley for her love and encouragement. Though I have only known her for a short time, her friendship over the past few months has brought much joy to my life that had been missing. And where would I be without my fellow

musketeers, stooges, dinosaurs, and partners in crime, Dr. Chris Widner and (soon-to-be Dr.) Scott Hale? Probably still trying to pass Strengths of Materials (Invar!). Thanks, guys, for all of the help, friendship, inside jokes, and everything else that we have shared over the course of obtaining these three degrees.

Thanks to all of my fellow graduate students who have made grad school a little more bearable all of these years. And thanks to all of my fellow birders and all of the little birdies for keeping me distracted so that I did not go completely insane long, long ago.

Abstract

The behavior of a laboratory-scale pulsed combustor is characterized over a wide range of operating conditions. The behavior of the combustor is shown to be driven by two different mechanisms. Acoustic coupling with the tailpipe produces large-amplitude pressure oscillations which are nonlinear in nature due to interaction with the combustion reaction and turbulent mixing. Due to the highly nonlinear nature of the combustion reaction at lean conditions, the system dynamics undergo a bifurcation as the equivalence ratio approaches the lean flammability limit which introduces low-frequency combustion instabilities that are superimposed upon the acoustically driven pressure oscillations. Rapid consumption and slow restocking of the available fuel inventory leads to poor-quality combustion events, misfire and, eventually, unrecoverable flameout.

A control algorithm is presented which monitors the peak pressure during each cycle to detect when the available fuel inventory has been consumed and the pulsed combustor begins to experience poor-quality combustion events while the fuel inventory is restocked. The controller then injects a small pulse of supplemental fuel to hasten the restocking process and drive the system back toward a more stable mode of operation. The control strategy is shown to be effective at dampening the combustion instabilities which results in lower unburned-hydrocarbon emission levels and allows the operating regime of the combustor to be extended further toward the lean flammability limit.

Contents

List of Figures

List of Tables

Chapter 1

Introduction

1.1 A brief history of pulsed combustion

The earliest known studies of acoustically driven combustion oscillations date back to the eighteenth century. In 1777, Higgins placed a hydrogen flame inside a glass jar to demonstrate to his students that water is produced by combustion reactions by condensing and collecting the water in the jar. Much to his surprise, a musical tone was produced. Higgins found that differently sized and shaped jars produced tones with different amplitudes and frequencies. The experiment became a popular parlor trick at parties for some time before studies were conducted to examine the physics which produce the tones (Nicholson and Higgins 1802).

Details of the experiment were first published by Brugnatelli (Delarive 1803). Later studies by DeLuc, Tyndall, Faraday, Rijke, Rayleigh and others further explored the nature of the oscillations and their source (Zinn 1986). Rayleigh determined that the condition under which the flame would "sing", later dubbed the Rayleigh criterion, is as follows:

> If heat be given to the air at the moment of greatest condensation, or be taken from it at the moment of greatest rarefaction, the vibration is encouraged. On the other hand, if heat be given at the moment of greatest rarefaction, or abstracted at the moment of greatest condensation, the vibration is discouraged. (Rayleigh 1945)

Practical applications of acoustically driven combustion were not developed until the twentieth century. Early in that century, growing interest in gas turbines led to the development of several combustor designs which were to use pulsed combustion for propulsion or power generation. A series of patents were issued for combustor designs beginning with a mechanically valved design by Esnault-Pelterie in 1906. The first aerodynamically valved, or aerovalve, design, in which air is drawn into the combustor by aerodynamic forces rather than mechanically injected, was proposed by Esnault-Pelterie's co-worker, Marconnet, in 1909 (Putnam *et al.* 1986). Other designs followed, but the first successful implementation of a pulsed-combustor design was the V-1 "buzz bomb" rocket used by Germany in World War II (Foa 1960).

The success of the V-1 rocket led to the post-war development of a wide variety of applications for pulsed combustors. A few designs were developed which sought to improve the performance of the V-1 rocket for aircraft propulsion; however, these pulse-jets produced a low specific thrust and were soon to be outperformed by the newly developed turbo-jet engine (Putnam *et al.* 1986). The Dyna-Jet, developed in 1946, was also used as a fog-generator by the United States Army and is now a favorite of model rocket and aircraft enthusiasts. A commercial version of the Dyna-Jet is still being produced by Curtis Dyna-Fog for use as insecticide foggers and sprayers (anon. 1998). The first heating application came in 1948 when Huber produced a pulsed-combustion water heater designed to maintain engine temperatures during shut-down. This design was later modified to heat air for residential applications as well as heating mass-transit vehicles. By 1961, Kitchen had

developed the Lucas-Rotax Pulsamatic boiler for residential water heating. A modified version of his design, known as the Hydro-Pulse, is still commercially available (Putnam *et al.* 1986). The success of the Pulsamatic helped inspire the development of the Lennox G14 Pulse® warm-air residential furnace introduced in 1982 (anon. 1999). The recent phenomenal success of the Hydro-Pulse boiler and the Lennox Pulse® furnace have lead to a renewed interest in the development of commercial and residential applications.

1.2   Basic principles of operation

A pulsed combustor works on a four-step cycle that is remarkably similar to the Diesel cycle. In fact, it can be argued that the internal combustion engine is merely an extreme example of a pulsed combustor in which the pressure oscillations are driven mechanically rather than acoustically. Pulsed combustor designs typically consist of a combustion chamber and an acoustically coupled tailpipe. Traditionally, the mixture is introduced intermittently either by mechanical means (flapper valves, fuel injection, *etc.*) or by allowing aerodynamic forces to draw the mixture into the combustor as needed. Recent studies have shown that it is possible to produce pulsed combustion with the mixture introduced at a constant rate through critical-flow orifices (Richards *et al.* 1991, republished as Richards *et al.* 1993).

The typical pulsed-combustion cycle is depicted in **Figure 1.1**. During the first step of the cycle, the fresh mixture in the combustion chamber is compressed and heated and to the auto-ignition point resulting in a combustion reaction which raises the combustor pressure. In mechanically and aerodynamically valved designs, the high combustor pressure restricts the flow of fresh charge into the combustion chamber, quenching the combustion
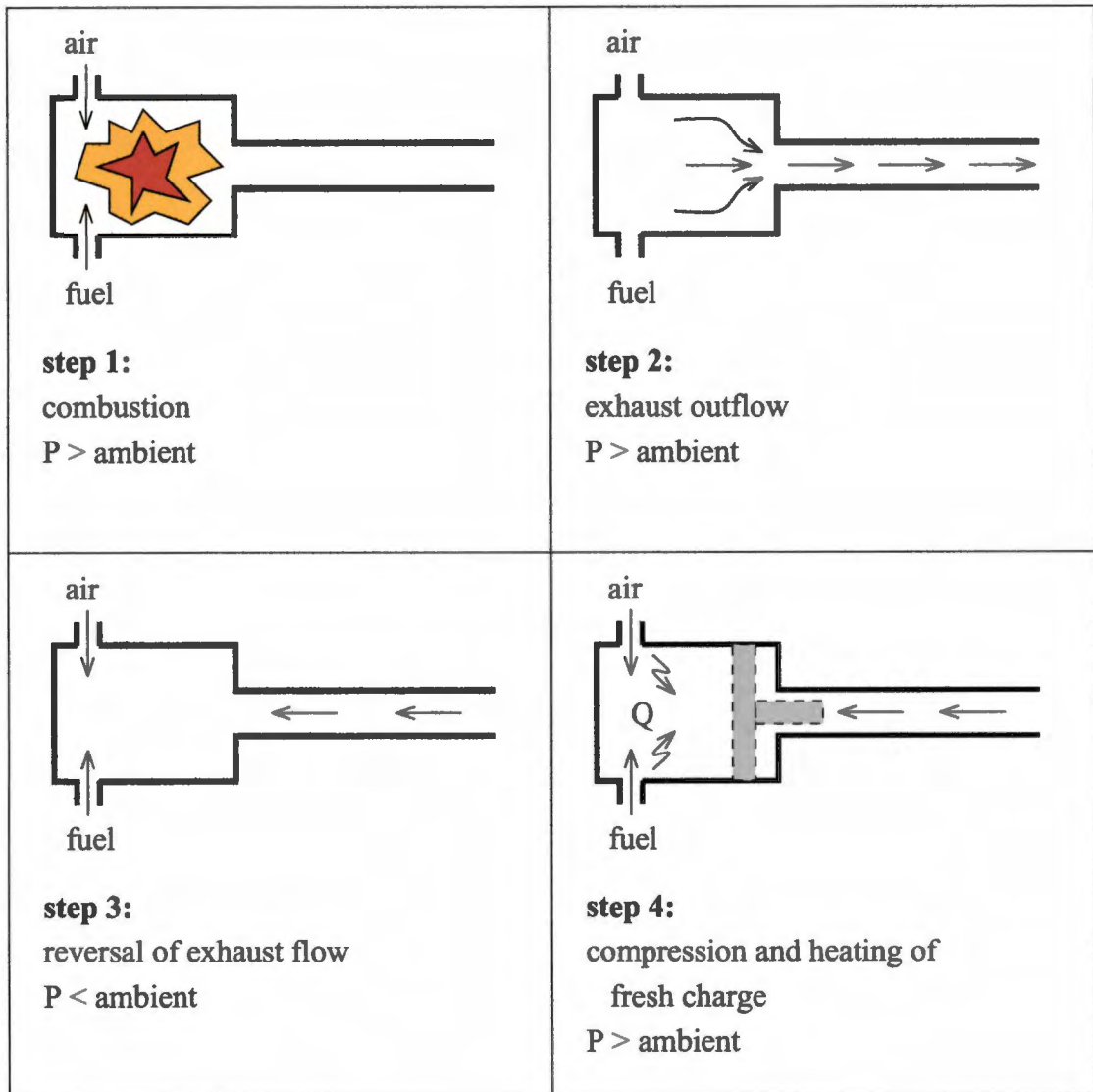
Figure 1.1: *Sketch outlining the four-step cycle typical of pulsed combustors.*

reaction and leading to the second step. During the second step, the exhaust gases expand through the tailpipe reducing the pressure inside the combustion chamber. As the exhaust gases exit, they gain enough momentum to evacuate the combustor until the combustor pressure drops below ambient pressure. During the third step, the reduction in combustor pressure allows fresh charge to enter the combustion chamber and causes the exhaust-gas flow to slow and eventually reverse, reintroducing residual gases to the combustion chamber. During the fourth step, the momentum of the residual exhaust gases and the incoming fresh charge pressurizes the combustor to slightly above ambient pressure. Heat transfer from the combustor walls and the hot residual gases heat the mixture to the auto-ignition point, thus restarting the cycle. The average time needed to complete one cycle is determined by the fundamental acoustic frequency of the combustor.

1.3 Benefits over steady-flow combustors

Pulsed combustion has long been known to have several significant advantages over steady-flow, constant-pressure combustion processes. Historically, these advantages were poorly understood and difficult to quantify. Without knowledge of how the benefits were derived, early pulsed combustor designs were developed largely by trial-and-error. The lack of a thorough thermodynamic understanding of the principles of pulsed combustion likely has lead to their limited use (Zinn 1986; Putnam *et al.* 1986). Late in the twentieth century, a number of studies began to quantify the benefits of pulsed combustion and develop an understanding of the mechanisms involved.

1.3.1 Convective transport

The oscillatory flow in pulsed combustor tailpipes has been shown to produce significantly higher convective heat and mass transfer rates than steady-flow combustors. Early studies of oscillatory flow found heat transfer rates that ranged from 70% less (Alhaddad and Coulman 1982) to 240% greater (Hanby 1969) than those for steady turbulent flow at similar mean Reynolds numbers. However, the test conditions used in these studies varied considerably from one another and few investigated the effects of varying the test conditions. Many of the studies which predicted lower transfer rates were conducted at oscillatory conditions atypical of pulsed-combustor operation (*e.g.*, lower frequencies and smaller amplitude oscillations) (Dec *et al.* 1992). High convective transfer rates provide obvious benefits for heating and drying applications. However, without a thorough understanding of the mechanisms involved in producing those increases, it is difficult to design a system to take full advantage of those benefits. Many theories were proposed to describe the increased transfer rates, but none were adequate to fully explain the behavior.

In the late 1980s, experiments began at Sandia National Laboratories in order to quantify the heat and mass transfer rates from the tailpipe of an experimental pulsed combustor, to determine the effect various parameters such as pulse frequency, combustor-pressure amplitude and flow rate have upon the heat transfer rate and to discover the mechanisms responsible for the increased convective transfer rates. A two-color laser Doppler velocimetry system was used to make spatially and temporally resolved velocity measurements inside the tailpipe of the pulsed combustor (Keller and Saito 1987; Dec *et al.* 1991). Spatially resolved temperature measurements inside the tailpipe were obtained using two-line atomic fluorescence (Dec and Keller 1986). Additionally, temperature measurements made using a thin-film thermocouple coating the inner surface of the tailpipe

and a fast-response thermocouple inbedded within the tailpipe wall were used to obtain cycle-resolved measurements of the heat flux being conducted through the tailpipe (Dec and Keller 1990). Mass transfer rates were determined by measuring the evaporation rate of water passed through a sintered, stainless steel cylinder placed in the tailpipe (Gemmen *et al.* 1991).

The heat transfer Nusselt number was found to vary greatly with the root-mean-square of the combustor pressure, increasing with increased combustor pressure. The Nusselt number was also found to increase slightly with frequency; varying the flow rate had little or no effect. In all test cases, Nusselt numbers were found to exceed those of a steady-flow combustor at similar mean Reynolds numbers, in some cases by as much as a factor of three (Dec and Keller 1989). Mass transfer Nusselt numbers were found to be up to 25% greater than those for steady-flow combustors (Gemmen *et al.* 1991, republished as Gemmen *et al.* 1993). Based upon analysis of the spatially and temporally resolved velocity and temperature measurements, Dec *et al.* (1992) were able to discount most of the previously purposed theories and show that the flow inside the pulsed-combustor tailpipe has small-scale turbulence superimposed upon the larger-amplitude acoustically driven oscillations.

Using techniques developed to describe convective transport in forced and buoyancy-driven turbulent flow (Arpaci 1986; Arpaci and Selamet 1991), Arpaci *et al.* (1991) developed a model to predict heat transfer rates for oscillating turbulent flows by determining the appropriate spatial scale of the small turbulent vortices which were shown to exist within the larger, acoustically driven flow oscillations. Most previous studies attempted to correlate experimental Nusselt number data from pulsed combustors to those predicted by quasi-steady theory; however, quasi-steady models do not adequately agree with ex-

perimental results at all operating conditions and cannot account for the frequency effects noted by Dec and Keller (1989). The model developed by Arpaci *et al.* attempts to develop heat transfer relations which fully and accurately account for the minute scale of the turbulence fluctuations which Dec *et al.* (1992) found in the pulsed combustor. The model shows exceptional agreement with the experimental results of Dec and Keller (1989), including those experiments in which the acoustic frequency is varied. Furthermore, the model collapses to the traditional quasi-steady and steady turbulent heat transfer relations at the appropriate conditions. Based upon the agreement with experimental results, superpositioning of micro-scaled turbulence upon the large-scale acoustically driven oscillations currently provides the best explanation for the enhanced convective transport seen in pulsed combustors (Arpaci *et al.* 1991, republished as Arpaci *et al.* 1993).

1.3.2   Pollutant emission levels

Pulsed combustors have long been known to produce significantly lower levels of pollutant emissions — particularly NO_x — than steady-flow combustors. Studies at Sandia have shown that high heat transfer rates and rapid mixing of the hot exhaust gases with cooler combustor gases help to limit the time that the exhaust gases spend at high temperatures. Keller and Hongo (1990) found that the majority of NO_x production in pulsed combustors occurs near the flame front. The exhaust gases reach thermal equilibrium at a much lower temperature before leaving the combustion chamber. As a result, the rate of NO_x production decreases as the exhaust gases move toward the tailpipe. In contrast, the exhaust gas in steady combustors were found to remain at a much higher temperature throughout the combustion chamber resulting in near constant NO_x production rates throughout the combustion chamber. Keller *et al.* (1994) were able to reduce NO_x and CO

emissions in the Sandia pulsed combustor to ≤ 5 ppm at 3% O_2 by operating in a lean, premixed mode and promoting fine-scale mixing of the fresh and residual charges at the inlet.

1.4   Limits of operation

To make full use of the benefits of pulsed combustion, it would be desirable to operate the combustor at lean conditions to increase the fuel efficiency and further reduce pollutant emission levels. Unfortunately, recent studies have shown that, as with many other combustion systems, pulsed combustors become unstable at lean conditions, leading to misfire and, eventually, unrecoverable flameout. The instabilities often develop well above the lean flammability limit.

At the former Morgantown Energy Technology Center (METC) — currently part of the National Energy Technology Laboratory — Richards *et al.* constructed an experimental thermal pulse combustor and developed a simple analytical model to predict its behavior. The combustor is modeled as a well-stirred reactor coupled with an acoustic oscillator. Richards *et al.* were able to show good correlation between the analytical model and experimental observations. Both the analytical model and the experimental combustor exhibit steady combustion, pulsed combustion and flame extinction at various operating conditions (Richards *et al.* 1991).

Daw *et al.* (1992) showed that, due to the nonlinearity of the Arrhenius rate law, the METC analytical model follows a classic period-doubling route to chaos as the mass flow rate of the mixture is increased. Pressure time-series traces from the METC combustor, recorded at operating conditions similar to those for which chaotic behavior is predicted,

demonstrate similarities to the model predictions suggesting that the combustor does in fact exhibit deterministically chaotic behavior. Daw *et al.* speculated that the cycle-to-cycle variation in the magnitude of the pressure oscillation may result in reduced combustion efficiency and increased pollutant emission levels (Daw *et al.* 1992; Daw *et al.* 1994; Daw *et al.* 1995). The nonlinear behavior of pulsed combustors has been independently confirmed in experimental and analytical studies (Sterling and Zukoski 1991; Sterling 1993; Margolis 1994).

The behavior of a pulsed combustor similar to the METC design has been characterized as part of the current study. As will be discussed in detail in later chapters, as the mixture is made increasingly lean, nonlinear combustion instabilities are observed to develop which lead to misfire and eventual flameout of the combustor. An analytical model has been developed which indicates that the instabilities develop due to nonlinearities inherent to the reaction mechanism at lean conditions (Edwards *et al.* 1997; Edwards *et al.* 1998; Edwards *et al.* 2000).

1.5   Control of combustor behavior

Daw *et al.* (1992) were the first to suggest that, due to the nonlinear nature of pulsed combustion, linear control algorithms would prove less effective in reducing cyclic variation and extending the practical operating regime of pulsed combustors than control strategies based upon nonlinear dynamics. In studies by Rhode *et al.* and In *et al.*, various nonlinear control techniques were successfully applied to the METC analytical model.

Rhode *et al.* (1995) applied several control techniques to the METC model using the friction factor of the tailpipe as a control perturbation. A derivative control scheme was

shown to be capable of eliminating the pulsed behavior and forcing the combustor model into steady operation. An adaptive map-based scheme was used to stabilize the pulsed behavior allowing operation at higher mass flow rates than otherwise possible.

In *et al.* (1997) developed a maintenance-of-chaos control algorithm to extend the operating regime of the METC analytical model. The controller monitors the pressure temporal record predicted by the model and detects the occurrence of certain patterns, or mediating trajectories, which lead to flameout. In *et al.* showed that it is possible to prevent flameout in the model by momentarily imposing a slight decrease in the mass flow rate of the mixture whenever a mediating trajectory is detected to push the system behavior away from flameout and back toward more stable trajectories.

1.6   Scope of the current study

For the current study, a laboratory-scale pulsed combustor has been designed and constructed based upon a modified version of the METC design. The behavior of the combustor has been characterized over a wide range of operating conditions. At lean conditions, nonlinear combustion instabilities were found to develop which reduce the quality of combustion and lead to misfire and flameout. An analytical model developed to help determine the source of the combustion instabilities suggests that the instabilities result from the nonlinear nature of the combustion reaction. Based upon the information gained in this study, a control strategy similar in principle to the one used by In *et al.* (1997) has been developed which is capable of stabilizing the behavior of the experimental combustor at lean conditions and extending the practical operating regime by detecting events which proceed misfire and injecting a small amount of supplemental fuel to push the system toward a more stable operating mode.

Chapter 2

Background

2.1 Thermal pulse combustion

2.1.1 Experimental combustor

The pulsed combustor used in the current study is derived from the thermal pulse combustor developed by Richards *et al.* (1991) at METC. In the METC combustor, shown schematically in **Figure 2.1**, fuel and air enter the combustor through separate, opposing inlets each equipped with a critical-flow orifice to maintain constant flow rates. The impinging inlet streams form a jet-stirred reaction zone. An alumina rod installed along the centerline of the combustor provides an additional heat source for ignition. A piezoelectric pressure transducer is used to monitor the combustor-pressure oscillations and a thermocouple is attached to the exterior-wall of the combustion chamber to provide a wall temperature to be used as a reference. The operating condition of the thermal pulse combustor is defined by the equivalence ratio of the fresh mixture and a characteristic flow time, τ_f, which approximates the time the mixture resides in the combustion chamber and

12

Alumina Centerbody
Optional - See Text

Fuel

Spark Plug

Tail Pipe

Combustor

Air

Blank Flange   Fuel Inlet   Spark Plug Opening

22.0   48.0   17.8

Air Inlet

38.0   43.0   102.0   610.0
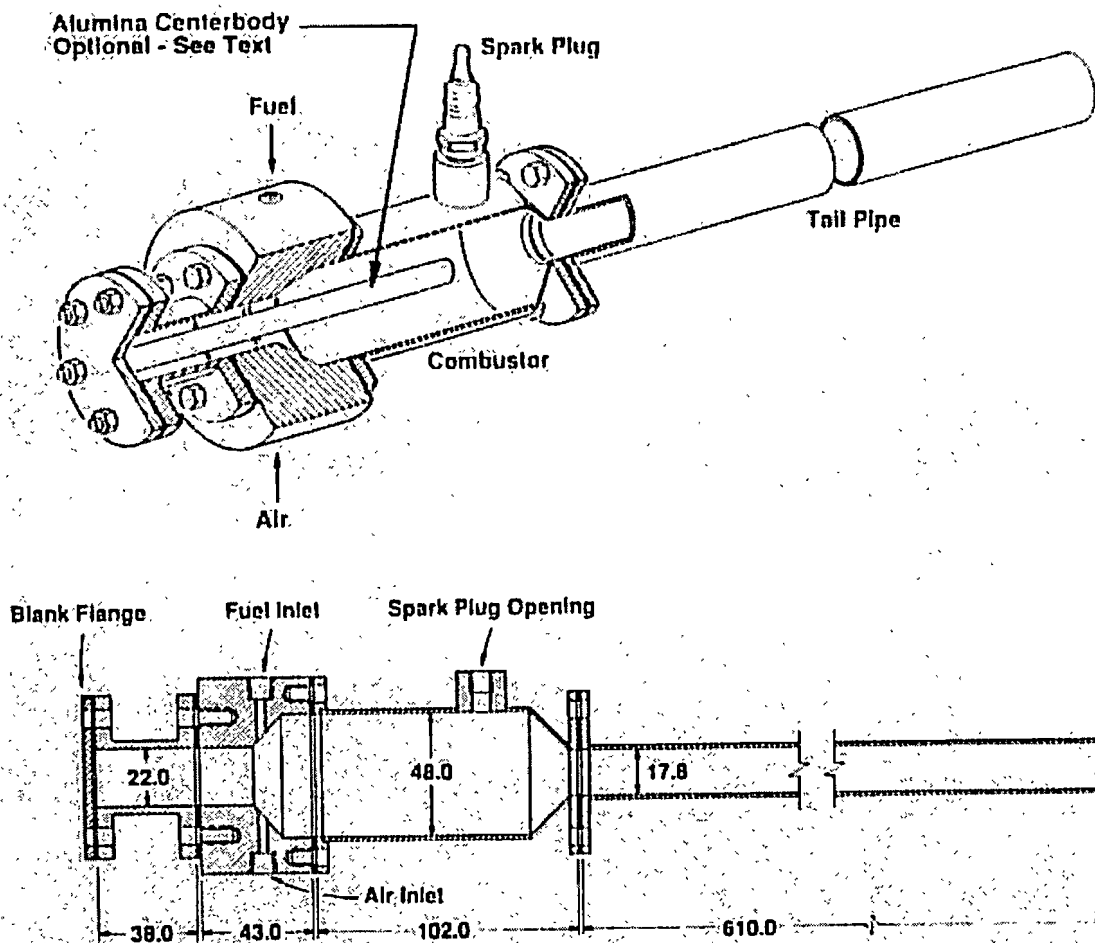
Figure 2.1: *Schematic of the thermal pulse combustor developed at METC. Dimensions are in mm (Richards et al. 1991).*

is determined by the equation

$$\tau_f = \frac{\rho_o V}{\dot{m}_a + \dot{m}_f}$$

(2.1)

where ρ_o is the ambient density and V is the volume of the combustion chamber.

Richards *et al.* (1991) conducted a series of experiments at a few disparate operating conditions. The thermal pulse combustor was found to exhibit three modes of operation depending upon the operating conditions: steady combustion, pulsed combustion and flame extinction. That the combustor would operate in a pulsed mode with constant inlet flows is noteworthy as, previously, mechanically or aerodynamically valved inlets had been considered necessary to produce pulsed combustion.

The behavior of the combustor was found to rely heavily upon the combustor-wall temperature — hence the moniker, thermal pulse combustor. Self-sustained combustion was found not to be possible at low wall temperatures (*e.g.*, below ~ 900 K). At these conditions, the combustor behavior is characterized by occasional explosive reactions followed by a series of decaying-amplitude oscillations which occur at the fundamental acoustic frequency (Morris *et al.* 1990). At higher wall temperatures, the behavior of the combustor was found to be either steady or pulsating depending upon the equivalence ratio and flow time.

As the equivalence ratio was decreased while holding the mass flow rate of the mixture constant, the behavior of the thermal pulse combustor was found to go through a transition from low-amplitude (~ 50 kPa, peak-to-trough) pressure oscillations with a frequency of approximately 167 Hz at an equivalence ratio of $\phi = 0.85$ to higher-amplitude (~ 100 kPa, peak-to-trough), lower-frequency (110 Hz) oscillations at an equivalence ratio of $\phi = 0.68$ (**Figure 2.2**). The transition between the two modes of behavior is not smooth; rather, at the intermediate equivalence ratios, behavior is characterized by intermittent transitions
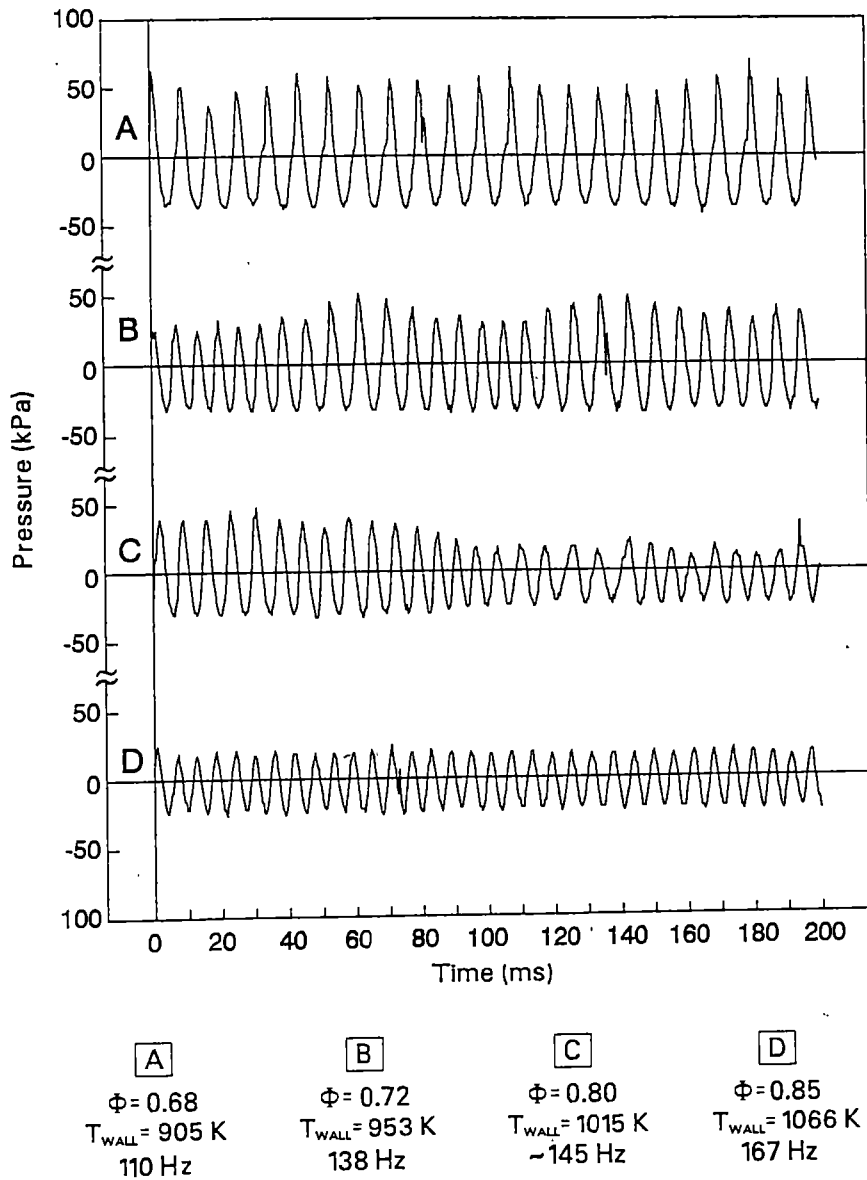
Figure 2.2: *Combustor-pressure traces showing the effects of equivalence ratio upon the behavior of the METC thermal pulse combustor (Richards et al. 1991).*

between the two modes. Similar behavior was observed by holding equivalence ratio constant and increasing flow time (**Figure 2.3**). Long flow times (*e.g.,* $\tau_f \geq 74$ ms) were found to produce steady combustion.

While the tests performed by Richards *et al.* provided insight into the behavior of the thermal pulse combustor, the limited number and disparate conditions of test runs and the limited amount of data collected at each condition leaves something to be desired. A thorough, systematic characterization of the behavior of the thermal pulse combustor over a wide range of operating conditions has yet to be performed.

2.1.2 Analytical model

In addition to the experimental combustor, Richards *et al.* (1991) developed an analytical model to explain the behavior of the physical system. The combustor is modeled as a well-stirred reactor acoustically coupled to the tailpipe with the geometry shown in **Figure 2.4**. Reactants are premixed and enter at a constant mass flow rate through a single inlet. The combustor-wall temperature is maintained constant at some specified value. The pressure, temperature and mass fraction of fuel are assumed to be uniform throughout the combustion chamber and are related to the values at the tailpipe entrance by assuming isentropic acceleration through the nozzle connecting the combustion chamber and the tailpipe. The friction factor, f, in the tailpipe is assumed constant, and ambient pressure is assumed at the tailpipe exit.

Conservation equations for mass, energy and species are applied to the combustion chamber and coupled with conservation equations for mass and momentum in the tailpipe. Combustion is described by a bi-molecular rate law written specifically for stoichiometric conditions (which limits the accuracy of the model at non-stoichiometric conditions).
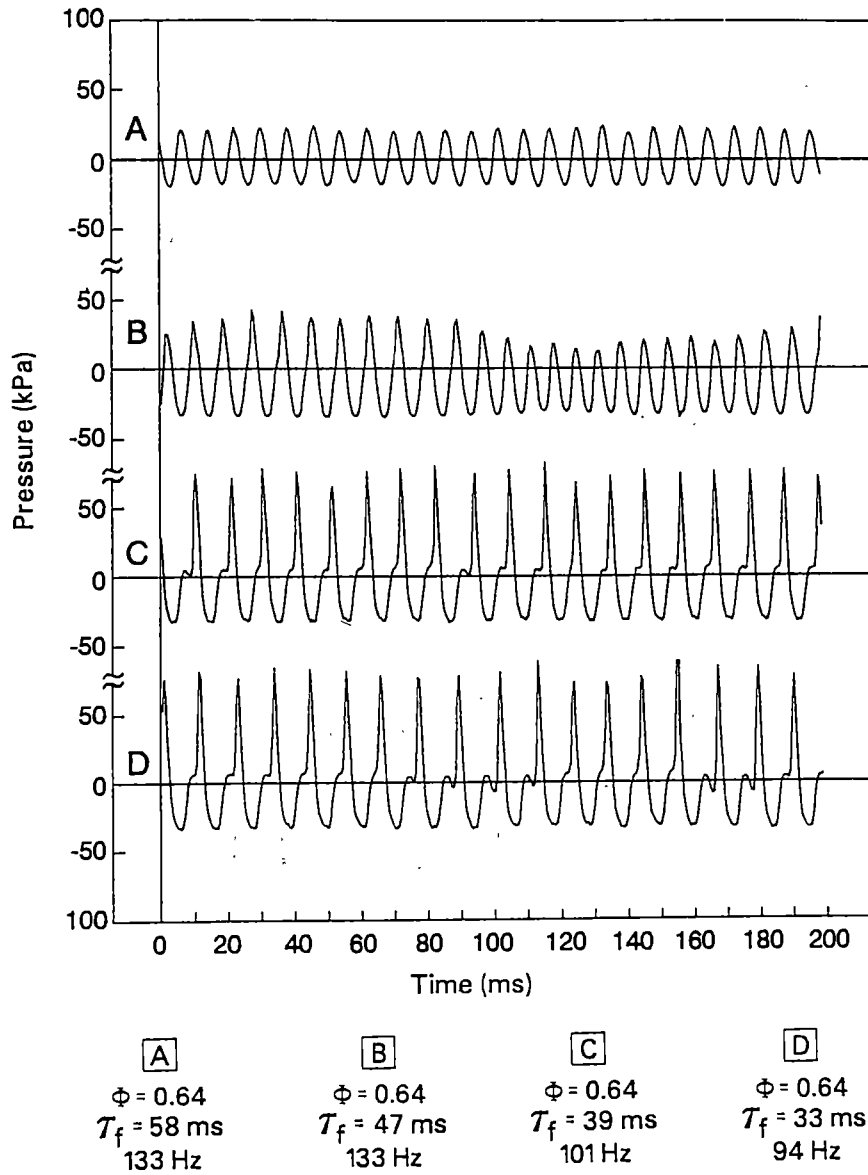
Figure 2.3: *Combustor-pressure traces showing the effects of flow time on the behavior of the METC thermal pulse combustor (Richards et al. 1991).*
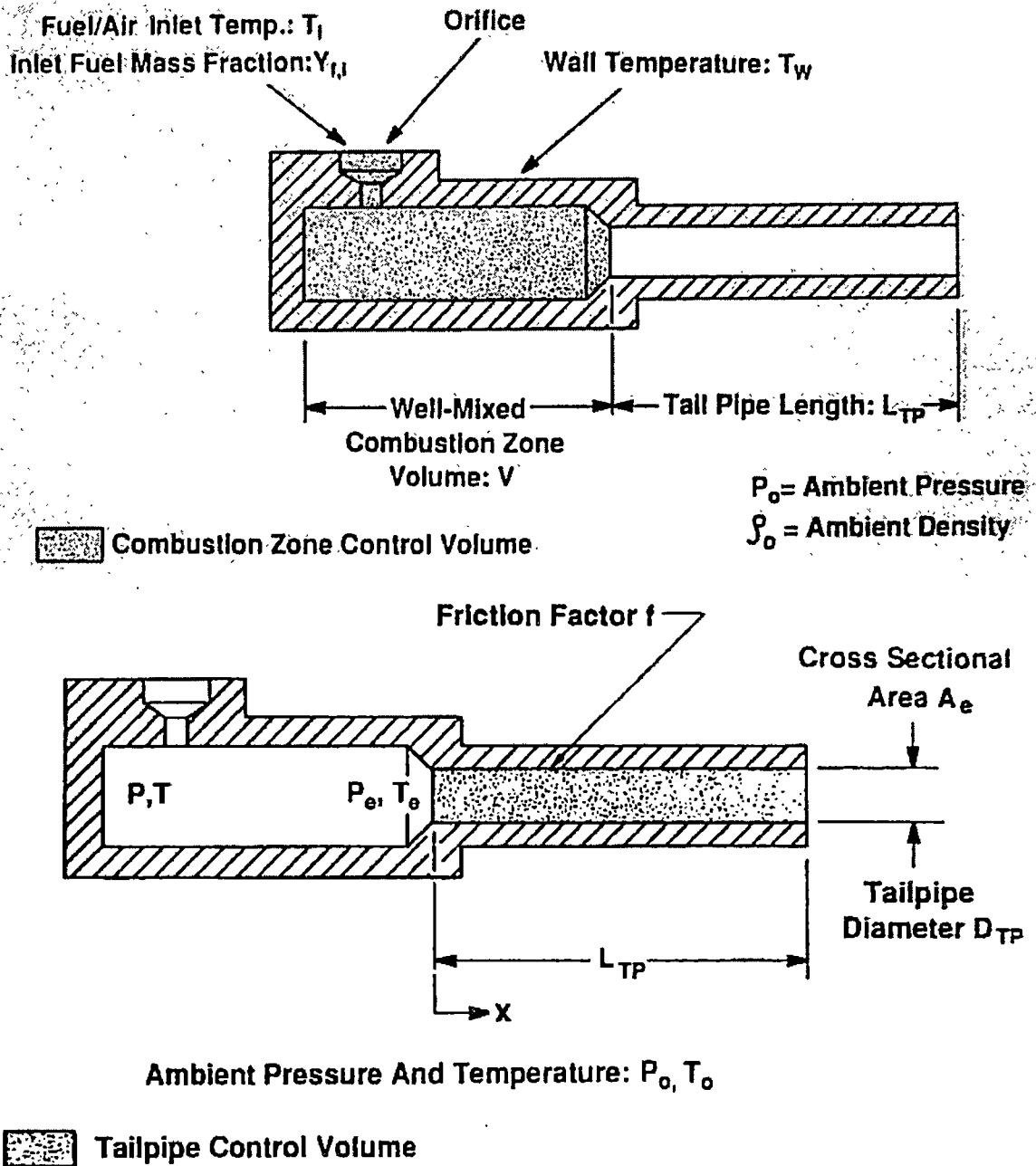
Figure 2.4: *Geometry of the METC analytical model (Richards et al. 1991).*

Simplifications and non-dimensionalization of the governing equations yields a set of four coupled, nonlinear ordinary differential equations (ODEs) for the non-dimensional forms of temperature,

$$\frac{d\tilde{T}}{dt} = k\left(\frac{1}{\tau_f} + \frac{1}{\tau_{HT}} + \frac{1}{\tau_c}\right)\frac{\tilde{T}}{\tilde{P}} - \left[(k-1)\frac{Z_{te}}{\rho_o} + \frac{1}{\tau_f} + \frac{k}{\tau_{HT}} + \frac{T_o}{T_w}\right]\frac{\tilde{T}^2}{\tilde{P}}, \quad (2.2)$$

pressure,

$$\frac{d\tilde{P}}{dt} = k\left(\frac{1}{\tau_f} + \frac{1}{\tau_{HT}} + \frac{1}{\tau_c}\right) - \left(\frac{Z_{te}}{\rho_o} + \frac{1}{\tau_{HT}}\frac{T_o}{T_w}\right)\tilde{T}, \quad (2.3)$$

mass fraction of fuel,

$$\frac{dY_f}{dt} = \frac{1}{\tau_f}\left(Y_{f,i} - Y_f\right)\frac{\tilde{T}}{\tilde{P}} - \frac{1}{\tau_c}\left(\frac{C_p T_o}{\Delta H_R}\right)\frac{\tilde{T}}{\tilde{P}}, \quad (2.4)$$

and velocity at the tailpipe entrance,

$$\frac{d\tilde{U}}{dt} = \left(\tilde{P}_{te} - 1\right)\frac{R_u T_o A_e \tau_f}{L_{TP} V}\frac{\tilde{T}_{te}}{\tilde{P}_{te}} - \frac{V f}{2 D_{TP} A_e \tau_f}\frac{\tilde{U}^3}{|\tilde{U}|}. \quad (2.5)$$

The various parameters in the governing equations include the ratio of tailpipe mass flow rate to combustion-chamber volume, Z_{te}; a characteristic heat transfer time,

$$\tau_{HT} = \frac{V \rho_o C_p T_o}{A_s U T_w}; \quad (2.6)$$

and a characteristic combustion time,

$$\frac{1}{\tau_c} = A'\frac{\Delta H_R}{C_p T_o}\frac{\tilde{P}^2}{\tilde{T}^{3/2}} Y_f^2 e^{-\tilde{T}_a/\tilde{T}}. \quad (2.7)$$

The METC model predicts three modes of behavior: steady combustion, pulsed combustion and flameout. As the combustor-wall temperature is reduced while holding the flow time constant, the model predicts a transition from steady combustion to pulsed combustion to flameout. During the pulsed-combustion regime, reductions in wall temperature

are predicted to result in increased amplitude and decreased frequency. These predictions closely match with the experimental observations. The effects of equivalence ratio cannot be explored since the reaction-rate equation used in the model is only valid at stoichiometric conditions (Richards *et al.* 1991).

2.2 Nonlinearity in pulsed combustors

Daw *et al.* investigated the behavior of the METC pulsed combustor and analytical model more closely, suspecting that the trends observed by Richards *et al.* (1991) were signs of deterministic chaotic behavior. Various techniques were used to confirm that the experimental pulsed combustor does exhibit nonlinear behavior. The nonlinearity of the Arrhenius rate law and the high dimensionality of the METC model led Daw *et al.* to suspect that the model might predict deterministic chaotic behavior despite the fact that it does not account for turbulent mixing. As shown in **Figure 2.5**, as flow time is shortened, the model does in fact predict that the combustor will follow a classic period-doubling route to chaos (Moon 1987). Daw *et al.* proposed that chaotic behavior could be present in many combustion systems and, due to the resulting fluctuations in pressure and temperature, could lead to reduced combustion efficiency and increased emission levels of pollutants such as NO_x (Daw *et al.* 1992; Daw *et al.* 1994; Daw *et al.* 1995).

The nonlinear nature of pulsed combustion has been independently confirmed by other studies. Analytical model studies performed at Sandia found that nonlinear coupling of various acoustic modes will produce nonlinear pressure oscillations of the type found in pulsed combustors (Margolis 1994). Sterling (1993) found that the combustor-pressure oscillations in a laboratory-scale pulsed combustor were described by a limit cycle with a
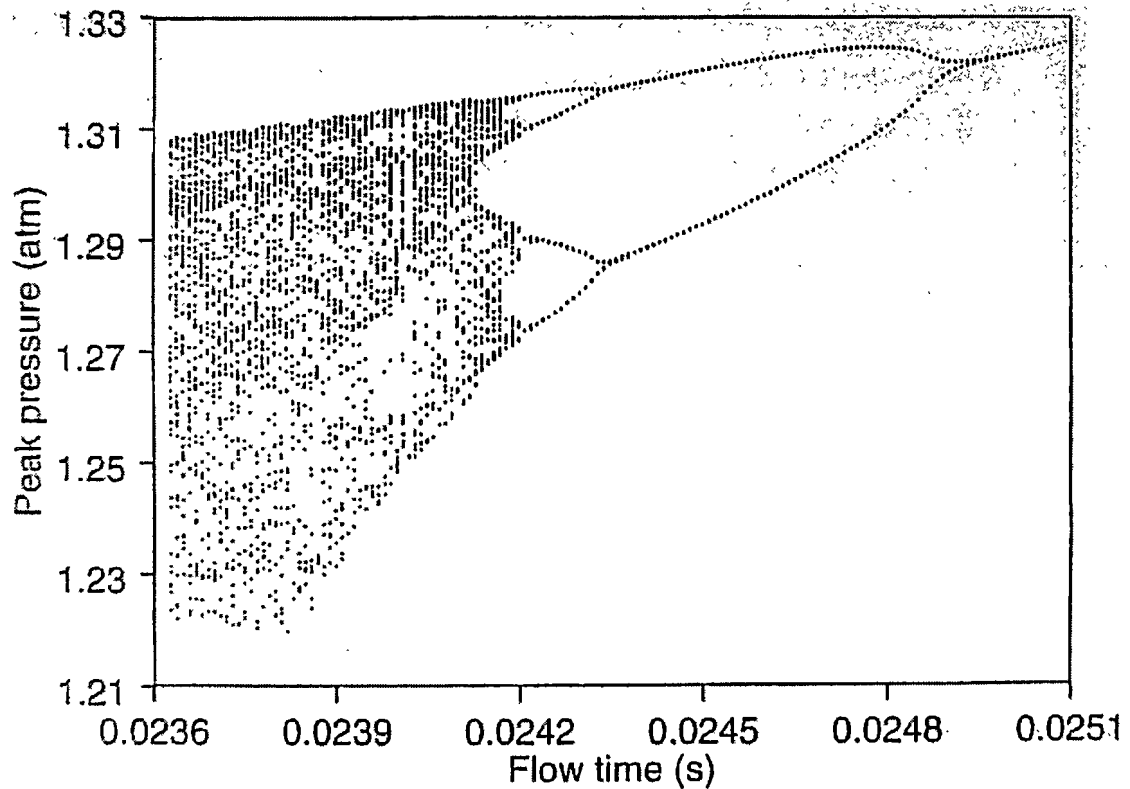
Figure 2.5: *Bifurcation diagram showing the period-doubling route to chaos predicted by the METC model as flow time is shortened (Daw et al. 1995).*

dimension greater than one. Sterling proposed that the combustion reaction was the source of the nonlinearity rather than nonlinear acoustic effects. An analytical model developed around this premise was shown to predict that the combustor will follow a period-doubling route to chaos as the mass flow rate of mixture is increased, in a manner similar to that predicted by Daw et al. (1992) (Sterling and Zukoski 1991; Sterling 1993).

2.3   Control of pulsed combustors

There has been considerable study dedicated toward applying active control to eliminate acoustically driven combustion oscillations because of the detrimental effect they can have upon delicate system components such as turbine blades. A review of these studies is beyond the scope of this study. A thorough review of active control techniques to eliminate acoustically driven combustion instabilities can be found in McManus *et al.* (1991) (republished as McManus *et al.* 1993).

Daw *et al.* (1992) speculated that the nonlinear nature of pulsed combustors would mean that linear control algorithms would be less effective at eliminating cyclic variability than would nonlinear control algorithms. A few studies have been conducted in which various nonlinear control methods were applied to the METC analytical model.

Rhode *et al.* (1995) applied a variety of control techniques to the METC model to eliminate the pressure oscillations or promote regular oscillations to delay the onset of chaos. The friction factor of the tailpipe was used as the control parameter in this study. A derivative control scheme was applied in which the friction factor was increased by adding to it a value proportional to the derivative of temperature with respect to time. The derivative control scheme was found to be effective at eliminating the pressure oscillations and forcing the model to operate in a steady mode. Adaptive map-based control schemes were found to be effective in promoting the oscillatory behavior. Using occasional and recursive proportional feedback, the map-based control scheme was able to prevent the model from going through the period-doubling route to chaos described by Daw *et al.* (1995) and avoid flameout, thus extending the operating regime of the model to include shorter flow times.

In *et al.* (1997) took a different approach toward controlling the behavior of the METC

model. In *et al.* sought to delay flameout of the model by maintaining the chaotic pressure oscillations. Characteristic trajectories which lead to flameout were identified and used to determine when to apply control actions to push the system away from flameout. When the model began to follow the mediating trajectory, a small perturbation was applied to the system by slightly increasing the flow time (*i.e.*, decreasing the mass flow rate of the mixture). Using this strategy, In *et al.* were also able to extend the operating regime of the model to include shorter flow times.

Chapter 3

Experimental Apparatus and Procedure

3.1 Overview of combustor design and instrumentation

The pulsed combustor used in this study is based upon the thermal pulse combustor design developed at METC in which the mixture is introduced at a constant flow rate and combustion is self-sustained by heat transfer from the hot combustor walls (Richards *et al.* 1991). A series of modifications were made to the original design over the course of the study before arriving at the final configuration.

3.1.1 Combustor design and construction

The pulsed combustor used in this study is shown schematically in **Figure 3.1**; a photograph of the combustor is shown in **Figure 3.2**. The design consists of a main body, comprised of a mixing chamber and a combustion chamber, and an acoustically coupled tailpipe. The main body was constructed by boring out the 5.1-cm (2-in) diameter mixing and combustion chambers from 6.35-cm (2.5-in) diameter 306 stainless steel round-stock.
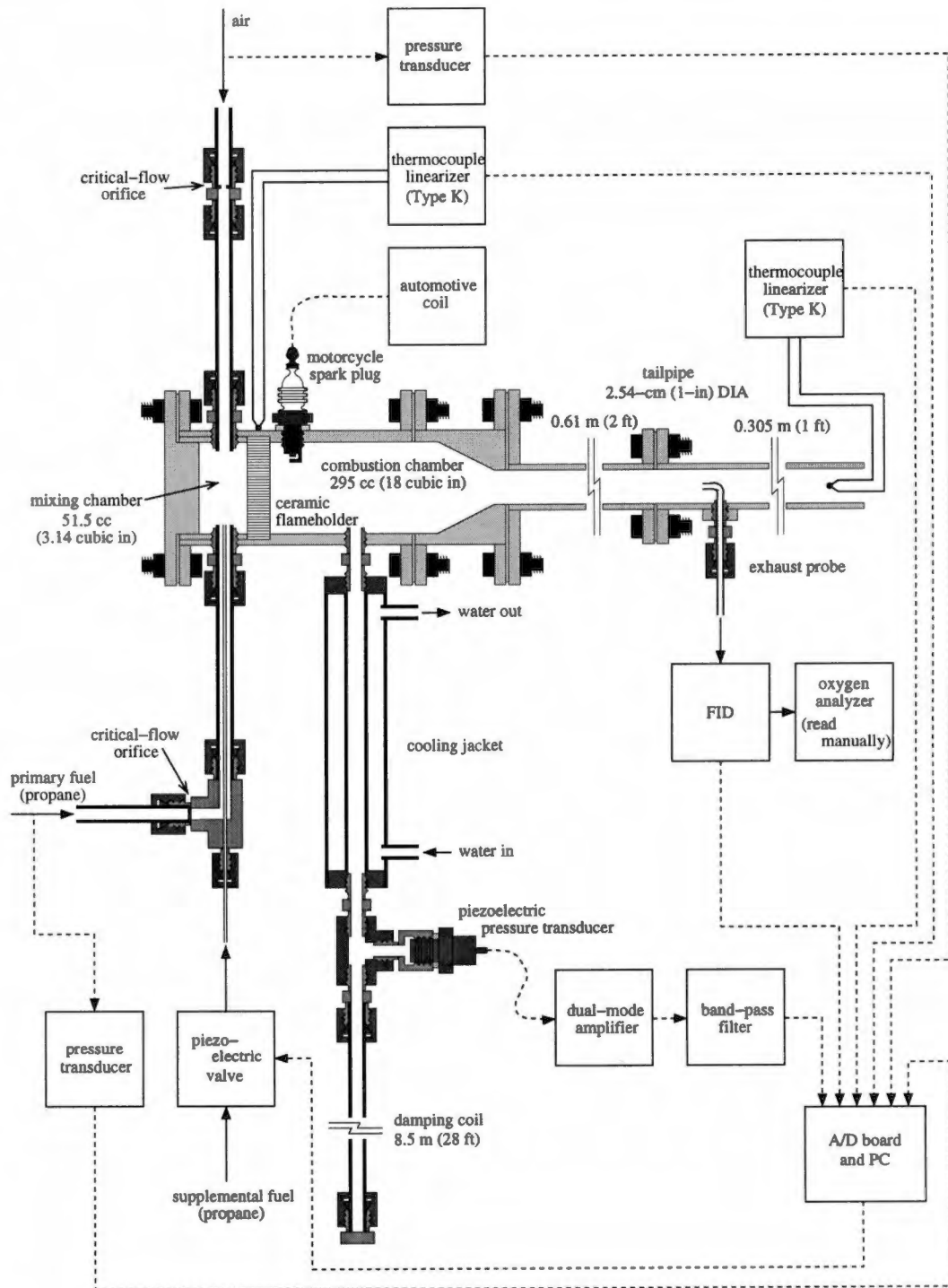
Figure 3.1: *Schematic of the pulsed-combustor design and instrumentation. Note that the swirl-inducing vanes are not shown in this view.*
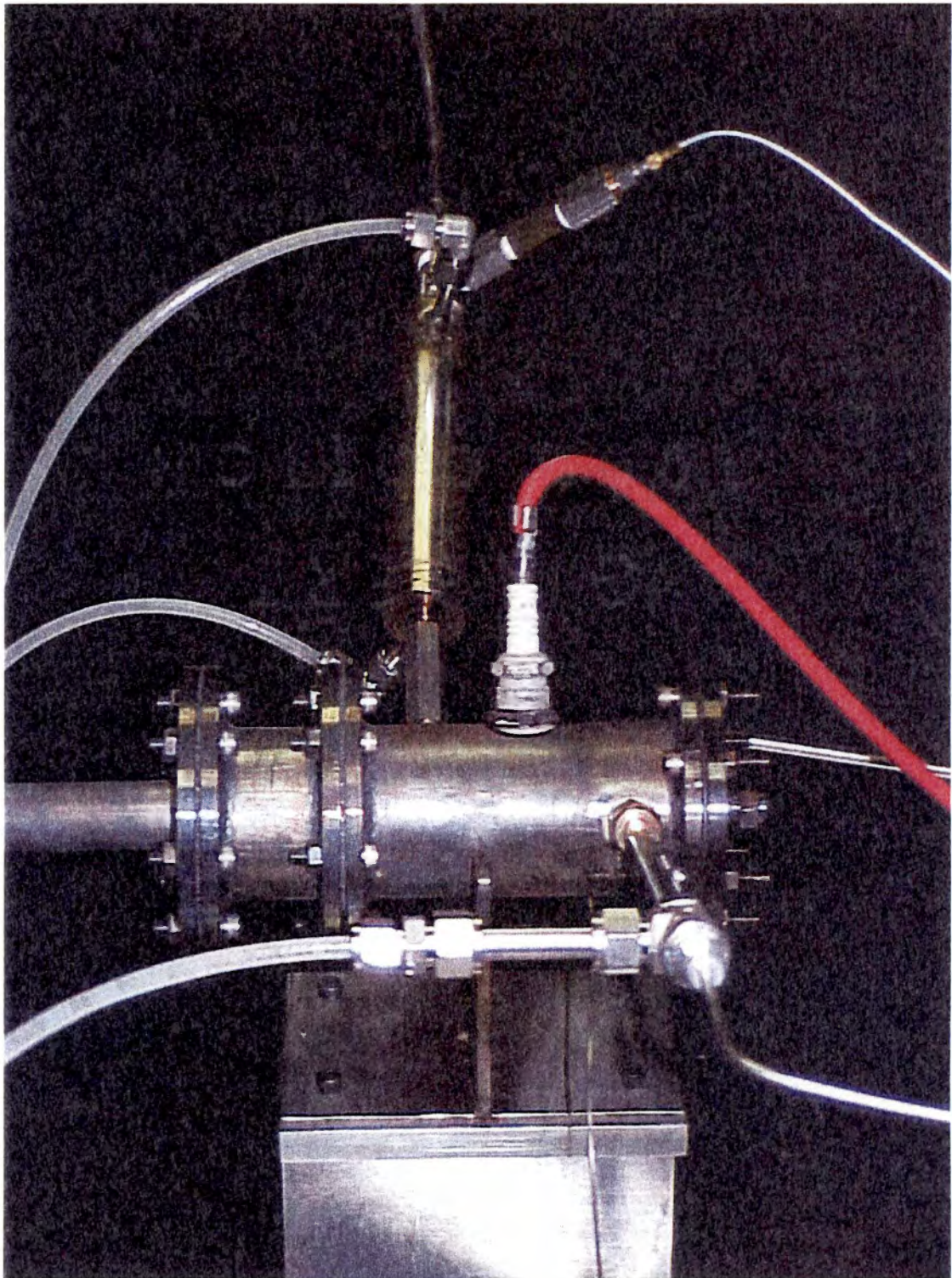
Figure 3.2: *Photograph of the pulsed combustor.*

The mixing chamber has an internal volume of 51.5 cc (3.14 in^3) and the combustion chamber has an internal volume of 295 cc (18 in^3). The tailpipe is constructed of 2.54-cm (1-in) stainless steel tubing which has an inner diameter of 1.9 cm (0.75 in). A conical section is included to make the transition from the combustion chamber to the tailpipe. The modular design of the tailpipe allows the length to be varied from 30.5 to 91.4 cm (1 to 3 ft) in 30.5-cm (1-ft) increments. A tailpipe length of 91.4 cm (3 ft) was used in this study unless otherwise specified.

The mixing chamber and combustion chamber are separated by a square-celled honeycomb ceramic flameholder that provides a stable location onto which the flame can anchor and acts as a heat source which helps sustain the combustion reaction after start-up. The ceramic chosen is a Celcor™ substrate from Corning International traditionally used in catalytic converters. The main components of the ceramic are silicon dioxide, alumina, and magnesium oxide. The flameholders are constructed by milling a 5.7-cm (2.25-in) diameter disk from a 6.35-mm (1/4-in) plate of the ceramic material. A cell density of 200 cells-per-square-inch was chosen. With this density, the cell openings have a hydraulic diameter of 1.5 mm (0.06 in) which is smaller than the quenching diameter for an air-propane mixture, 1.8 mm (0.07 in) (Turns 1996). This prevents the flame from propagating through the ceramic, thus anchoring it to the surface of the flameholder. Although the ceramic has a manufacturer-specified softening temperature of 1410°C (2570°F), the flameholder suffers thermal damage and must be replaced after several hours of combustor operation. The flameholder is held in place between a stainless steel sleeve inserted in the mixing chamber and a shoulder on the combustion-chamber side. An endcap allows easy access to the combustor interior so that the flameholder may be replaced and that the swirl vanes on the air and fuel inlets may be positioned.

A motorcycle spark plug installed in the combustion chamber immediately downstream of the ceramic flameholder and energized by an automotive coil is used to ignite the mixture during start-up. The energy released by the combustion reaction heats the combustor walls and the ceramic flameholder which in turn heat the incoming fresh charge. Eventually, enough energy is supplied by the flameholder and combustor walls to auto-ignite the fresh charge and initiate a self-sustaining combustion reaction. At this point, the energy supplied by the spark plug is no longer required to sustain combustion; however, for safety concerns, the spark plug is typically left on during operation.

Analysis of the pressure inside the combustion chamber was found to be the most effective method of characterizing the behavior of the system. A piezoelectric pressure transducer (Kistler, model 206) connected to a static-pressure tap located 4.75 cm (1.875 in) downstream of the ceramic flameholder is used to monitor the combustor pressure. Since the transducer is susceptible to thermal damage when exposed to the high temperatures of the combustor wall and exhaust gases, the tap is water-cooled to prevent overheating.

3.1.2 Supplying the mixture

The plumbing system for the combustor includes three separate lines which supply the air, primary fuel and supplemental fuel as shown in **Figures 3.3** and **3.4**. Air and fuel enter the mixing chamber in opposing streams. Each inlet has a swirl-inducing vane to enhance mixing. The air supply is obtained from building air which is normally available at a pressure of 689 kPa_g (100 psig). Two, 689-kPa_g (100-psig) propane tanks are used to supply the primary and supplemental fuel.

The mass flow rates of air and primary fuel are intended to be maintained constant regardless of the pressure oscillations occurring within the combustion chamber. To ac-
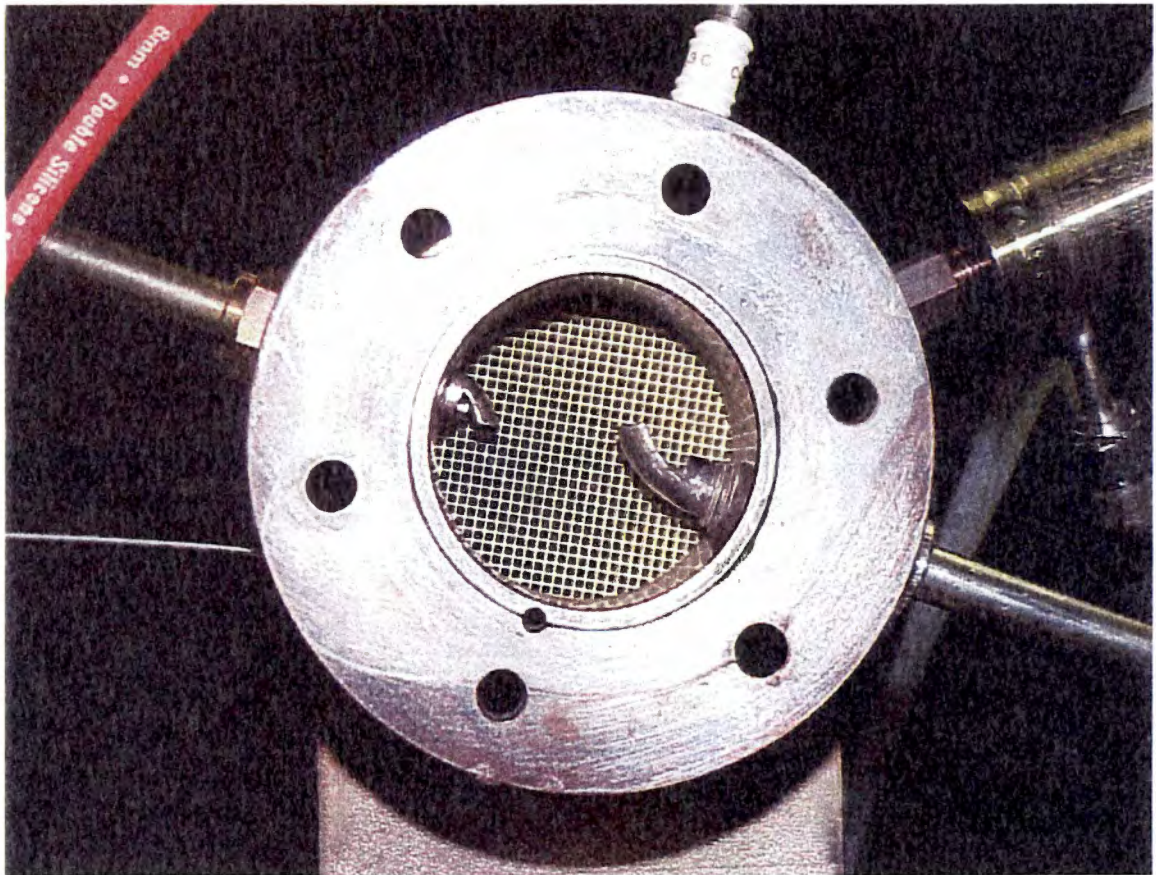
Figure 3.3: *Interior design of the mixing chamber showing the swirl inlets and ceramic flameholder.*
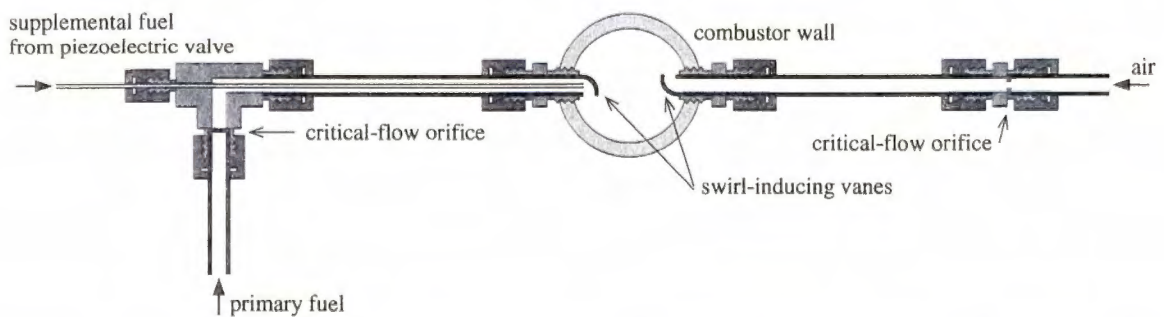
Figure 3.4: *Sketch of a pulsed-combustor cross-section showing the fuel and air inlet configuration including the swirl-inducing vanes and critical-flow orifice placement.*

complish this, the air and primary fuel supply lines each contain a critical-flow orifice as shown in **Figure 3.4**. As long as the supply pressure upstream of each orifice exceeds the critical pressure required for the Mach number to equal 1.0 at the orifice throat,

$$P_{crit,x} = P \left(\frac{k_x + 1}{2} \right)^{\frac{k_x}{k_x - 1}}, \tag{3.1}$$

where P is the pressure inside the combustion chamber and k_x is the specific-heat ratio of air or fuel, the flow will be choked and the mass flow rate will remain constant despite the downstream pressure oscillations. Tests were conducted in which pressure transducers were used to measure the pressure on either side of the critical-flow orifices while the pulsed combustor was operating to insure that the combustor-pressure oscillations do not cause the orifices to become unchoked. For choked flow with $M = 1$, the mass flow rates of air and primary fuel are given by

$$\dot{m}_x = P_{o,x} \frac{\pi d_x^2}{4} \sqrt{\frac{k_x}{R_x T_{o,x}}} \left(\frac{k_x + 1}{2} \right)^{\frac{k_x + 1}{2 - 2k_x}} \tag{3.2}$$

and thus depend upon only the orifice diameter, d_x; the supply pressure, $P_{o,x}$; and the supply temperature, $T_{o,x}$. Small changes in the mass flow rates are accomplished by varying the supply pressures using a pressure regulator installed in each line, upstream of the critical-flow orifice. Larger changes in mass flow rate are achieved by replacing the critical-flow orifices with larger- or smaller-diameter orifices. The supply temperatures are assumed to be maintained constant at room temperature.

The operating condition of the combustor is defined by two operating parameters: the equivalence ratio and a characteristic flow time. The equivalence ratio, ϕ, is defined as the ratio of the stoichiometric air-to-fuel ratio to the actual air-to-fuel ratio being supplied to

the mixing chamber via the air and primary fuel supply lines,

$$\phi = \frac{AF_{stoich}}{AF_{actual}}. \tag{3.3}$$

Thus, $\phi > 1$ for rich conditions; $\phi = 1$ at stoichiometric conditions; and $\phi < 1$ for lean conditions. The characteristic flow time, τ, is a reference value which is inversely related to the mass flow rate of the mixture and is meant to serve as a crude estimation of the average time the mixture spends inside the combustion chamber. The flow time is determined as

$$\tau = \frac{\text{internal volume of combustion chamber}}{\text{standardized volumetric flow rate of the mixture}}. \tag{3.4}$$

Consequently, a low mass flow rate corresponds to a long flow time and a high mass flow rate corresponds to a short flow time. It should be noted that the flow time is only a reference value which is used to specify the operating condition. The flow time does not accurate predict the time that a particle would actually reside in the combustion chamber due to the conversion of the volumetric flow rate to standard conditions and the pulsating nature of the flow inside the pulsed combustor.

It can be seen that both the equivalence ratio and the flow time — and thus the operating condition of the combustor — depend solely upon the mass flow rates of air and fuel. As previously mentioned, the use of critical-flow orifices in the supply lines allows the mass flow rate of air and primary fuel to be set by controlling the supply pressure and selecting an orifice with an appropriate diameter. Therefore, the operating condition of the combustor may be controlled in a similar manner.

The air and primary fuel lines are constructed of stainless steel tubing with Swagelok® fittings. The critical-flow orifices are constructed of 0.127-mm (0.005-in) steel shim-stock, die-punched and drilled to the appropriate size. This construction method is inexact and results in orifices which are not perfectly circular. The effective diameters of the critical-

flow orifices are approximated by placing the orifice under a microscope and measuring the diameter along two axes then averaging the two values. If the two diameter measurements are found to vary by more than ±25.4 μm (±0.001 in), that orifice is not used. The orifices are placed against the shoulder of a Swagelok® fitting and held in place by the tubing as shown in **Figure 3.4**.

3.1.3   Acoustic frequency

The pulsed combustor is designed to operate as a Helmholtz combustor with a small-diameter tailpipe acoustically coupled to a larger-diameter combustion chamber. With this configuration, the fundamental acoustic frequency, at which the combustor should pulse, is given by

$$f_H = \frac{a}{2\pi} \sqrt{\frac{A_t}{L_t\, V_c}} \tag{3.5}$$

where a is the speed of sound, A_t and L_t are the cross-sectional area and length of the tailpipe, respectively, and V_c is the internal volume of the combustor. The configuration of the current design results in an acoustic frequency of approximately 100 Hz, assuming properties of air at an exhaust-gas temperature of 1000 K.

The pressure tap also has the potential to act as an acoustic resonator. The original design used a 15-cm (6-in) long pressure tap. With this length, the pressure tap would have an acoustic frequency of approximately 85 Hz. There was concern that this acoustic mode would interfere with the combustor behavior or the ability to measure the pressure oscillations accurately. A 8.5-m (28-ft) long damping coil was added to the length of the pressure tap to reduce the acoustic frequency to approximately 10 Hz.

3.1.4 Control

As will be discussed in Chapter 6, the mass flow rate of fuel was found to be an effective control parameter for modifying the combustor dynamics. Various injection techniques and locations for a supplemental fuel supply were tested, but the best results were obtained by injecting the supplemental fuel coaxial with the primary fuel supply as shown in **Figure 3.4**. When a control action is required, a small pulse of fuel is introduced through the supplemental fuel line using a low-flow piezoelectric valve (Maxtex, model MV-112) capable of cycling at 250 Hz. The throughput of the valve is determined by the voltage applied and the supply pressure of the gas and can be varied over a range of 0 to 2500 cc/min SA (0 to 0.088 cfm SA).

The system used to control the injection of supplemental fuel is shown in **Figures 3.5** and **3.6**. When a control action is deemed necessary, the controller applies a voltage drop (6 V) across a solid-state relay, closing the relay and completing the circuit between the piezoelectric valve and the 80-V power supply. The piezoelectric valve then opens allowing additional fuel to enter the pulsed combustor. A rotameter installed upstream of the piezoelectric valve is used to measure the average flow rate of supplemental fuel. A surge tank is installed to decouple the piezoelectric valve and the rotameter and to insure a more steady flow of fuel throughout the duration of the control action. The controller terminates the control action by removing the voltage drop across the relay, breaking the circuit and causing the piezoelectric valve to close.

3.1.5 Instrumentation

Several instruments are used to determine the operating condition and monitor the dynamic behavior of the combustor. A 486-33MHz personal computer (PC) equipped with a
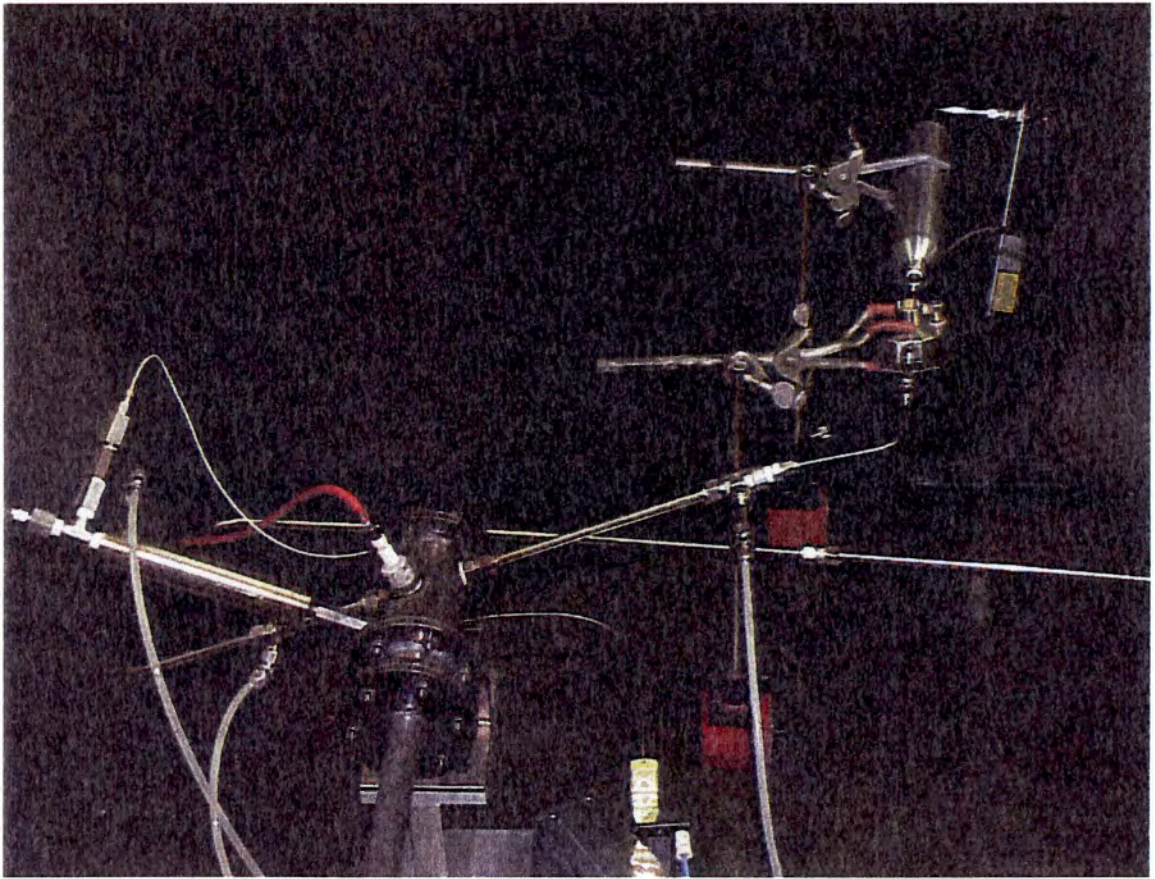
Figure 3.5: *Photograph of the pulsed combustor which shows the supplemental fuel-injection system used to introduce the control perturbations.*
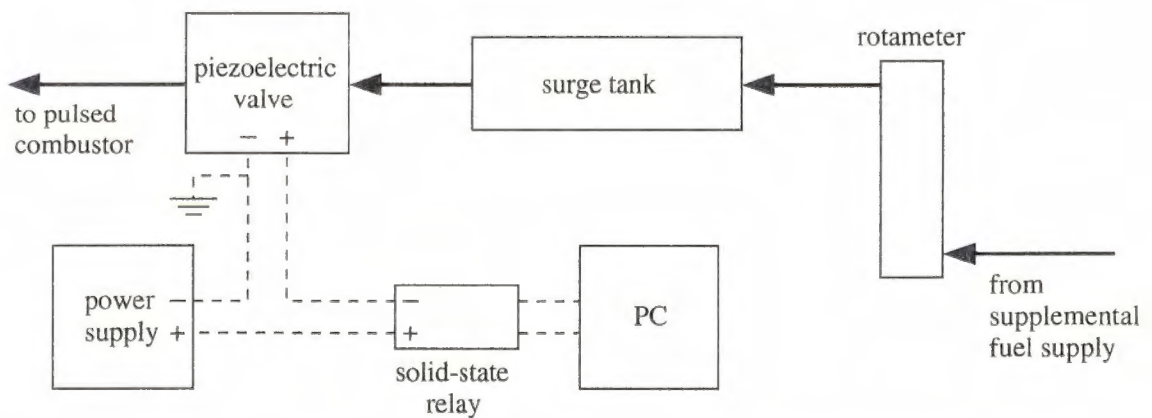
Figure 3.6: *Schematic of supplemental fuel-injection system used to introduce control perturbations.*

12-bit analog-to-digital (A/D) conversion card (National Instruments, model AT-MIO-16) is used to collect and reduce the data and make control decisions. This process is controlled by a C++ code written in-house by the Chaos Research Group at the University of Tennessee, Knoxville (written by Dean Edwards incorporating graphic routines written by Dr. Nicolaas van Goor).

The operating condition of the combustor is defined by the equivalence ratio and flow time which depend upon the supply pressures, supply temperatures and diameters of the critical-flow orifices that are installed. The diameters of the orifices are measured during construction and the supply temperatures are always assumed to be at standard room temperature. Therefore, only the supply pressures need be monitored while the combustor is in operation. To accomplish this, a resistance-type pressure transducer (Cole-Parmer, model 68971-10) is placed upstream of the critical-flow orifice in the air and primary fuel lines. The transducers have a manufacturer-specified operating range of 0 to 689 kPa_g (0 to 100 psig), an accuracy of ±0.1%FS, a time response of 1 ms and 4 to 20 mA output. The transducer output is routed to a digital reader with an accuracy of ±0.1%FS. Replacing a jumper on the input connections of the digital reader with a 100-Ω resistor provides a voltage drop which can be read by the A/D card.

A piezoelectric pressure transducer (Kistler, model 206) which measures oscillations about the time-averaged mean pressure is used to monitor the combustor pressure. A dual-mode amplifier (Kistler, model 5004) is used to process the raw signal from the transducer and amplify it to a readable range. The transducer has a manufacturer-specified range of 0 to 551.3 kPa (0 to 80 psi), a threshold of 6.89 Pa (0.001 psi) and a rise time of 3 μs. It is capable of detecting pressure oscillations occurring at frequencies as low as 0.05 Hz — lower-frequency oscillations are filtered out as the transducer adjusts to the varying mean

pressure. The transducer and amplifier each have a manufacturer-specified accuracy of ±1%. The amplified signal is band-passed using an analog filter (Rockland, model 852). The high-pass filter is set at 0.1 Hz to eliminate any DC-bias and the low-pass filter is set at half the sampling frequency to eliminate aliasing. The pressure-transducer signal is sampled using the PC or, for higher sampling rates, a digital oscilloscope (Nicolet, model 440) capable of sampling frequencies up to 10 MHz.

A shielded, Type-K thermocouple is attached to the exterior wall of the combustor near the location of the ceramic flameholder to provide an approximation of the combustion-chamber wall temperature at the flame front. While the reading is below the actual inside wall temperature, this reading is adequate to determine when steady state has been achieved and to provide a reference point to help insure accurate duplication of test conditions. The average exhaust-gas temperature is measured by a second Type-K thermocouple installed at the tailpipe exit. A thermocouple reader and linearizer (Extech, model KR401030) is used to provide a 0°C reference point and to linearize the output of each thermocouple. The output of the thermocouple readers are connected to the A/D card.

A viewing port is installed in the exhaust system which allows the observer to look up the tailpipe into the combustion chamber. Correlations can then be made between events seen in the pressure traces and the actual combustion events that are observed to occur inside the combustor.

A flame ionization detector, or FID, (Thermo Environmental Instruments, model 51) is used to sample the exhaust gases to measure the unburned-hydrocarbon (UHC) emission levels. The FID has a manufacturer-specified detection range of 0.1 to 10,000 ppm with an accuracy of ±2% of the reading. The 5-s response time of the FID is too slow for cycle-

resolved measurements. Instead, readings are time-averaged over a period of 1–2 min. An oxygen analyzer (Beckman, model OM-11 EA) is used to measure the concentration of oxygen in the exhaust gases.

The instantaneous amount of fuel injected during each control perturbation could not be easily measured; therefore, the following procedure was developed to determine the time-averaged mass flow rate of supplemental fuel. A surge tank and rotameter (Omega, model FL-3404G-NV) are installed upstream of the piezoelectric valve. The surge tank serves as damping volume to decouple the rotameter from the discontinuous flow through the valve. Thus, the rotameter sees a near-steady flow rate equal to the time-averaged throughput of the valve. The time-averaged mass flow rate is used to determine the effective equivalence ratio, $\bar{\phi}$, which would exist were the control perturbations introduced at a steady rate via the primary fuel supply.

The data-acquisition and control (DAC) code has a graphical user interface (GUI) which presents the data graphically and allows data-collection and control settings to be changed quickly and easily. The code monitors the combustor pressure and displays it on a strip chart. The air and primary fuel supply pressures are monitored so that the operating condition of the pulsed combustor can be determined based upon user-specified values for the diameters of the critical-flow orifices. An option in the code allows the operator to continuously monitor the wall and exhaust-gas temperatures, as well as the operating condition, on strip charts to insure that equilibrium has been reached prior to data collection. Real-time data-analysis techniques available with the DAC code include Fourier transform and time-return maps.

The DAC code is capable of sampling the combustor pressure at frequencies up to 1000 Hz. Data collection is initiated and terminated by the operator. The number of data

points which may be collected is limited only by the amount of hard-drive space available. The combustor-pressure data are written to an `ASCII` data file. Immediately prior to and following data collection, the code determines the operating condition of the pulsed combustor and writes it, as well as the wall temperature and exhaust-gas temperature and composition, to a log file. Other statistics including the date, time, data-collection rate, number of data points collected and control settings are also written to the log file.

The control algorithm (discussed in Chapter 6) is built into the DAC code. Control can be activated and deactivated at any time by the operator, and control settings can be varied easily through the GUI. When control is active, the state of the control signal is recorded in the data file along with the combustor-pressure signal. The state of the control signal is indicated by the following system which corresponds to the voltage of the control signal being sent to the relay: "1" – control is in stand-by mode, "2" – control is in learning mode, "0" – control is active but no control action is being taken, "6" – control is active and a control action is being taken. With this information, it is possible to reconstruct the control activation/deactivation sequence from the data file.

3.2   Uncertainty analysis

The operating condition of the pulsed combustor is defined by the equivalence ratio and a characteristic flow time. Both operating parameters depend solely upon the mass flow rates of air and primary fuel which, in turn, depend upon the diameters of the critical-flow orifices and the supply pressures and temperatures. An uncertainty analysis was performed to determine how uncertainties in these measurements affect the accuracy in determining the operating condition and the ability to accurately reproduce the operating condition of

a given test.

The uncertainty in measuring the diameters of the critical-flow orifices were found to have the largest effect upon the accuracy of determining the equivalence ratio and flow time. However, while accuracy is important, the primary concern is the ability to accurately reproduce a given test condition. Since the same set of critical-flow orifices would be used in reproducing a test condition, the uncertainties in the diameter of the orifices have no effect upon the repeatability of test conditions.

3.2.1   Uncertainty in determining equivalence ratio

In this study, the equivalence ratio, ϕ, is defined as the ratio of the stoichiometric air-to-fuel ratio to the actual air-to-fuel ratio of the mixture as supplied by the air and primary fuel,

$$\phi = AF_{stoich}\frac{\dot{m}_f}{\dot{m}_a}. \tag{3.6}$$

Since the mass flow rates of air and primary fuel are maintained constant by the critical-flow orifices, the equivalence ratio can be evaluated using Equation 3.2 to yield

$$\phi = AF_{stoich}\frac{d_f^2}{d_a^2}\frac{P_{o,f}}{P_{o,a}}\sqrt{\frac{T_{o,a}}{T_{o,f}}}\sqrt{\frac{k_f R_a}{k_a R_f}}\left(\frac{k_f+1}{2}\right)^{\left(\frac{k_f+1}{2-2k_f}\right)}\left(\frac{k_a+1}{2}\right)^{\left(\frac{k_a+1}{2k_a-2}\right)}. \tag{3.7}$$

The uncertainty in determining the equivalence ratio is then evaluated using the Kline-McClintock method (Figliola and Beasley 1995). Uncertainty in the measurement of the orifice diameters and supply pressures and temperatures are assumed to contribute to the uncertainty in equivalence ratio. For simplicity, the specific heat ratios of air and fuel are

considered to be known with no uncertainty. This treatment yields

$$
u_\phi = \pm \left[\left(\frac{\partial \phi}{\partial d_a} u_d \right)^2 + \left(\frac{\partial \phi}{\partial d_f} u_d \right)^2 + \left(\frac{\partial \phi}{\partial P_{o,a}} u_{P_o} \right)^2 + \left(\frac{\partial \phi}{\partial P_{o,f}} u_{P_o} \right)^2 \right.
$$
$$
\left. + \left(\frac{\partial \phi}{\partial T_{o,a}} u_{T_o} \right)^2 + \left(\frac{\partial \phi}{\partial T_{o,f}} u_{T_o} \right)^2 \right]^{1/2} . \tag{3.8}
$$

Evaluation of the partial derivatives in Equation 3.8 and division by the equivalence ratio yields

$$
\frac{u_\phi}{\phi} = \pm \sqrt{ \left(2\frac{u_d}{d_a} \right)^2 + \left(2\frac{u_d}{d_f} \right)^2 + \left(\frac{u_{P_o}}{P_{o,a}} \right)^2 + \left(\frac{u_{P_o}}{P_{o,f}} \right)^2 + \left(\frac{1}{2} \frac{u_{T_o}}{T_{o,a}} \right)^2 + \left(\frac{1}{2} \frac{u_{T_o}}{T_{o,f}} \right)^2 } . \tag{3.9}
$$

The individual contributions to the overall uncertainty are considered as follows. The critical-flow orifices are constructed by die-punching a disc from 0.127-mm (0.005-in) steel shim-stock and drilling the appropriately sized hole using a drill press and a specially constructed jig. This construction method is inexact and results in orifices which are not perfectly circular. The effective diameters of the critical-flow orifices are approximated by placing the orifice under a microscope and measuring the diameter along two axes then averaging the two values. If the two diameter measurements are found to vary by more than $\pm 25.4 \, \mu$m (± 0.001 in), that orifice is not used. This leads to an assumed uncertainty in average diameter of $u_{ave} = \pm 12.7 \, \mu$m ($\pm 0.0005$ in). The microscope (Scherr Tumico, model 98-0001) has a manufacturer-specified resolution of $\pm 2.54 \, \mu$m (± 0.0001 in), however, actual measurement of the orifices is felt to be possible only to a resolution of $e_r = \pm 12.7 \, \mu$m (± 0.0005 in). Based upon this, the estimated uncertainty in the orifice diameter is considered to be given by

$$
u_d = \pm \sqrt{e_r^2 + u_{ave}^2} \tag{3.10}
$$

which yields a value of $u_d = \pm 18.0 \, \mu$m (± 0.0007 in).

Supply pressures are monitored using resistance-type pressure transducers placed in the plumbing system upstream of each critical-flow orifice and connected to digital readers. The pressure transducers and digital readers both have a manufacturer-specified accuracy of $\pm 0.1\%$FS which translates to ± 0.7 kPa ($\pm$ 0.1 psi) and results in a combined overall instrument error of $u_o = \pm 1.0$ kPa (± 0.15 psi). During test runs, pressure fluctuations often occur in the supply lines (especially in the building-air supply) but are limited in magnitude by the pressure regulators in each line. These fluctuations are accounted for by including a contribution, $u_{pf} = \pm 0.7$ kPa (± 0.1 psi), to the uncertainty in supply pressure. Finally, since the pressure transducers measure gage pressure, the readings are converted to absolute pressure by adding the atmospheric pressure, assumed to be 99.9 kPa$_a$ (14.5 psia) at the elevation of the laboratory. Day-to-day fluctuations in atmospheric pressure due to meteorological conditions are accounted for by including a conservative contribution to the uncertainty in supply pressure, $u_{atm} = \pm 1.6$ kPa (± 0.5 in of Hg). The uncertainty in supply pressure measurement due to these contributions is assumed to be given by

$$u_{P_o} = \pm \sqrt{u_o^2 + u_{pf}^2 + u_{atm}^2}. \tag{3.11}$$

This treatment yields an uncertainty in supply pressure of $u_{P_o} = \pm 2.0$ kPa (0.3 psi).

The supply temperatures are not monitored but are assumed to be the same as the room temperature for the laboratory. Based upon Equation 3.9, it appears that the supply-temperature uncertainties are the smallest contribution to the overall uncertainty in equivalence ratio. A temperature of 21.4°C (70°F) is assumed in calculation of the operating conditions with a conservative uncertainty of $u_{T_o} = \pm 5.6$°C (± 10°F).

Results of the uncertainty analysis for the operating conditions used in this study are shown in **Table 3.1**. As can be seen, the accuracy error in determining equivalence ratio is quite large, ranging from $\pm 7.3\%$ to $\pm 10.4\%$ and increasing with flow time. The uncer-

Table 3.1: *Uncertainty in accurately evaluating and reproducing the operating condition of the pulsed combustor for the test cases used in this study.*

(a) $\tau = 50$ ms

measurement uncertainties	air	fuel
diameter of critical-flow orifice	2362 ± 18 μm (0.093 $\pm$ 0.0007 in)	508 ± 18 μm (0.020 $\pm$ 0.0007 in)
supply pressure	538 ± 2 kPa$_g$ (78 $\pm$ 0.3 psig)	317–724 ± 2 kPa$_g$ (46–105 $\pm$ 0.3 psig)
supply temperature	21.4 ± 5.6 °C (70 $\pm$ 10 °F)	21.4 ± 5.6 °C (70 $\pm$ 10 °F)

	ϕ	τ
accuracy error	$\pm 7.3\%$	$\pm 1.8\%$
repeatability error	$\pm 1.5\%$	$\pm 1.0\%$

(b) $\tau = 75$ ms

measurement uncertainties	air	fuel
diameter of critical-flow orifice	2235 ± 18 μm (0.088 $\pm$ 0.0007 in)	406 ± 18 μm (0.016 $\pm$ 0.0007 in)
supply pressure	372 ± 2 kPa$_g$ (54 $\pm$ 0.3 psig)	248–744 ± 2 kPa$_g$ (36–108 $\pm$ 0.3 psig)
supply temperature	21.4 ± 5.6 °C (70 $\pm$ 10 °F)	21.4 ± 5.6 °C (70 $\pm$ 10 °F)

	ϕ	τ
accuracy error	$\pm 9.0\%$	$\pm 1.9\%$
repeatability error	$\pm 1.7\%$	$\pm 1.1\%$

Table 3.1: *(continued)*

(c) $\tau = 100$ ms

measurement uncertainties	air	fuel
diameter of critical-flow orifice	2057 ± 18 μm (0.081 $\pm$ 0.0007 in)	356 ± 18 μm (0.014 $\pm$ 0.0007 in)
supply pressure	331 ± 2 kPa$_g$ (48 $\pm$ 0.3 psig)	124–751 $\pm$ 2 kPa$_g$ (18–109 $\pm$ 0.3 psig)
supply temperature	21.4 ± 5.6 °C (70 $\pm$ 10 °F)	21.4 ± 5.6 °C (70 $\pm$ 10 °F)

	ϕ	τ
accuracy error	$\pm$10.4%	$\pm$2.0%
repeatability error	$\pm$2.2%	$\pm$1.1%

tainty in critical-orifice diameter has the largest contribution to accuracy error. The use of smaller-diameter orifices to produce longer flow times are responsible for the majority of the increase in accuracy error with flow time. The repeatability error in equivalence ratio is significantly smaller, ranging from $\pm$1.5% to $\pm$2.2%. Again, the error is seen to increase with flow time; however, the increase is not as dramatic as with the accuracy error. While the accuracy error may cause some concern about the ability to determine the actual equivalence ratio of the mixture, especially for high equivalence ratios, the repeatability error is quite low, allowing for accurate reproduction of test conditions. The accuracy of the equivalence ratio calculations were checked using two independent experimental methods. Each orifice was calibrated over a range of mass flow rates using a hot-film anemometer to measure the average velocity in each supply line. Secondly, the oxygen analyzer was used to measure the oxygen content of the exhaust gases over a

range of equivalence ratios for each combination of critical-flow orifices used. Both tests confirmed that the equivalence calculations were accurate within the specified uncertainty levels.

3.2.2 Uncertainty in determining flow time

The characteristic flow time, τ, is a reference value which is meant to crudely approximate of the average time the mixture resides inside the combustion chamber as determined by dividing the combustor internal volume by the standardized volumetric flow rate of the fresh mixture. The mass flow rate of the mixture can be assumed to be equal to the sum of the mass flow rates of air and primary fuel introduced to the combustor. The density of the mixture changes with its composition which not only depends upon the equivalence ratio at which the combustor is operating but which also changes as combustion occurs. Therefore, the density of air at standard conditions is used to standardize the flow time calculation. Thus, the flow time is given by

$$\tau = \frac{V_c\, \rho_{SSL}}{\dot{m}_a + \dot{m}_f}. \qquad (3.12)$$

Substituting for the mass flow rates from Equation 3.2 yields

$$\tau = \frac{V_c\, \rho_{SSL}}{P_{o,a}\dfrac{\pi d_a^2}{4}\sqrt{\dfrac{k_a}{R_a T_{o,a}}}\left(\dfrac{k_a+1}{2}\right)^{\frac{k_a+1}{2-2k_a}} + P_{o,f}\dfrac{\pi d_f^2}{4}\sqrt{\dfrac{k_f}{R_f T_{o,f}}}\left(\dfrac{k_f+1}{2}\right)^{\frac{k_f+1}{2-2k_f}}} \qquad (3.13)$$

As with equivalence ratio, the Kline-McClintock method is used to estimate the uncertainty in determining the flow time. Assuming no uncertainty in the determination of the

specific-heat ratios for air and fuel, the uncertainty in flow time is given as

$$
u_\tau = \pm \left[\left(\frac{\partial \tau}{\partial d_a} u_d \right)^2 + \left(\frac{\partial \tau}{\partial d_f} u_d \right)^2 + \left(\frac{\partial \tau}{\partial P_{o,a}} u_{P_o} \right)^2 + \left(\frac{\partial \tau}{\partial P_{o,f}} u_{P_o} \right)^2 \right.
$$
$$
\left. + \left(\frac{\partial \tau}{\partial T_{o,a}} u_{T_o} \right)^2 + \left(\frac{\partial \tau}{\partial T_{o,f}} u_{T_o} \right)^2 \right]. \tag{3.14}
$$

Notice that the internal volume of the combustor and the density of the mixture are assumed not to contribute to the overall uncertainty in flow time, despite the fact that both have a significant uncertainty associated with their value. Since the same internal volume and density values are used in each flow time calculation, the uncertainty in internal volume and density have no effect upon the ability to accurately perform repeated evaluations at the same operating condition, which, as stated earlier, is the primary concern. Evaluating the partial derivatives in Equation 3.14 and dividing through by τ yields

$$
\frac{u_\tau}{\tau} = \pm \left[\left(2C_a \frac{u_d}{d_a} \right)^2 + \left(2C_f \frac{u_d}{d_f} \right)^2 + \left(C_a \frac{u_{P_o}}{P_{o,a}} \right)^2 + \left(C_f \frac{u_{P_o}}{P_{o,f}} \right)^2 \right.
$$
$$
\left. + \left(\frac{1}{2} C_a \frac{u_{T_o}}{T_{o,a}} \right)^2 + \left(\frac{1}{2} C_f \frac{u_{T_o}}{T_{o,f}} \right)^2 \right] \tag{3.15}
$$

where

$$
C_x = \frac{\dot{m}_x}{\dot{m}_a + \dot{m}_f}. \tag{3.16}
$$

Using the same approximations for the individual contributions as before, the accuracy and repeatability errors in the flow time were evaluated for the operating conditions used in this study with the results shown in **Table 3.1**. Both the accuracy and repeatability errors are much smaller for the flow time than for the equivalence ratio. The accuracy error ranges from $\pm 1.8\%$ to $\pm 2.0\%$, and the repeatability error ranges from $\pm 1.0\%$ to $\pm 1.1\%$.

3.3   Experimental procedure

A typical experimental run begins by first insuring that the laboratory exhaust system and carbon monoxide detector are functioning properly. Cooling water is introduced to the pressure-tap cooling jacket and the spark plug is activated. The FID and oxygen analyzer must be calibrated before each run. Breathing-quality air and a span gas composed of 983 ppm of propane with air as the base gas are used to zero the FID and establish a calibration point. Nitrogen and breathing-quality air are used to zero and calibrate the oxygen analyzer.

The remaining data-collection instruments are then activated and checked to insure proper operation. The DAC code is initiated and a series of tests are performed to insure that the code is operating properly and that valid data are being received from the data-collection instruments.

After donning ear protection, the air supply is sufficiently pressurized to insure choked flow. With the fuel cut-off valve closed, the primary and supplemental fuel supply lines are pressurized and the power supply for the piezoelectric valve is turned on. A slightly rich mixture has proven best for a quick, efficient start-up. After a final safety check, the fuel cut-off valve is opened allowing fuel to enter the combustor through the primary fuel supply line.

Start-up of the pulsed combustor is rather dramatic. The spark plug supplies a localized ignition source which is incapable of initiating self-sustained combustion throughout the combustion chamber. Instead, the initial stage of start-up is characterized by a series of extremely intense combustion events as a combustible mixture builds in the combustion chamber until ignited by the spark plug. The flame kernel introduced by the spark plug consumes all the available fuel in a rapid combustion event. Another combustion event
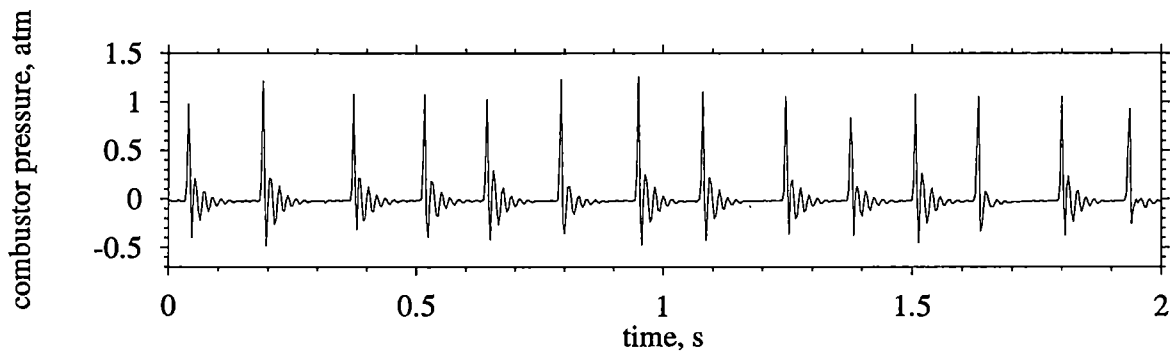
Figure 3.7: *Pressure trace collected during the initial stages of combustor start-up. This stage of start-up is characterized by occasional, intense combustion events. The signal depicts oscillations about the time-averaged mean combustor pressure.*

cannot occur until a sufficient fuel inventory has once again built up in the vicinity of the spark plug. **Figure 3.7** shows a combustor-pressure time series collected during this initial stage of start-up. As can be seen, the combustion events are characterized by a large pressure spike which may exceed 1 atm above ambient pressure followed by a decaying oscillation which occurs at the acoustic frequency of the tailpipe. These combustion events produce a sound pressure level in excess of 120 db, and the rapid "banging" is often said to sound like automatic-rifle fire. The time between successive combustion events is dependent upon the time required for the fuel concentration to rise to a combustible level in the vicinity of the spark plug. This behavior is very similar to that observed by Richards *et al.* (1991) when operating at low combustor-wall temperatures.

A few minutes of this behavior are often required until the ceramic flameholder and combustor walls are heated to a temperature sufficient to auto-ignite the fuel and initiate a global, self-sustained combustion reaction. Observations through the viewing port in the exhaust system show that the flame front initially forms in the combustion chamber and more heating of the ceramic is required before the flame attaches to the ceramic
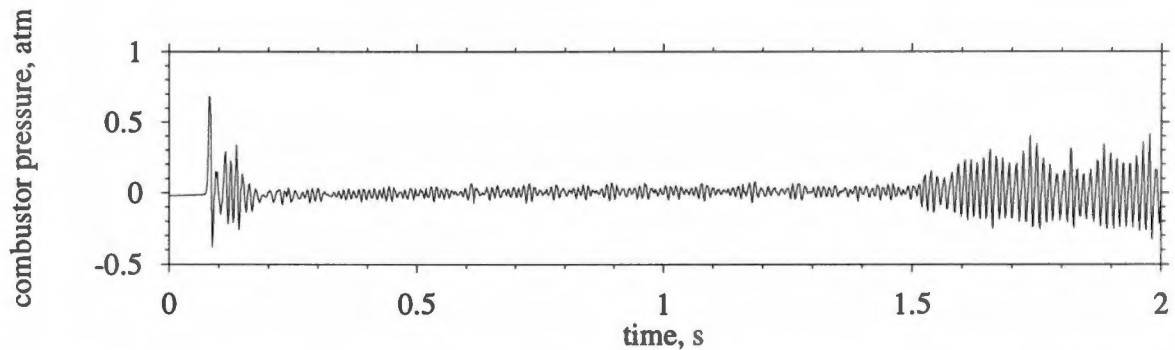
Figure 3.8: *Pressure trace collected during combustor start-up showing the initiation of self-sustained combustion and the subsequent attachment of the flame to the ceramic flameholder. The signal depicts oscillations about the time-averaged mean combustor pressure.*

flameholder. **Figure 3.8** shows a pressure trace collected as self-sustained combustion is initiated and the flame becomes attached to the flameholder. While the flame front is located in the combustion chamber, the combustor operates in a steady mode with small, random fluctuations about the mean pressure. Once the flame is attached to the ceramic flameholder, the combustor begins to operate in a pulsed mode, as evident by the higher-amplitude oscillations in combustor pressure. Once the combustion reaction becomes self-sustained and the flame is anchored to the ceramic flameholder, the spark plug has no effect upon combustion quality (see Section 4.4.1) and may be deactivated; however, it is usually left on for safety and to hasten recovery from flameout.

Once the flame has anchored to the flameholder, the air and primary fuel supply pressures are brought to the levels needed to produce the desired operating condition. The wall and exhaust-gas temperatures and exhaust-gas composition are monitored to insure that the system has reached equilibrium at the new operating condition before data are collected.

In case of emergency, the combustor may be shut-down by closing the fuel cut-off valve. In normal shut-down procedure, the fuel supplies are cut off at their source allowing the fuel supply lines to be partially evacuated. The air supply is typically left on for several minutes to help evacuate any residual fuel from the combustor. When flameout occurs during operation of the combustor, the fuel cut-off valve is closed as soon as possible. A rapid restart may be achieved by increasing the equivalence ratio to slightly rich conditions and reopening the fuel cut-off valve with the spark plug energized.

Chapter 4

Characterization of combustor dynamics

4.1 Analysis of combustor behavior

One of the primary goals of this study is to perform a thorough, systematic analysis of the behavior of the pulsed combustor over a wide range of operating conditions. This was accomplished by operating the pulsed combustor at three different flow times and reducing the equivalence ratios from slightly rich conditions to the point at which flame extinction occurred. The combustor pressure, combustion-chamber wall temperature and exhaust-gas temperature and composition were monitored to detect changes in behavior at the various operating conditions. Visual observations were made through the viewing port in the exhaust system in order to correlate any observed trends in the data to the actual events observed to occur inside the combustion chamber. Long data sets (approximately 60,000 records) were collected at high sampling rates (up to 5000 Hz) to insure that statistically significant information could be obtained from the various data-analysis techniques used

50
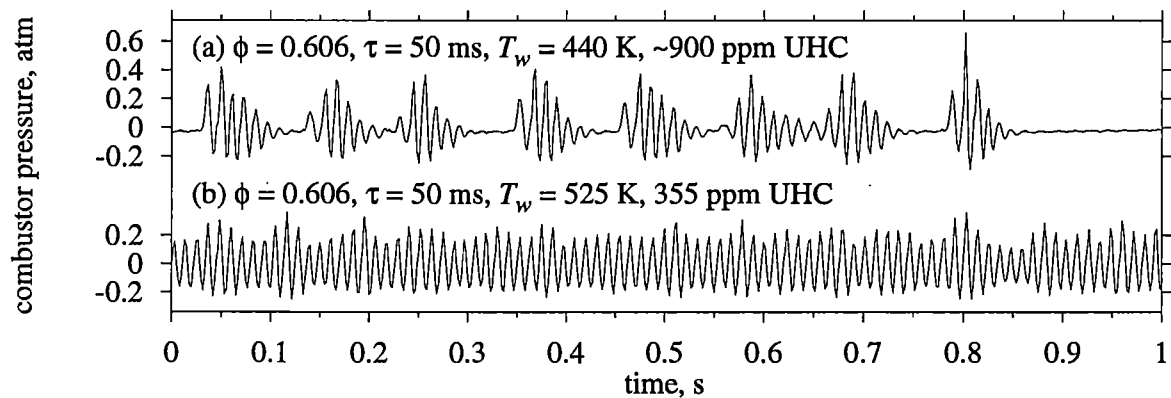
Figure 4.1: *Combustor-pressure time-series segments which demonstrate the effect of combustor-wall temperature, T_w, upon the performance of the pulsed combustor. The signals depict oscillations about the time-averaged mean combustor pressure.*

to characterize the behavior of the combustor.

4.1.1 Wall-temperature effects

Richards *et al.* (1991) were able to show both experimentally and analytically that the combustion-chamber wall temperature has a significant effect upon the behavior of the thermal pulse combustor, hence the name. Similar effects were found during the current study. High wall temperatures were found to enhance the combustion quality, especially at very lean conditions where flameout can be delayed by increasing the temperature of the combustion-chamber wall and the ceramic flameholder. **Figure 4.1** shows two combustor-pressure time series recorded while the pulsed combustor was operating at an equivalence ratio of $\phi = 0.606$ and a flow time of $\tau = 50$ ms. The pressure time series shown in **Figure 4.1(a)** was collected while the combustor was being operated normally, whereas the pressure time series shown in **Figure 4.1(b)** was collected with the combustor insulated as shown in **Figure 4.2** to reduce the heat loss to the surroundings and raise the wall temper-
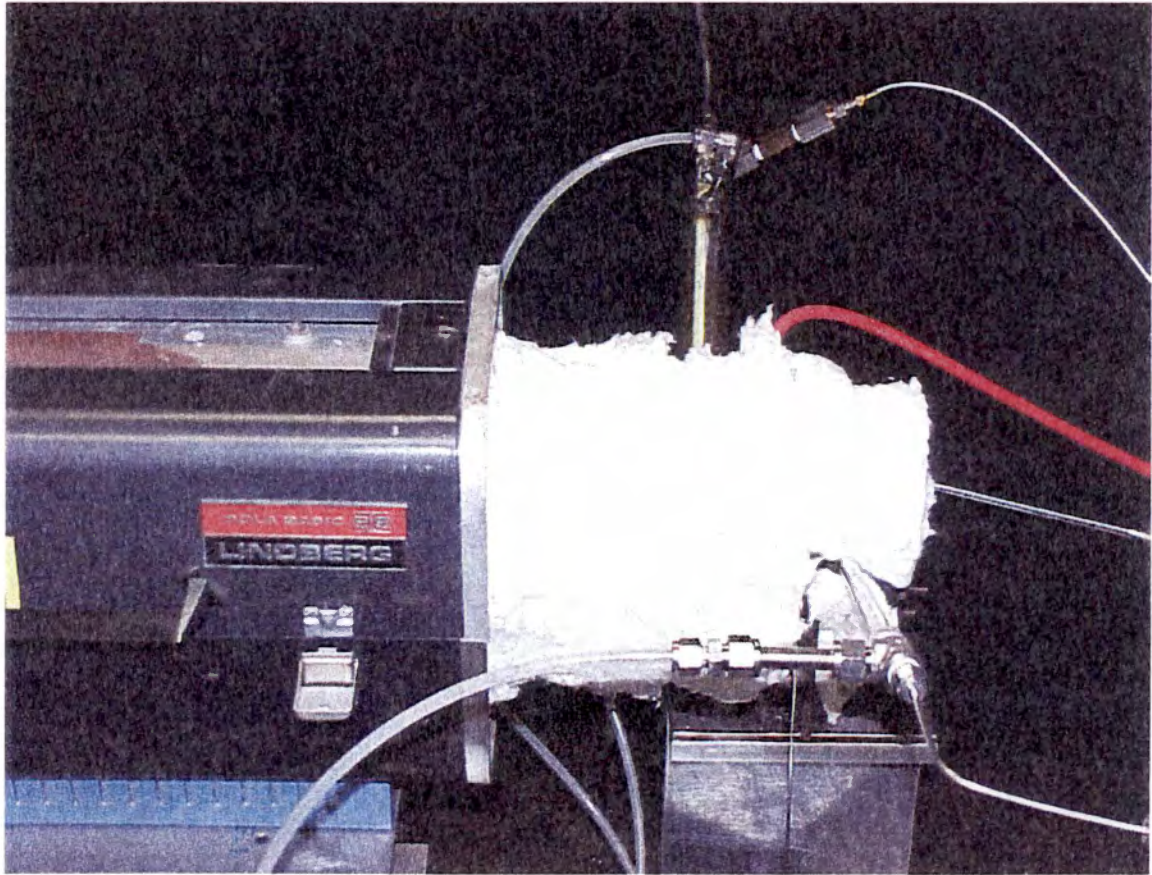
Figure 4.2: *Photograph showing the pulsed combustor with the tailpipe placed in a thermocouple furnace and the combustion chamber wrapped in ceramic insulation to reduce heat loss and elevate the wall temperature.*

ature. Without insulation, the steady-state wall temperature is 440 K, and the combustor behavior is very unstable with frequent misfires which eventually lead to an unrecoverable flameout. With insulation, the wall temperature reaches steady state at 525 K, and the combustor behavior is much more stable without any occurrence of misfire and relatively small cycle-to-cycle variations in the magnitude of the combustor-pressure oscillations.

At a given operating condition, the pulsed combustor will eventually reach thermal equilibrium at a steady-state temperature. As should be expected, due to differences in

the amount of heat release at different operating conditions, the value of the steady-state temperature varies with the operating condition. It was also found that the steady-state temperature can vary over repeated test runs conducted on different days but at the same operating condition. The changes in behavior are greater than can be explained by the uncertainty in reproducing a given operating condition which suggests that other factors, such as day-to-day fluctuations in the heat loss from the combustor due to changes in the ambient conditions of the test facility, could be responsible.

The dependence of the behavior of the combustor upon the wall temperature has serious implications for engineering systems in which the pulsed combustor is used for heating applications. It seems clear that the rate of heat transfer from the combustor has a dramatic effect upon the stability of the system, especially at lean operating conditions. In this study, no effort has been made to actively control the heat transfer rate from the combustor to explore how engineering applications of the pulsed combustor might be affected by this wall-temperature dependence. However, the wall temperature is monitored to ensure that the combustor has reached steady state before data collection is initiated to avoid hysteresis error which would otherwise occur when changing the operating condition during a test run. Also, in comparing data collected at similar operating conditions but on different test runs, care has been taken to insure that the wall temperature for those tests are similar.

4.1.2   Equivalence-ratio effects

By comparing pressure time series collected at similar mass flow rates but different equivalence ratios, Richards *et al.* (1991) found that the thermal pulse combustor undergoes a transition from high-amplitude pulsations to low-amplitude pulsations as the equivalence ratio is lowered. During transition between the two modes, the combustor behavior inter-

mittently switches between the high- and low-amplitude oscillations.

In the current study, the behavior of the pulsed combustor was also found to be highly dependent upon the equivalence ratio of the fresh charge introduced into the combustion chamber. At all operating conditions, the behavior of the system is dominated by large pressure oscillations which occur at the acoustic frequency of the combustor. At most operating conditions, there is significant variability in behavior from one cycle to the next indicating that there are cycle-to-cycle fluctuations in the quality of the combustion events. This cyclic variability is easily detectable by observing the cycle-to-cycle fluctuations in the magnitude of the combustor-pressure oscillations. At near-stoichiometric and slightly lean equivalence ratios, the cyclic variability is relatively small and appears to be random in nature. As the equivalence ratio approaches the lean flammability limit, combustion instabilities begin to develop which greatly increase the cyclic variability in combustion quality. The combustion instabilities force the combustor into a characteristic pattern of misfire and recovery and eventually lead to an unrecoverable flameout.

The onset of the combustion instabilities was investigated by holding the flow time constant and decreasing the equivalence ratio from slightly rich conditions to the point at which the combustor experiences an unrecoverable flameout. **Figure 4.3** illustrates the onset of the combustion instabilities using typical time-series segments of the combustor pressure, measured relative to the time-averaged mean pressure, recorded over a range of equivalence ratios at a flow time of $\tau = 50$ ms. The combustor pressure undergoes large-magnitude oscillations at the acoustic frequency of the combustor, which is approximately 100 Hz; however, the temperature of the exhaust gases decreases with equivalence ratio causing the frequency of the oscillations to decrease by as much as 20 Hz over the range of equivalence ratios shown here.
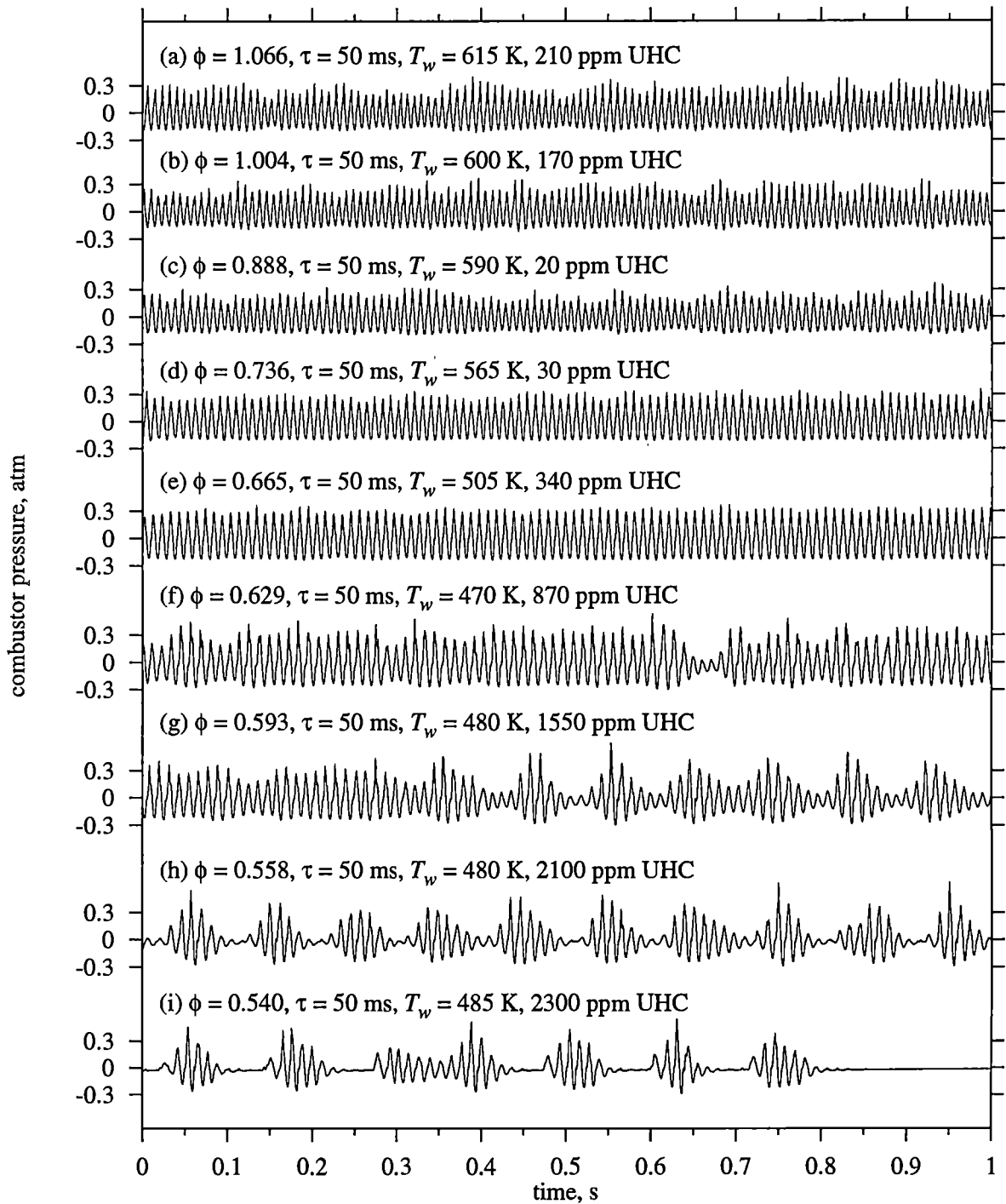
Figure 4.3: *Combustor-pressure time-series segments recorded at a flow time of* τ = *50 ms showing the onset of combustion instabilities as equivalence ratio is decreased. The signals depict oscillations about the time-averaged mean combustor pressure.*

At near-stoichiometric conditions (**Figures 4.3(a)–4.3(c)**), there is significant variability in the combustion quality from one cycle to the next as evidenced by the cycle-to-cycle fluctuations in the magnitude of the combustor-pressure oscillations. As seen through the observation port, at these operating conditions, the flame remains attached to the ceramic flameholder but occasionally flickers.

As the mixture is made increasingly lean (**Figure 4.3(d)**), the average amplitude of the combustor-pressure oscillations increases slightly and the cycle-to-cycle fluctuations in magnitude decrease significantly until the combustor-pressure oscillations become fairly regular with relatively minor cyclic variability (**Figure 4.3(e)**). The occurrence of flame flicker diminishes greatly at these conditions.

With further reductions in equivalence ratio, the cyclic variability again begins to increase. Occasionally, the combustion quality becomes extremely poor resulting in a near misfire (*e.g.*, at $t = 0.65$ s in **Figure 4.3(f)**). The pulsed combustor begins to experience intermittent shifts between a relatively stable mode of operation and a mode in which the combustion quality alternates between good and extremely poor in a periodic pattern with a frequency on the order of 10 Hz (**Figure 4.3(g)**). Similar intermittencies were observed by Richards *et al.* (1991).

As the equivalence ratio approaches the lean flammability limit (**Figures 4.3(h)** and **4.3(i)**), the system begins to visit the more stable mode less frequently — if ever. During the poor-quality combustion events, the system actually begins to misfire as confirmed by visual observations in which the flame is seen to be extinguished. Misfire is followed by a rapid recovery in which the magnitude of the combustor-pressure oscillations becomes quite large before the system slowly decays toward another misfire. The frequency of the misfire-and-recovery pattern is on the order of 10 Hz; however, the frequency decreases

slightly as the equivalence ratio is decreased. With less energy being released due to the frequent misfires, the combustor wall and the ceramic flameholder begin to cool. Eventually, at the edge of the lean flammability limit, the cooling is sufficient to extinguish the self-sustaining reaction, at which point the pulsed combustor experiences an unrecoverable flameout (**Figure 4.3(i)** at $t = 0.8$ s), even with the spark plug firing.

The changes in the behavior of the combustor are very noticeable to the human ear and it suspected that acoustic sensors could be used to monitor the behavior of the combustor without the intrusiveness created by the pressure tap. The decrease in acoustic frequency with equivalence ratio — due to decreasing exhaust-gas temperature — is very evident. At moderately lean conditions where the behavior is the most stable, the combustor produces a smooth roar. At higher equivalence ratios where there is significant cyclic variability in combustion quality, the combustor sounds much more rough and irregular. At very lean conditions where the behavior is dominated by the combustion instabilities, the sound produced by the combustor is often compared to the sound made by a hot rod or a Harley-Davidson® motorcycle.

The actual onset of the combustion instabilities is evident in power-spectral-density (PSD) plots of the combustor pressure (**Figure 4.4**). The combustion instabilities appear as a peak on the order of 10 Hz in the power spectrum which is first detected at an equivalence ratio of $\phi = 0.665$ (**Figure 4.4(e)**) at this flow rate. At this operating condition, the development of the instabilities is not readily obvious in the pressure traces (**Figure 4.3**); however, the UHC emission levels begin to increase sharply at this point (see **Figure 4.3**) suggesting that combustion quality has decreased. At higher equivalence ratios (**Figures 4.4(a)–4.4(d)**), the power spectrum is dominated by peaks at the fundamental acoustic frequency and its harmonics. Once the instabilities begin to de-
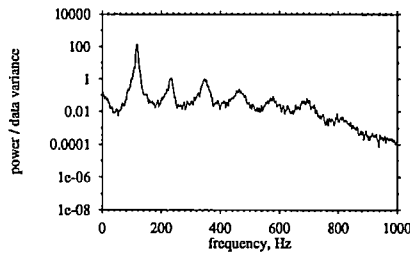
(a) $\phi = 1.066, \tau = 50$ ms
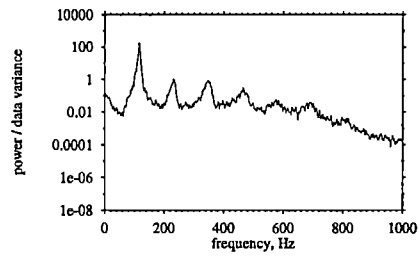
(b) $\phi = 1.044, \tau = 50$ ms
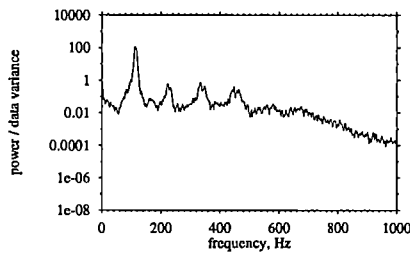
(c) $\phi = 0.888, \tau = 50$ ms
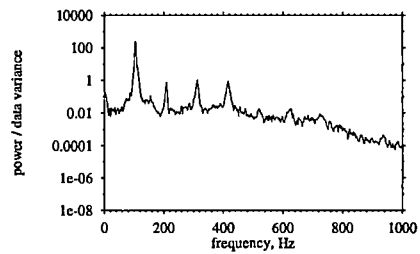
(d) $\phi = 0.736, \tau = 50$ ms
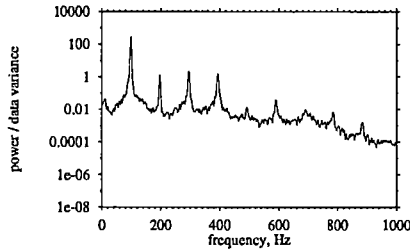
(e) $\phi = 0.665, \tau = 50$ ms
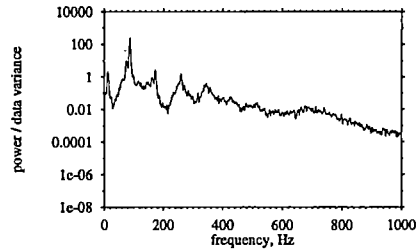
(f) $\phi = 0.629, \tau = 50$ ms
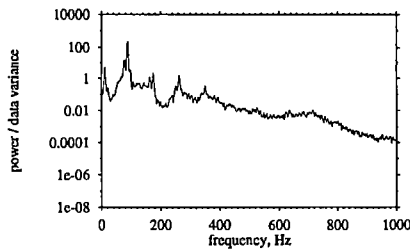
(g) $\phi = 0.593, \tau = 50$ ms
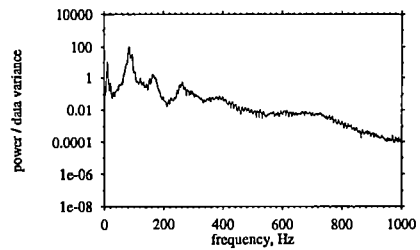
(h) $\phi = 0.558, \tau = 50$ ms

Figure 4.4: *PSD plots of the combustor pressure for a range of equivalence ratios at a flow time of $\tau = 50$ ms.*

velop, the harmonics become less powerful. As the equivalence ratio approaches the lean flammability limit, the power of the combustion instabilities continues to grow until, at an equivalence ratio of $\phi = 0.558$ (**Figure 4.4(h)**), it is almost of the same order as that of the acoustically driven oscillations.

4.1.3   Flow-time effects

Richards *et al.* (1991) found that decreasing the mass flow rate of the mixture (*i.e.*, lengthening the flow time) resulted in changes in the behavior of the thermal pulse combustor similar to those observed by decreasing the equivalence ratio. At very long flow times, the combustor was found to operate in a steady mode. Various analytical models have been shown to predict that pulsed combustors will follow a period-doubling route to chaos as the mass flow rate of the mixture is increased (Daw *et al.* 1995; Sterling 1993).

In this study, the effects of flow time (*i.e.*, mass flow rate) upon the behavior of the pulsed combustor were investigated by repeating the equivalence-ratio experiments at different mass flow rates and comparing the results. **Figure 4.5** shows a set of time-series traces of the combustor-pressure oscillations, relative to the time-averaged mean pressure, for a range of equivalence ratios at a flow time of $\tau = 100$ ms. Comparison with **Figure 4.3** readily shows that the behavior of the pulsed combustor is similar at both flow rates with a few exceptions. Most obviously, the overall amplitude of the combustor-pressure oscillations is significantly smaller at longer flow times (very noticeable to the human ear) due to the lower mass flow rate of mixture.

The effects of equivalence ratio upon the behavior of the pulsed combustor are similar for all flow times; however, the onset of the combustion instabilities is delayed to lower equivalence ratios as the flow time is lengthened. This seemingly allows the oper-
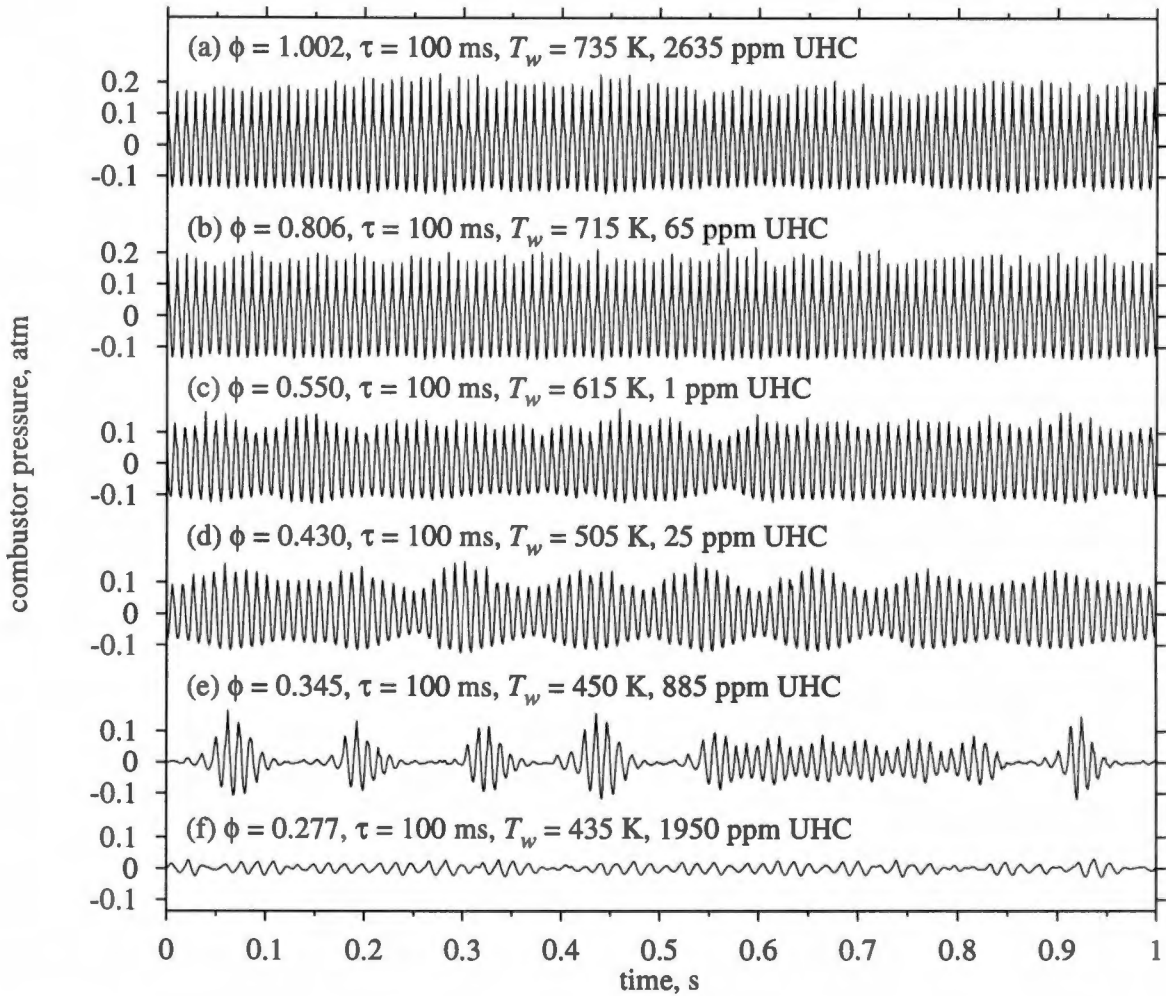
Figure 4.5: *Combustor-pressure time-series segments collected over a range of equivalence ratios at a flow time of $\tau = 100$ ms. The signals depict oscillations about the time-averaged mean combustor pressure.*

ating range of the pulsed combustor to be extend further toward, and even past, the lean flammability limit simply by decreasing the mass flow rate of the mixture. For example, at $\tau = 50$ ms, flameout occurs at an equivalence ratio of $\phi \approx 0.54$ whereas it is delayed until an equivalence ratio of $\phi \approx 0.30$ at a flow time of $\tau = 100$ ms. Also, at long flow times and very low equivalence ratios, the pulsed combustor will often operate in a steady mode (**Figure 4.5(f)**). Though this mode of operation is unstable and dependent upon high wall temperatures, it has only been observed at long flow times which corresponds to the results obtained by Richards *et al.* (1991).

The extended operating range of the pulsed combustor at longer flow times is felt to result from poor mixing of the inlet streams. At low mass flow rates, the inlet streams are believed to have insufficient momentum to mix thoroughly resulting in a stratified charge with a localized equivalence ratio which far exceeds the equivalence ratio of the injected mixture. Visual observation through the viewing port in the exhaust system confirm the presence of a "hotspot" on the ceramic flameholder indicating localized combustion. As mentioned in Chapter 3, the ceramic flameholders suffer thermal damage after several hours of use. **Figure 4.6** shows two flameholders which show very different damage patterns. The flameholder in **Figure 4.6(a)** has a nearly symmetric damage pattern suggesting thorough mixing and a uniform global reaction. The highly localized thermal damage shown in **Figure 4.6(b)** is an extreme example of the thermal damaged caused by poor mixing and a stratified charge.

The poor mixing limits the ability to compare the behavior of the combustor at various flow rates to that predicted by the METC analytical model which assumes a well-mixed reaction zone. Premixing of the air and fuel should resolve this problem; however, as this is not the primary goal of the current study, the effects of premixing were not thoroughly
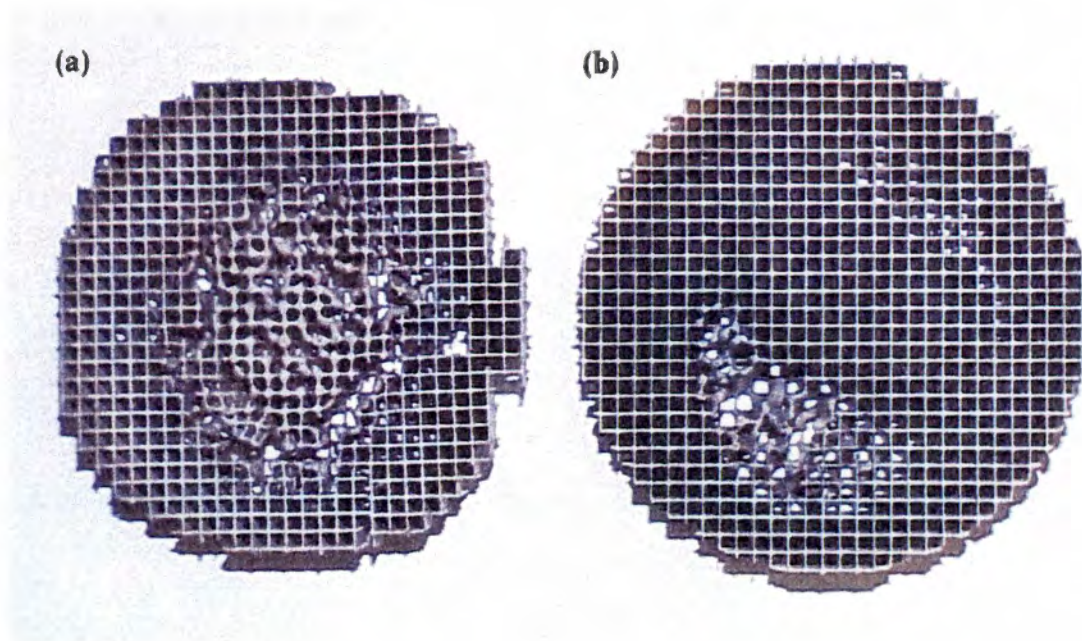
Figure 4.6: *Photograph demonstrating the thermal damage suffered by the ceramic flame-holder. Note the differences in the damage pattern resulting from poor mixing of the inlet streams.*

investigated.

4.1.4 Exhaust-gas analysis

The FID was used to analyze the composition of the exhaust gases over the range of operating conditions discussed above. **Figure 4.7** shows the UHC emission levels detected in the exhaust gases over a range of operating conditions. The relationship between UHC emission levels and equivalence ratio has a similar trend at different flow times but is shifted further lean as flow time increases. Looking at a single flow time, several trends are noted. There is a central range of equivalence ratios over which combustion is very efficient and the UHC emission levels are nearly undetectable. At higher and lower equivalence ratios, the UHC emission levels increase sharply as does the variability in the reading indicated
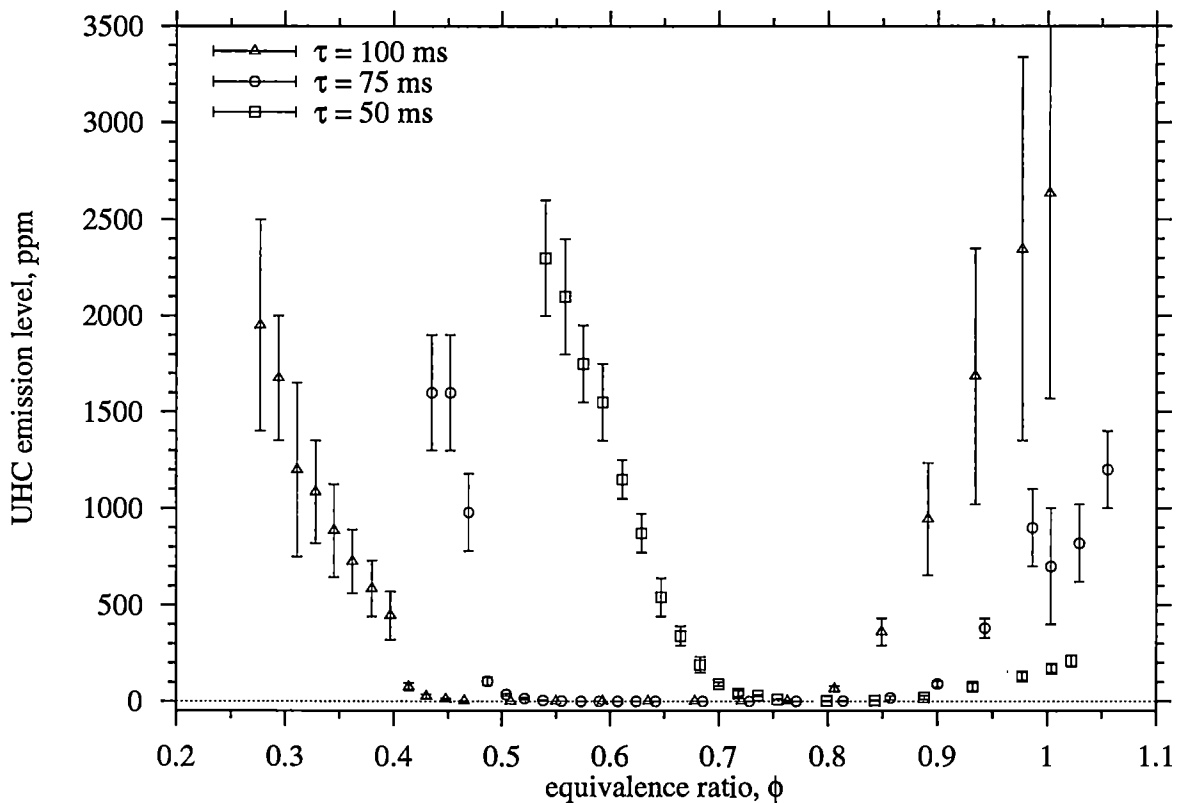
Figure 4.7: *UHC emission levels detected in the exhaust gases of the pulsed combustor over a range of operating conditions without control.*

by the size of the error bars.

Comparing **Figure 4.7** with the combustor-pressure time series (*e.g.,* **Figures 4.3** and **4.5**), it is seen that the lowest UHC emission levels occur at equivalence ratios where the combustor pressure is most stable with the least amount of cycle-to-cycle fluctuation in magnitude. As the equivalence ratio approaches the lean flammability limit, the UHC emission levels increase, as does the severity of the magnitude fluctuations. A similar, yet less-severe trend is seen as the equivalence ratio is brought toward stoichiometry. The correlation between increased cyclic variability and increased UHC emissions is quite intuitive. Obviously, large amounts of UHC will be released due to misfire near

the lean flammability limit as well as the cyclic variability in combustion quality at near-stoichiometric conditions.

4.2 Analysis of the combustion instabilities

If control is to be applied to dampen or eliminate the combustion instabilities, the nature and source of the combustion instabilities must first be determined. If, as is believed, the instabilities are nonlinear in nature, linear control techniques would be much less effective at achieving control of the system than would nonlinear control techniques. Knowledge of the mechanisms that are responsible for the development of the combustion instabilities would allow a control perturbation to be chosen which will have a direct effect upon the instabilities.

The instabilities have been shown to occur periodically with a frequency on the order of 10 Hz. The acoustic frequency of the pressure tap also being on the order of 10 Hz might indicate that the instabilities are the result of acoustic coupling with the pressure tap. However, were that the case, the instabilities should be present at all operating conditions instead of developing as the equivalence ratio of the mixture approaches the lean flammability limit. As discussed in detail in Section 4.4.2, acoustic coupling with the pressure tap can be ruled out as a possible source of the combustion instabilities by a simple experimental test.

Since the combustion instabilities develop as the equivalence ratio approaches the lean flammability limit, it is suspected that the source of the instabilities is the nonlinear relationship between reaction rate and equivalence ratio at lean conditions. Such nonlinear combustion instabilities have recently been shown to develop at lean conditions in a vari-

ety of combustion systems including internal combustion engines (Green *et al.* 1999; Daw *et al.* 1998; Wagner *et al.* 1998a; Wagner *et al.* 1998b; Daw *et al.* 1996).

The cycle-to-cycle variability in combustion quality and the development of the combustion instabilities observed in the combustor-pressure time series become more evident by applying techniques to filter out the acoustically driven oscillations such as plotting the peak-to-trough magnitude of the combustor pressure for each cycle as in **Figure 4.8**. At the most stable operating condition (**Figure 4.8(e)**), there is little cycle-to-cycle fluctuation in magnitude and no clear pattern is visible in the fluctuations. However, as the mixture is made increasingly lean (**Figures 4.8(f)–4.8(h)**), the cycle-to-cycle fluctuations in combustor-pressure magnitude become quite large and clearly occur in an increasingly periodic pattern with a frequency of roughly 10 Hz. This pattern is representative of the misfire-and-recovery pattern that is characteristic of the behavior of the pulsed combustor at very lean conditions. At near-stoichiometric and slightly lean operating conditions (**Figures 4.8(a)–4.8(d)**), the cycle-to-cycle fluctuations in magnitude are larger as well; however, there are no evident patterns to the fluctuations.

Time asymmetry has been shown to be an effective tool for detecting nonlinearity in system dynamics. Simply put, a system exhibits time asymmetry when it is possible to discern the direction of time. In other words, if the behavior of a system appears different in reverse than it does going forward, then the behavior is temporally asymmetric or irreversible. Time asymmetry is a property of nonlinear systems and its presence rules out linear or Gaussian-driven behavior (Finney 2000; Daw *et al.* 2000; Green *et al.* 1999; Timmer *et al.* 1999; Stam *et al.* 1998; Diks *et al.* 1995; Lawrance 1991; Cox 1981; Weiss 1975).

The presence of time asymmetry often can be detected by visual inspection of a time
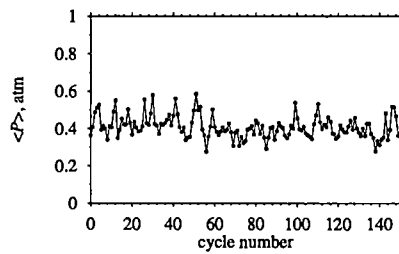
(a) $\phi = 1.066, \tau = 50$ ms
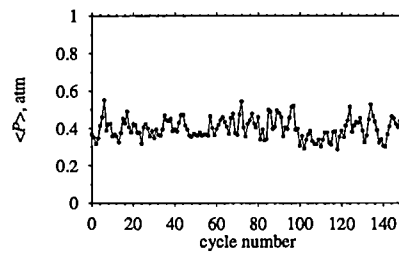
(b) $\phi = 1.004, \tau = 50$ ms
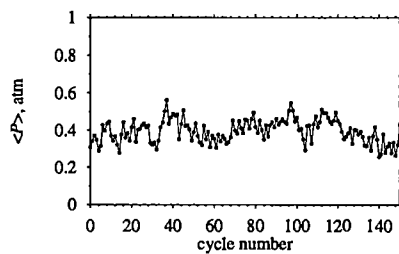
(c) $\phi = 0.888, \tau = 50$ ms
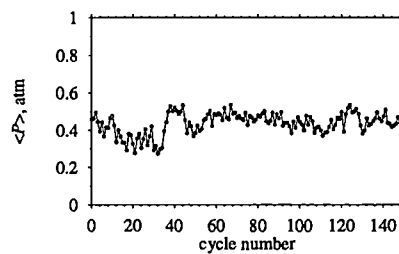
(d) $\phi = 0.736, \tau = 50$ ms
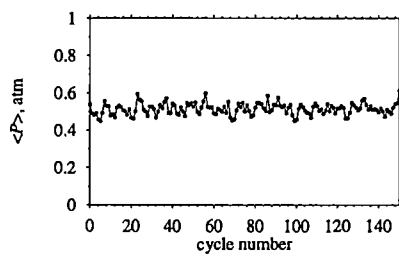
(e) $\phi = 0.665, \tau = 50$ ms
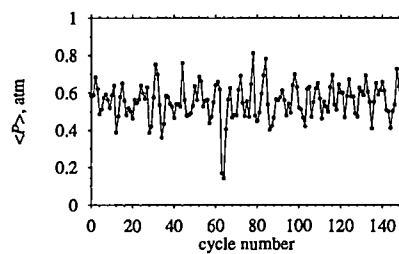
(f) $\phi = 0.629, \tau = 50$ ms
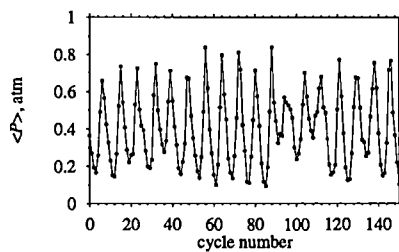
(g) $\phi = 0.593, \tau = 50$ ms
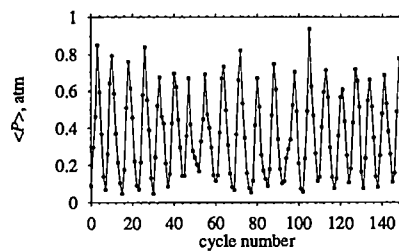
(h) $\phi = 0.558, \tau = 50$ ms

Figure 4.8: *Fluctuation in combustor-pressure cycle magnitude over a range of equivalence ratios at a flow time of* $\tau = 50$ ms.

series. **Figure 4.9** shows forward and backward time-series segments of the combustor pressure and the combustor-pressure cycle magnitude which demonstrate the characteristic misfire-and-recovery pattern seen at lean conditions. Examination of the combustor-pressure time series shows that the combustion instabilities do in fact appear to exhibit temporal asymmetry. The misfire-and-recovery pattern typically consists of a slow decay toward misfire followed by a rapid recovery. This asymmetry is also detectable in the cycle-magnitude traces. The combustion instabilities produce decidedly asymmetric magnitude traces typical of limit-cycle behavior rather than a symmetric pattern typical of sinusoidal behavior. The combustor-pressure magnitude traces show a bias toward shorter rise times during recovery (typically three or four successive uprising points) and longer fall times leading to misfire (typically four or five successive downsloping points). At higher equivalence ratios (see **Figure 4.8**), no such bias is immediately obvious, and the behavior appears much more random.

In order to get a more quantitative measure of the time irreversibility, the difference symbolization statistic, S_Δ, was used to evaluate the time asymmetry in the combustor-pressure magnitude over a range of equivalence ratios for a fixed flow time as shown in **Figure 4.10**. The data record is symbolized by assigning a value for each datum based upon the first difference: "-1" for decreasing slope, "0" for zero slope, "$+1$" for increasing slope. S_Δ is generated by summing the resulting symbol string. Temporally reversible data should have an equal number of data rises and falls; therefore, the null hypothesis is that $S_\Delta = 0$ for temporally reversible data records. To assign a statistical significance to the values of S_Δ for the original data record, temporally reversible surrogate data sets are constructed by randomly shuffling the original data record. For temporally reversible data records, shuffling should not affect the value of S_Δ, whereas the value of S_Δ for temporally
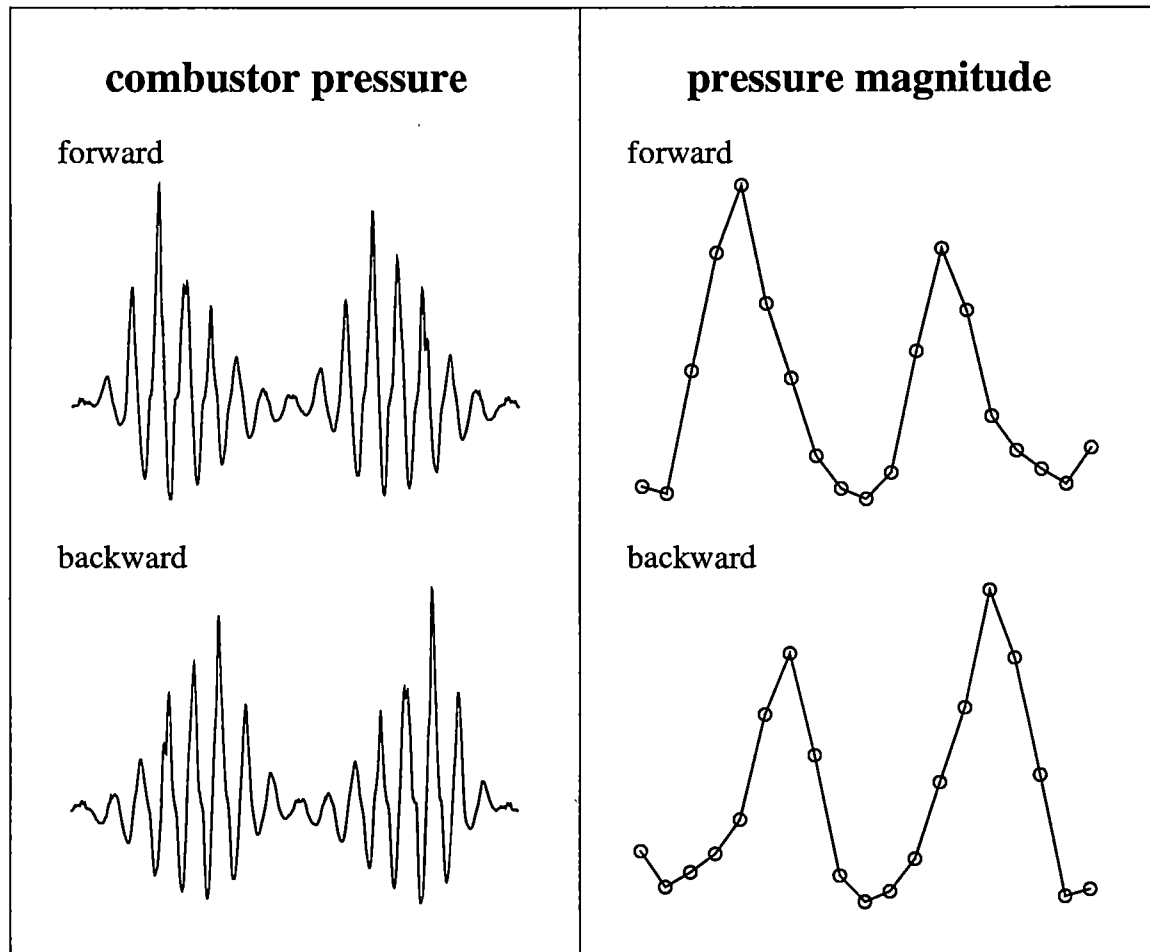
Figure 4.9: *Forward and backward time-series segments of the combustor pressure and the combustor-pressure cycle magnitude which demonstrate the temporally asymmetric and, therefore, nonlinear nature of the combustion instabilities.*
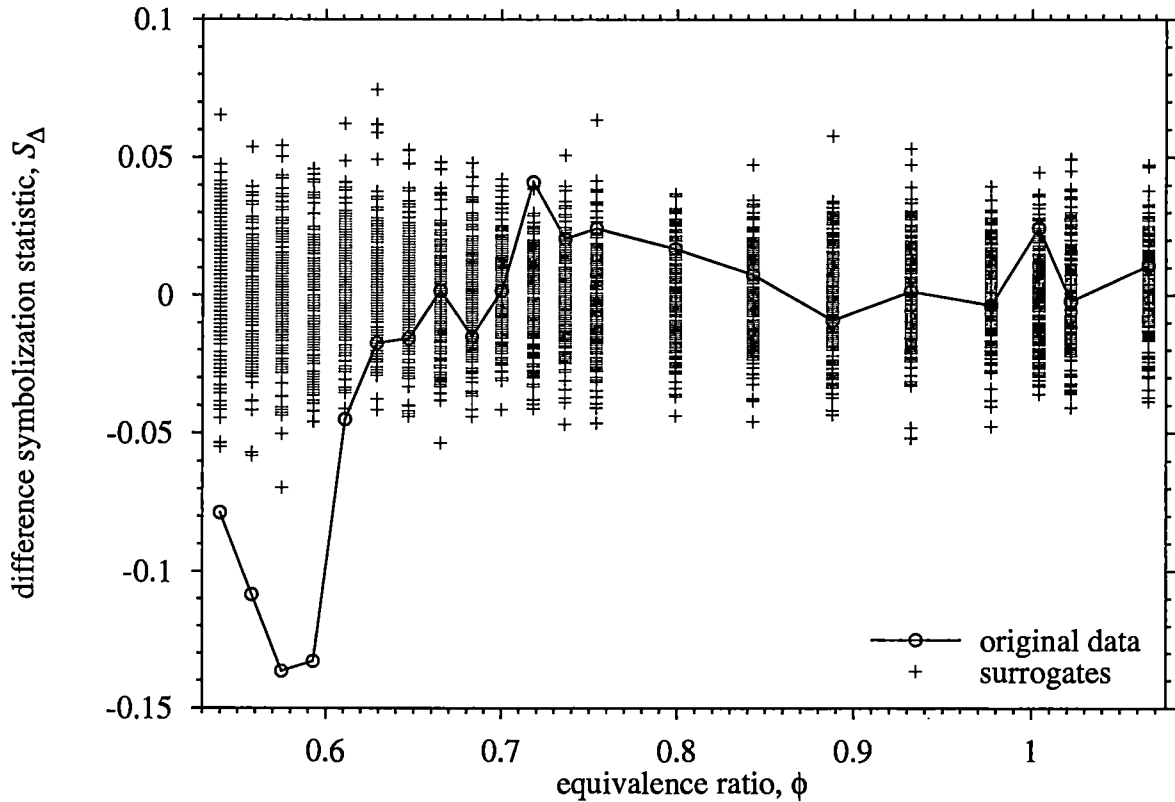
Figure 4.10: *Difference symbolization statistic, S_Δ, for combustor-pressure cycle magnitudes over a range of equivalence ratios at a flow time of $\tau = 50$ ms.*

irreversible data records should be significantly different than the value obtained for the surrogate data sets.

Figure 4.10 shows S_Δ for the original pressure-magnitude data and 200 surrogate data sets over a range of equivalence ratios for a flow time of $\tau = 50$ ms. At this flow rate, for equivalence ratios from $\phi = 1.066$ to $\phi = 0.629$, S_Δ for the original time series falls within the error bounds of the surrogates indicating time reversibility. At lower equivalence ratios where the combustion instabilities strongly affect the behavior of the combustor, S_Δ falls outside the error bounds of the surrogate data sets indicating statistically significant temporally irreversibility at these conditions. There appears to be a trend toward more

negative values of S_Δ as the mixture is made increasingly lean; however, it is not certain that this trend is statistically significant. While this test is not stringent enough to definitively detect the actual onset of the combustion instabilities, it is sufficient to show that the combustion instabilities do introduce significant temporal asymmetry indicating that they are nonlinear in nature (Finney 2000).

The nonlinear nature of the combustion instabilities can also be seen in the return maps shown in **Figure 4.11** which were generated by plotting the root-mean-square (RMS) of the combustor pressure summed over one cycle as a function of that for the previous cycle. The RMS combustor pressure for each cycle is related to the amount of heat released during that cycle; thus, any cyclic variations in the RMS combustor pressure can be directly related to cyclic variations in the combustion quality.

At this mass flow rate, for equivalence ratios ranging from $\phi = 1.066$ to $\phi = 0.665$ **(Figures 4.11(a)–4.11(e))**, the return maps show an elongated "shotgun-blast" pattern in which the data points are scattered randomly about a steady, mean value. In other words, at near-stoichiometric and moderately lean conditions, the combustion quality is approximately the same for all cycles, and the cyclic variability observed in the combustor-pressure traces are stochastic in nature. Thus, a change in the combustion quality for a given cycle appears to have no effect upon the subsequent cycle.

When the equivalence ratio is reduced from $\phi = 0.665$ to $\phi = 0.629$ **(Figures 4.11(e)** and **4.11(f))**, a very noticeable change is observed in the return map. As the equivalence ratio approaches the lean flammability limit, the return maps begin to show more structure, developing into an asymmetric "oyster-shell" pattern. At these conditions, the fluctuations in combustion quality are not random in nature but, instead, follow a clear, periodic trend. Whereas at near-stoichiometric and moderately lean conditions, each cycle was indepen-

(a) $\phi = 1.066, \tau = 50$ ms

(b) $\phi = 1.004, \tau = 50$ ms

(c) $\phi = 0.888, \tau = 50$ ms

(d) $\phi = 0.736, \tau = 50$ ms

(e) $\phi = 0.665, \tau = 50$ ms

(f) $\phi = 0.629, \tau = 50$ ms

(g) $\phi = 0.593, \tau = 50$ ms

(h) $\phi = 0.558, \tau = 50$ ms
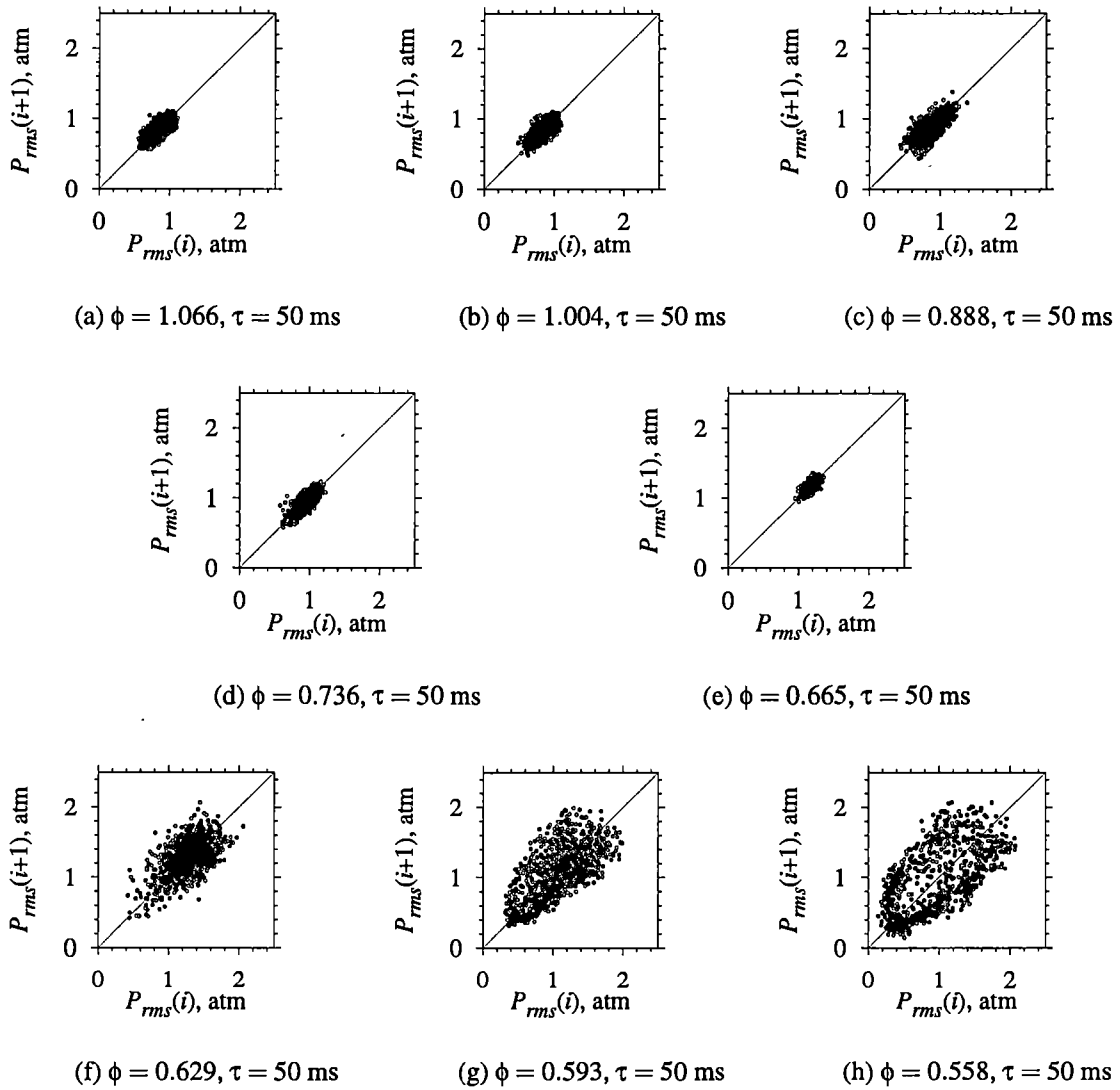
Figure 4.11: Return maps of P_{rms} over a range of equivalence ratios for a flow time of $\tau = 50$ ms.

dent from the others, at very lean conditions, information is being passed from one cycle to the next. The quality of the current combustion event directly affects not only the quality of combustion during the subsequent cycle, but the quality of combustion over several subsequent cycles, a sure indication of nonlinear behavior. This sudden change in the behavior of the system suggests that a bifurcation occurs in the system dynamics as the equivalence ratio is reduced.

4.3 Summary of combustor dynamics

The behavior of the pulsed combustor has proven to be very complex. The acoustically driven pressure oscillations are nonlinear in nature. Ideally, acoustic coupling is a linear process and should result in sinusoidal combustor-pressure oscillations. However, in the actual physical system, nonlinearities are introduced from numerous sources such as the combustion reaction, poor mixing of the inlet streams and turbulent mixing of the fresh charge with residual gases from the previous cycles. Therefore, it should not be surprising that the combustor-pressure oscillations are quite complex in nature. In addition to the fundamental nonlinearity of the combustor-pressure oscillations, a bifurcation in the system dynamics is observed to occur as the equivalence ratio of the mixture is reduced. The bifurcation introduces a second nonlinear oscillation which is superimposed upon the acoustic oscillations.

Figure 4.12 shows return maps which were created by plotting combustor-pressure measurements originally sampled at 5000 Hz against the third previous pressure measurement. At near-stoichiometric and moderately lean conditions (**Figures 4.12(a)** and **4.12(b)**), the combustor-pressure return maps follow a noisy stable limit cycle. The
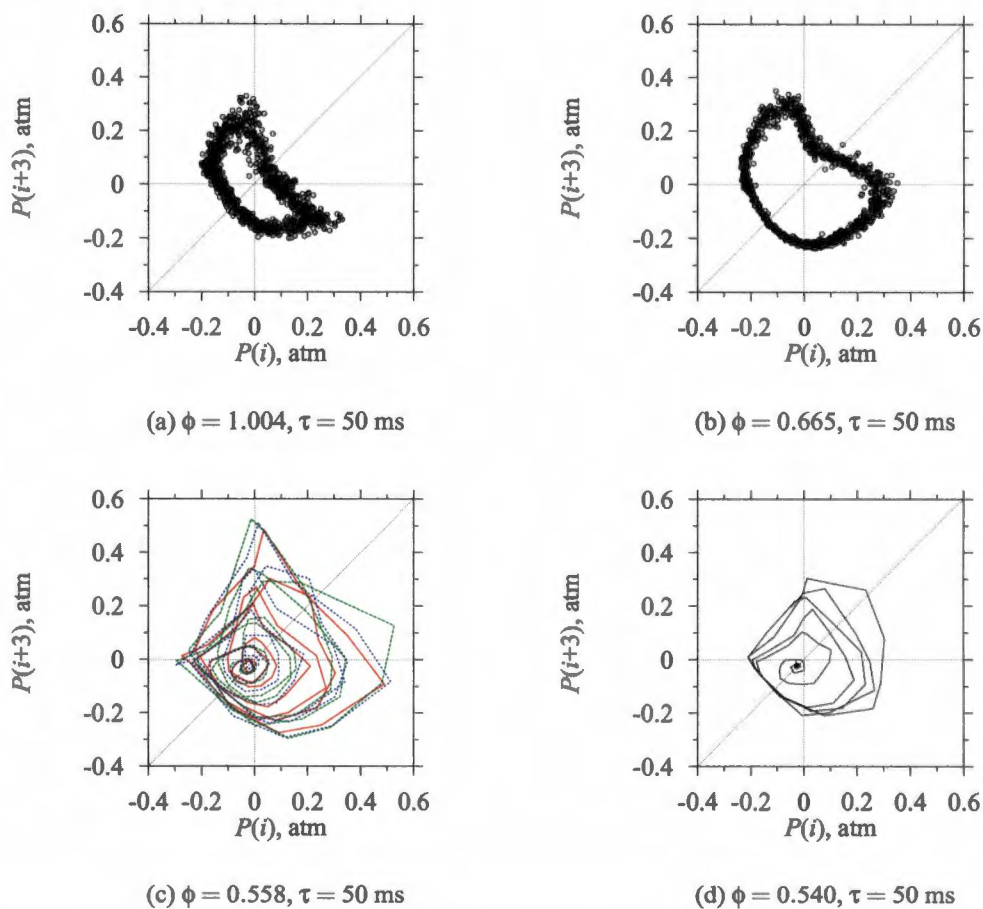
Figure 4.12: *Return maps constructed from the combustor-pressure time series over a range of equivalence ratios at a flow time of* $\tau = 50$ *ms.*

combustor-pressure oscillations follow a similar trajectory each cycle with only slight, random deviations. The cyclic variation in combustion quality at these conditions is believed to result from irregular mixing.

As the equivalence ratio approaches the lean flammability limit, the system undergoes a bifurcation. At these conditions, the return maps (**Figures 4.12(c)** and **4.12(d)**) clearly describe a different behavior than that seen at less-lean conditions. The combustor-pressure follows a trajectory that slowly spirals inward toward misfire before quickly spiraling back outward. **Figure 4.12(c)** shows the trajectories followed during three consecutive misfire-and-recovery events.

It is believed that the combustion instabilities result from nonlinearities inherent to the combustion reaction near the lean flammability limit. Strong combustion events are believed to consume the available fuel inventory. During the subsequent cycles, combustion quality is poor until a sufficient fuel inventory has been restocked. When the restocking of the fuel inventory becomes too slow, during the poor-quality combustion events, insufficient energy is released to maintain the combustor walls and the ceramic flameholder at a temperature which is sufficient to maintain the self-sustained combustion reaction. At this point, the pulsed combustor cannot recover from misfire and the system spirals inward toward flameout (**Figure 4.12(d)**). Similar behavior has been shown to occur in internal combustion engines (Green *et al.* 1999; Daw *et al.* 1998; Wagner *et al.* 1998a; Wagner *et al.* 1998b; Daw *et al.* 1996).

Near the bifurcation point, the system intermittently switches between the stable operating mode and the unstable mode characterized by repeated misfire and recovery. The system remains in the unstable mode until some disturbance pushes the system back across the bifurcation point. The system becomes entrained in the stable operating mode until an-

other disturbance pushes the system back to the unstable side of the bifurcation point. A modified version of the control strategy employed by In *et al.* (1997) should be able to detect when the trajectory of the combustor-pressure oscillations begin to deviate from the stable mode and spiral inwards toward misfire and then to apply an appropriate control perturbation to push the system back toward the stable mode. Once there, the nonlinear nature of the system should help entrain the system in the stable operating mode for an extended period of time before some disturbance eventually pushes the system back toward the unstable operating mode at which point another control action is required. Thus, control perturbations would only be required occasionally to push the system back toward stable operation when the mediating trajectories which lead to misfire are detected. Furthermore, from **Figure 4.8**, it appears that deviations from the stable operating mode can be detected by monitoring the magnitude of the combustor-pressure oscillations. All that remains is the selection of a proper control perturbation.

4.4 Various errata

There is some concern that operation of the spark plug and acoustic coupling with the pressure tap may affect the behavior of the pulsed combustor and/or the ability to measure the combustor pressure accurately. A series of tests were performed to determine what, if any, effect these factors might have.

4.4.1 Spark-plug effects

It is desirable to have the spark plug active during operation of the pulsed combustor for safety concerns and to assist in recovery from flameout. However, there was concern

that operation of the spark plug during data collection would result in electrical interference which could contaminate the low-voltage data signals from the piezoelectric pressure transducer, thermocouples and FID. The effect of spark-plug operation upon the dynamic behavior of the pulsed combustor was also of interest because of the possibility of using the spark plug to provide control perturbations. Therefore, a series of experiments were performed to determine the effects of firing the spark plug during operation of the pulsed combustor.

Figure 4.13 shows sample results of a PSD analysis conducted to determine if spark-plug operation affects the power spectrum of the combustor-pressure time series. At both operating conditions shown, the PSD is very similar with the spark plug on and off. There are no significant changes in the frequencies or amplitudes of the peaks in the power spectrum. There are no significant power differences at a frequency of 60 Hz which would indicate electrical interference in the pressure signal. Also, at very lean conditions, the power of the low-frequency peak in the neighborhood of 10 Hz, which corresponds to the combustion instabilities, shows no change when the spark plug is operated continuously, indicating that even continuous firing of the spark plug cannot prevent misfire and would therefore be a poor choice for applying control perturbations.

4.4.2 Pressure-tap effects

The combustion instabilities show a strong periodicity at a frequency on the order of 10 Hz, which happens to coincide with the acoustic frequency of the pressure tap. A series of experimental tests were conducted using two pressure-tap lengths, 15 cm (6 in) and 8.5 m (28 ft), with acoustic frequencies of approximately 85 Hz and 10 Hz, respectively, to determine if the combustion instabilities were the result of acoustic coupling

(a) $\phi = 0.691, \tau = 50$ ms   (b) $\phi = 0.663, \tau = 50$ ms
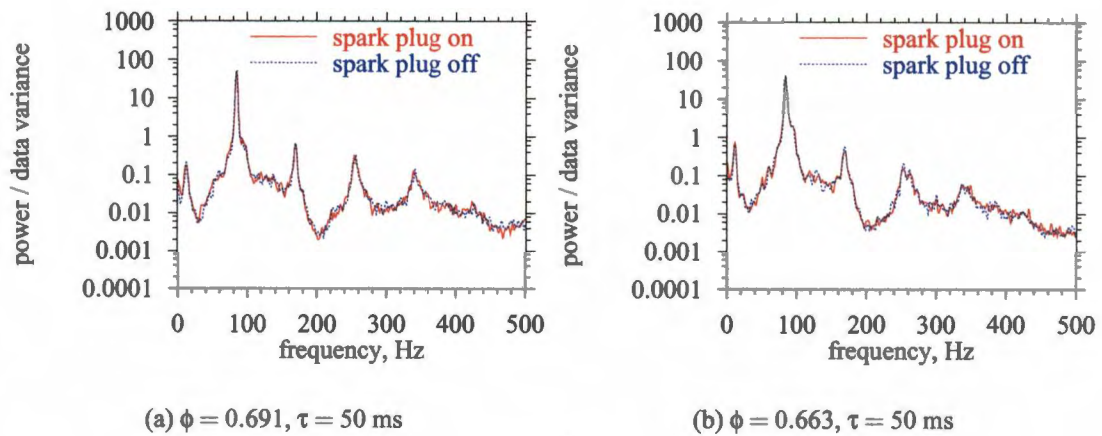
Figure 4.13: *PSD plots of the combustor pressure showing the effect of spark-plug activation.*

between the combustion chamber and the pressure tap.

In addition to the possibility of acoustic coupling promoting the combustion instabilities, due to the low natural frequency of the pressure tap, it is possible that the pressure tap acting as a highly damped, second-order system could severely inhibit accurate measurement of the 100-Hz combustor-pressure oscillations. To address this issue, Richards *et al.* (1991) compared measurements of the combustor-pressure oscillations in the METC thermal pulse combustor recorded by a pressure transducer mounted at the end of a 60-cm-long pressure tap to the measurements recorded by a second pressure transducer installed flush with the combustion-chamber wall. No differences in the shape of the waveforms were found; however, the amplitude of the oscillations as measured through the pressure tap were typically 10% less than the amplitude as measured by the flush-mounted transducer.

Figures 4.14 and **4.15** compare combustor-pressure time series collected at two oper-
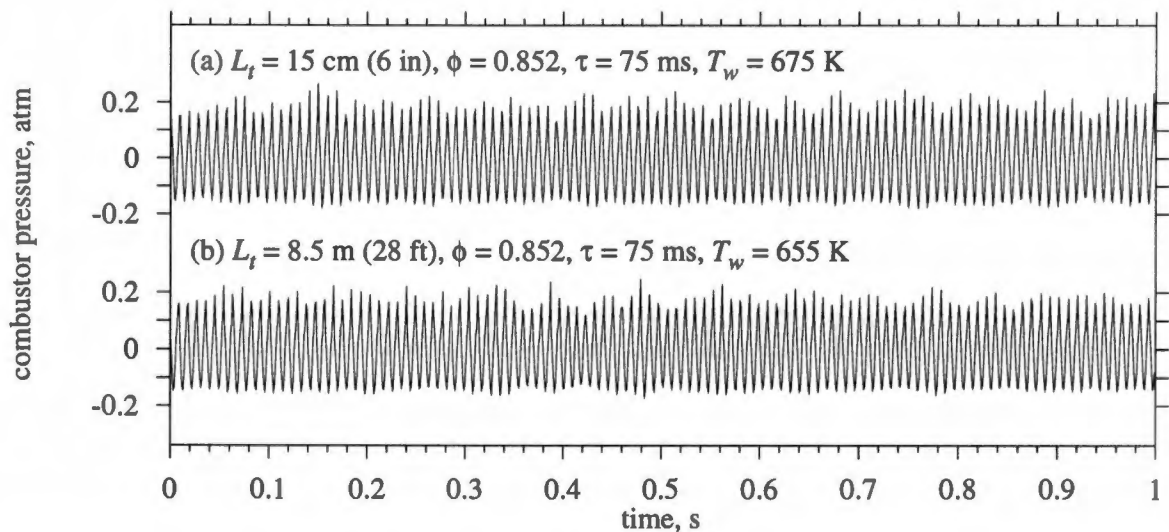
Figure 4.14: *Combustor-pressure time-series segments showing the effects of pressure-tap length. The signals depict oscillations about the time-averaged mean combustor pressure and were collected at an equivalence ratio of $\phi = 0.852$ and a flow time of $\tau = 75$ ms.*
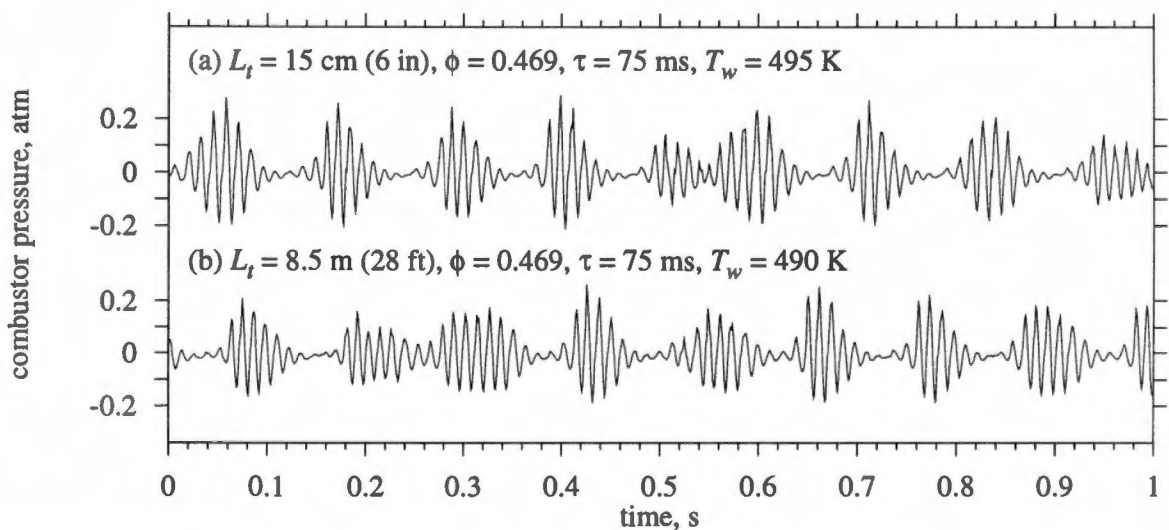
Figure 4.15: *Combustor-pressure time-series segments showing the effects of pressure-tap length. The signals depict oscillations about the time-averaged mean combustor pressure and were collected at an equivalence ratio of $\phi = 0.469$ and a flow time of $\tau = 75$ ms.*

ating conditions with different pressure-tap lengths. No obvious differences in behavior
can be detected at either operating condition. In particular, note that near the lean flamma-
bility limit **(Figure 4.15)**, the low-frequency combustion instabilities occur with similar
frequency for both pressure-tap lengths, despite the large difference in acoustic frequency.
Also, the combustor-pressure oscillations are of similar amplitude for both pressure-tap
lengths indicating that the extra damping volume does not further damp the amplitude of
the combustor-pressure oscillations.

The combustor-pressure data records collected using the two different pressure-tap
lengths have nearly identical power spectrums as shown in **Figure 4.16**. In particular,
near the lean flammability limit, **(Figure 4.16(b))**, there are no significant differences in
either the power or frequency of the low-frequency peak which corresponds to the com-
bustion instabilities. Again, this suggests that the combustion instabilities do not result
from acoustic coupling with the pressure tap.

(a) $\phi = 0.852, \tau = 75$ ms   (b) $\phi = 0.469, \tau = 75$ ms
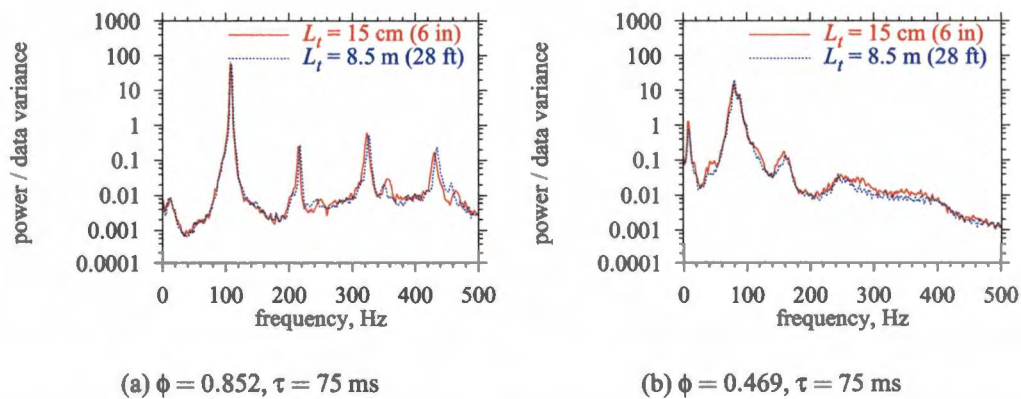
Figure 4.16: *PSD plots of the combustor pressure showing the effect of pressure-tap length.*

Chapter 5

Analytical model of the combustion instabilities

5.1 Model basics

If control is to be applied to dampen or eliminate the combustion instabilities, it would be desirable to know the source of the instabilities so that an appropriate control perturbation could be chosen which will have a significant effect upon the behavior of the system. The instabilities have been shown to be nonlinear in nature and to develop due to a bifurcation in system dynamics which occurs as the equivalence ratio approaches the lean flammability limit. It is believed that the nonlinear reaction mechanism is the source of the instabilities, and an analytical model has been developed to test this theory. The acoustically driven oscillations have been eliminated from the model so that the development of the low-frequency combustion instabilities may be detected more easily.

The model assumes that well-mixed reactants are introduced to the pulsed combustor at a constant mass flow rate through a single inlet. Combustion is described by an

Arrhenius rate law that is first-order with respect to fuel concentration. Tailpipe dynamics are not modeled, and exhaust gases are assumed to exit at a steady rate. Kinetic- and potential-energy effects are assumed to be negligible. For simplicity, the mixture inside the combustion chamber is assumed to behave as an ideal gas with properties equal to those of air. All properties are assumed to be uniform throughout the combustion chamber. The density of the mixture is assumed to remain constant. The mass fraction of oxidizer, air, is assumed to be much greater than that of fuel — especially at lean conditions — and, therefore, is assumed to remain constant for simplicity.

5.2 Model derivation

The analytical model is based upon conservation equations for mass, fuel, oxidizer and energy applied to the combustion chamber. With the given assumptions, the conservation of momentum yields no further useful information and therefore is not considered. Upon simplification, the governing equations yield a pair of coupled, nonlinear ODEs. A stability analysis is performed to determine the critical operating conditions where the combustor dynamics undergo changes.

5.2.1 Governing equations

Conservation of mass

The general form of the conservation-of-mass equation is given by

$$\frac{Dm}{Dt} = \sum \dot{m}_{in} - \sum \dot{m}_{out}.$$

(5.1)

The model assumes that the reactants are premixed and enter at a constant mass flow rate through a single inlet and that the exhaust gases leave through a single exit. The density of the mixture inside the combustor is assumed to remain constant and uniform. While at first this seems to be an erroneous assumption, it must be remembered that the acoustically driven oscillations have been removed from the model leaving a steady-flow case with relatively small fluctuations in pressure. The high percentage of excess air at lean conditions limits the difference in density between the fresh charge and the exhaust gases. Applying these simplifications and incorporating the definition of the characteristic flow time yields

$$\dot{m}_i = \dot{m}_e = \frac{V_c \, \rho_{SSL}}{\tau}. \tag{5.2}$$

Conservation of species: fuel

The general form of the conservation-of-mass equation written for fuel is given by

$$\frac{Dm_f}{Dt} = \sum \dot{m}_{f,in} - \sum \dot{m}_{f,out}. \tag{5.3}$$

Fuel enters through a single inlet and is partially consumed by the combustion reaction; unburned fuel exits with the exhaust gases. In addition to assuming the density of the mixture in the combustion chamber to be constant and uniform, the concentration of fuel is assumed to be uniform throughout the combustion chamber. These simplifications yield an ODE for the mass fraction of fuel in the combustion chamber,

$$V_c \, \rho \, \frac{dY_f}{dt} = Y_{f,i} \, \dot{m}_i - Y_f \, \dot{m}_e - \dot{m}_R \tag{5.4}$$

where $Y_{f,i}$ is the mass fraction of fuel present in the fresh charge as given by

$$Y_{f,i} = \frac{\phi}{\phi + AF_{stoich}} \tag{5.5}$$

and $\dot{m}_R$ is the rate of fuel consumption by the reaction as given by an Arrhenius rate law,

$$\dot{m}_R = A' V_c \rho^{N+1} Y_f Y_o^N e^{-E_A/R_u T}. \tag{5.6}$$

Substituting for the mass flow rates using Equations 5.2 and 5.6 yields

$$\frac{1}{Y_{f,i}} \frac{dY_f}{dt} = \frac{1}{\tau SG}\left(1 - \frac{Y_f}{Y_{f,i}}\right) - A' \rho^N Y_o^N \frac{Y_f}{Y_{f,i}} e^{-E_A/R_u T} \tag{5.7}$$

where SG is the specific gravity of the mixture inside the combustion chamber.

Conservation of species: oxidizer

The purpose of the model study is to analyze the onset of the combustion instabilities at very lean conditions where the large percentage of excess air insures that $Y_o \gg Y_f$; thus, Y_o can be treated as being essentially constant. The large air-to-fuel ratio for an air-propane mixture at stoichiometric conditions (15.64:1) insures that this assumption holds relatively well even at stoichiometry. Therefore, it is assumed that

$$Y_{o,i} \approx Y_{o,e} \equiv Y_o = \frac{AF_{stoich}}{\phi + AF_{stoich}}. \tag{5.8}$$

Conservation of energy

The general form of the first law of thermodynamics is given by

$$\frac{DE}{Dt} = \sum \dot{E}_{in} - \sum \dot{E}_{out}. \tag{5.9}$$

Energy is generated by the combustion reaction and transported by the incoming and outgoing streams and heat loss to the surroundings. The mixture in the combustion chamber is assumed to be at thermal equilibrium at all times. Neglecting changes in kinetic and potential energy and assuming density is constant and uniform, the first law becomes

$$V_c \rho \frac{de}{dt} = \dot{m}_i h_i - \dot{m}_e h_e + V_c q''' - \dot{Q}. \tag{5.10}$$

Substituting for the mass flow rates using Equation 5.2 and evaluating the generation and heat-loss terms yields

$$V_c \, \rho \, \frac{de}{dt} = \frac{V_c \, \rho_{SSL}}{\tau} (h_i - h_e) + A' \, \Delta H_R \, V_c \, \rho^{N+1} \, Y_f \, Y_o^N \, e^{-E_A/R_u T} - U \, A_s \, (T - T_\infty).$$

(5.11)

Assuming ideal-gas behavior allows the internal energy and enthalpy to be evaluated in terms of temperature. Further simplifications (such as setting $T_i = T_\infty$) yield an ODE for the temperature of the mixture in the combustion chamber,

$$\frac{dT}{dt} = \underbrace{\left(\frac{k}{\tau \, SG} + \frac{U \, A_s}{V_c \, \rho \, C_v} \right) (T_\infty - T)}_{\text{transport}} + \underbrace{A' \, \frac{\Delta H_R}{C_v} \, \rho^N \, Y_f \, Y_o^N \, e^{-E_A/R_u T}}_{\text{generation}}.$$

(5.12)

5.2.2 Non-dimensionalization

The governing equations were non-dimensionalized using the following definitions:

$$\lambda \equiv \frac{Y_f}{Y_{f,i}},$$

(5.13)

$$\theta \equiv \frac{T}{T_\infty},$$

(5.14)

and

$$\xi \equiv \frac{t}{\tau}.$$

(5.15)

The resulting ODEs for the conservation of fuel and energy are given by

$$\frac{d\lambda}{d\xi} = \frac{1}{SG} (1 - \lambda) - \frac{1}{SG} \tau_A \, \lambda \, e^{-\theta_A/\theta}$$

(5.16)

and

$$\frac{d\theta}{d\xi} = \tau_T \, (1 - \theta) + \tau_C \, \lambda \, e^{-\theta_A/\theta}$$

(5.17)

where θ_A is the non-dimensionalized activation temperature as given by

$$\theta_A = E_A/R_u T_\infty. \tag{5.18}$$

The behavior of the system is controlled by three characteristic time scales: two kinetic time scales,

$$\tau_A = SG A' \rho^N Y_o^N \tau \tag{5.19}$$

and

$$\tau_C = A' \frac{\Delta H_R}{C_v T_\infty} \rho^N Y_o^N Y_{f,i} \tau; \tag{5.20}$$

and a time scale describing the transport rate of energy by heat and mass transfer,

$$\tau_T = \left(\frac{k}{SG} + \frac{U A_s}{V_c \rho C_v} \tau \right). \tag{5.21}$$

5.2.3   Nullclines

In order to perform a stability analysis, it is necessary to solve for the nullclines of the two ODEs (Equations 5.16 and 5.17). Setting $\frac{d\lambda}{d\varsigma} = 1$ yields

$$\lambda = \frac{1}{1 + \tau_A e^{-\theta_A/\theta}} \tag{5.22}$$

and setting $\frac{d\theta}{d\varsigma} = 0$ yields

$$\lambda = \frac{\tau_T(\theta - 1)}{\tau_C e^{-\theta_A/\theta}}. \tag{5.23}$$

5.3 Model predictions

The necessary model parameters were estimated to match the experimental system as closely as possible and then varied to determine if oscillatory behavior would develop under realistic conditions. The final values chosen for the parameters are shown in **Table 5.1**.

Figures 5.1 and **5.2** show the species and energy nullclines and the solutions for the two ODEs over a range of equivalence ratios at a flow time of $\tau = 50$ ms and with other parameters as set in **Table 5.1** — note that the shape of the species nullcline is relatively unaffected by changes in equivalence ratio, thus only one solution is shown. At these conditions, the system undergoes a supercritical Hopf bifurcation as the equivalence ratio is reduced (Strogatz 1994). At near-stoichiometric conditions (**Figures 5.2(a)–5.2(b)**), the system exhibits a damped oscillation leading to a constant steady-state solution. As the equivalence ratio is reduced, the system reaches a bifurcation point after which the steady-state solution is oscillatory (**Figure 5.2(c)**). After the bifurcation, further reductions in equivalence ratio result in lower-amplitude and lower-frequency oscillations (**Figures 5.2(d)–5.2(e)**). Eventually, there is not enough fuel to sustain combustion and the system flames out (**Figure 5.2(f)**).

As shown in **Figures 5.3** and **5.4**, similar results may be obtained by increasing the heat transfer coefficient while maintaining an equivalence ratio of $\phi = 0.50$ and a flow time of $\tau = 50$ ms with all other parameters as given in **Table 5.1**. In this case, increasing the heat transfer coefficient reduces the combustor-wall temperature leading to the development of the instabilities. Eventually, combustion cannot be sustained and flameout occurs. The dependence of the behavior upon the heat transfer rate corresponds well to experimental results.

Table 5.1: *Final values used for the parameters in the analytical model.*

combustor volume	$V_c = 295$ cc
constant-volume specific heat	$C_v = 0.7175$ kJ/kg-K
specific-heat ratio	$k = 1.4$
specific gravity	$SG = 1$
ambient/supply temperature	$T_\infty = 295$ K
enthalpy of reaction	$\Delta H_R = 46{,}357$ kJ/kg
pre-exponential term in Arrhenius rate law	$A' = 1.3 \times 10^{14}$ kg^{N+1}/m^{3N}
order of the rate law in terms of oxidizer concentration	$N = 1.65$
non-dimensional activation temperature	$\theta_A = 26$
overall heat transfer coefficient	$U = 500$ kW/m^2-K
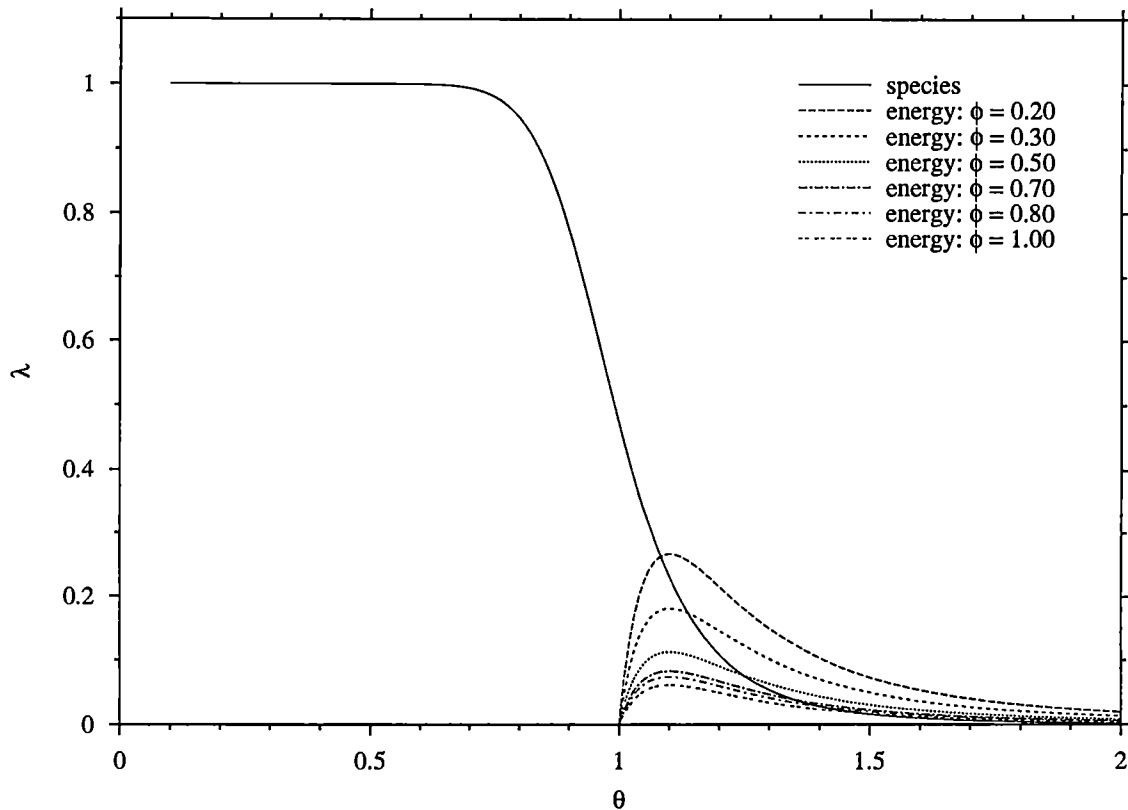
Figure 5.1: *Species and energy nullclines predicted by the analytical model over a range of equivalence ratios.*
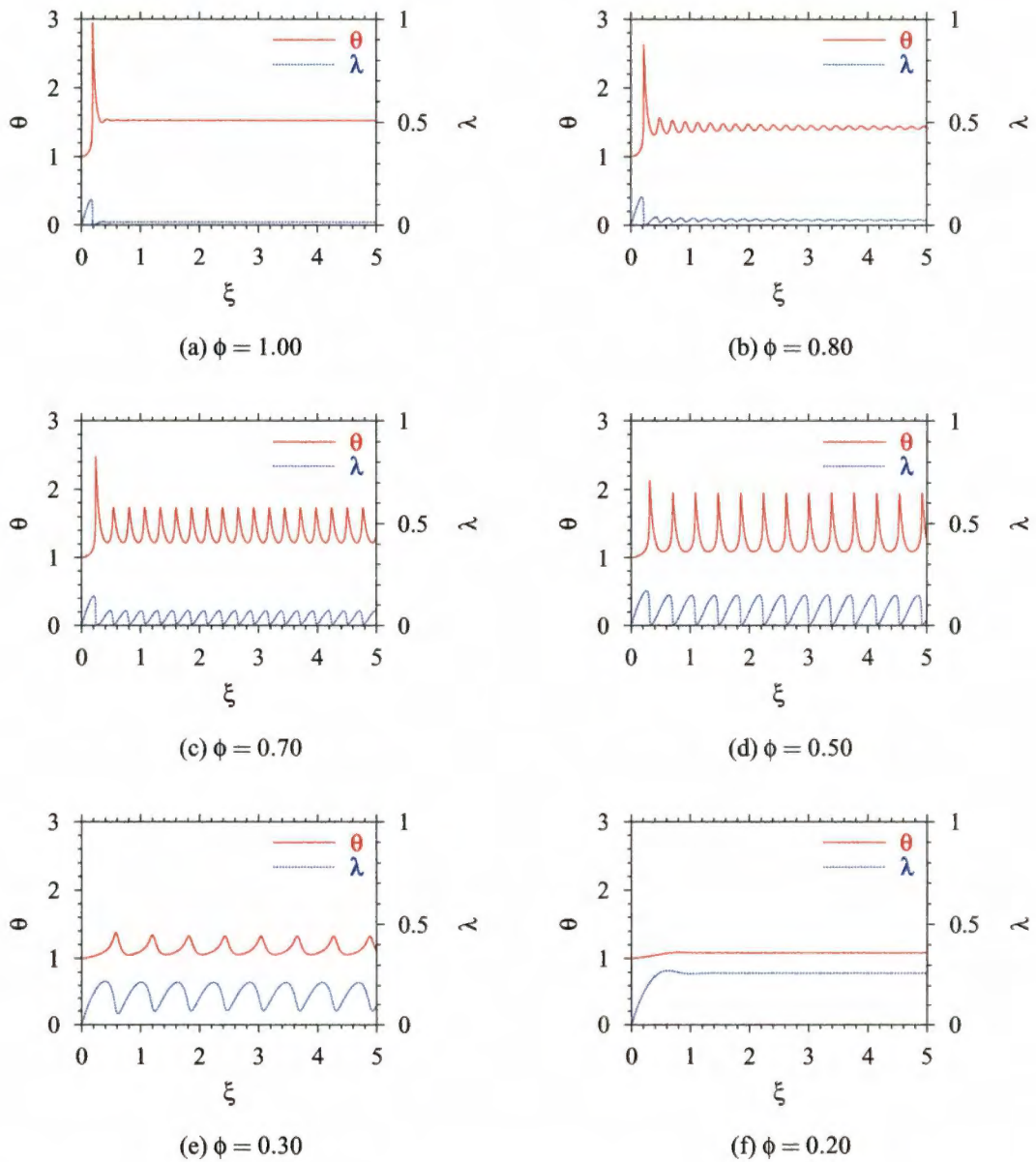
Figure 5.2: Non-dimensional temperature and mass fraction of fuel predicted by the analytical model over a range of equivalence ratios.
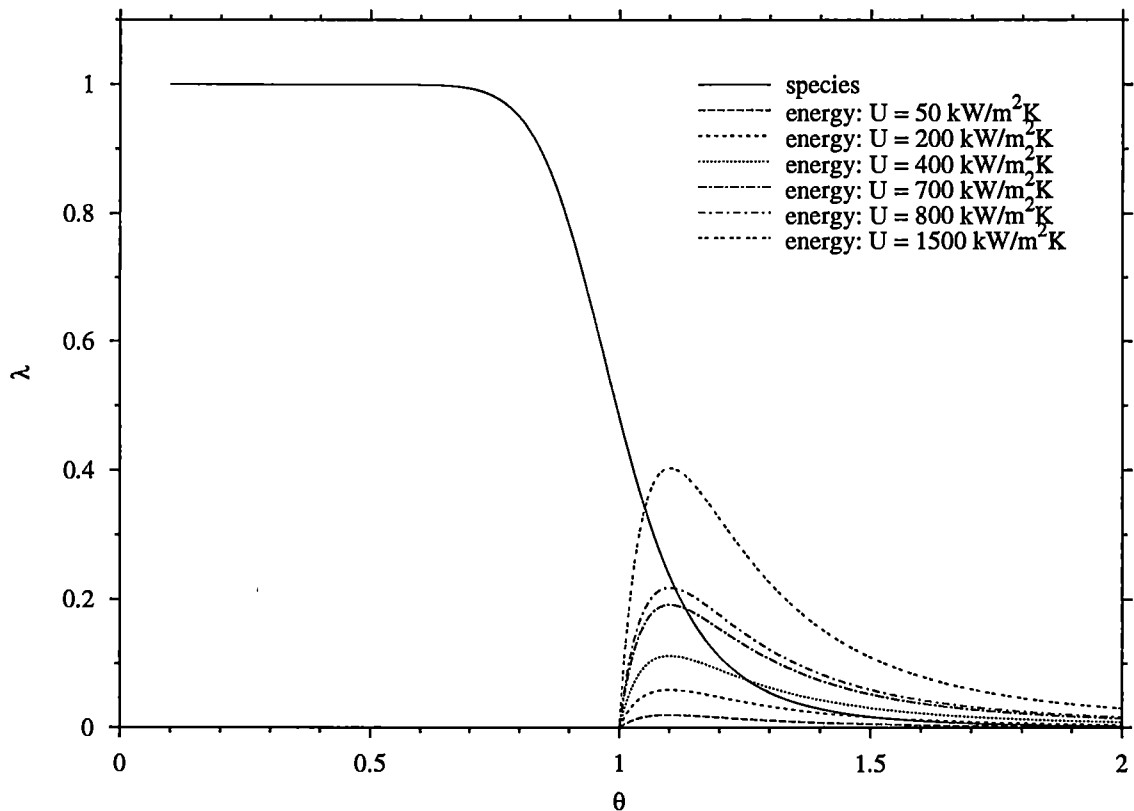
Figure 5.3: *Species and energy nullclines predicted by the analytical model for a range of heat transfer rates.*

5.4 Implications to the physical system

The analytical model suggests that, at certain conditions, a low-frequency oscillatory be-havior can develop in the pulsed combustor by processes other than acoustic coupling. The nonlinear Arrhenius rate law used to describe the combustion process can result in the development of combustion instabilities at lean conditions. The instabilities take the form of low-frequency oscillations resulting from the consumption and restocking of fuel. The nonlinear nature of the instabilities concurs with the observations in Section 4.2. While the conditions at which this occurs have not been shown to match those of the experimental
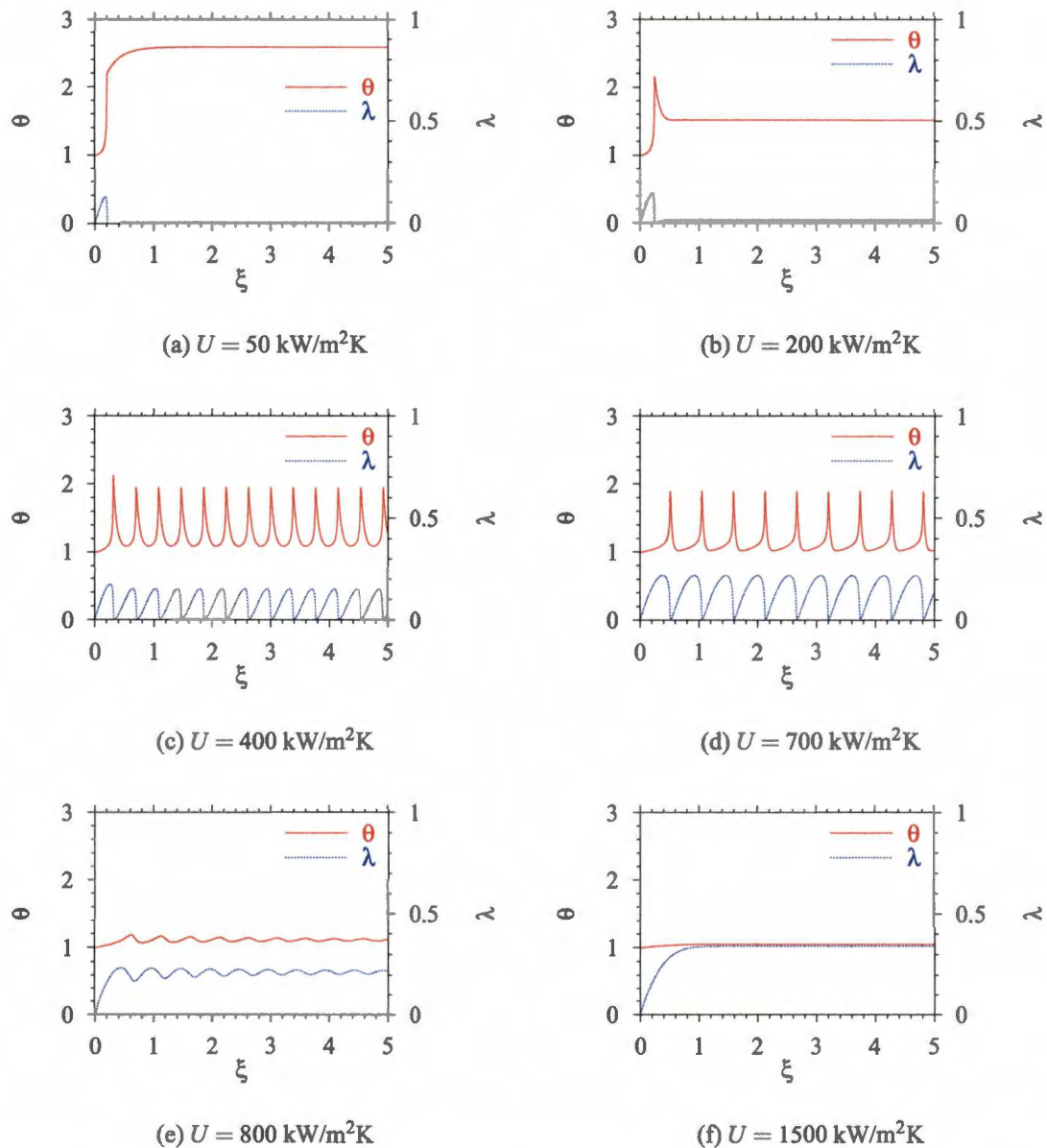
Figure 5.4: Non-dimensional temperature and mass fraction of fuel predicted by the analytical model for a range of heat transfer rates.

system, it is felt that the basic processes involved are correct.

Knowing that the low-frequency combustion instabilities are due to the nonlinearity of the combustion reaction as opposed to some acoustic modulation in the tailpipe has serious implications for control. Choosing a control perturbation which modifies the flow inside the tailpipe would not provide the most efficient means of controlling the behavior of the pulsed combustor. Instead, a control perturbation should be chosen which will directly affect the combustion reaction, such as injections of supplemental fuel to hasten the restocking process.

Chapter 6

Application of control

6.1 Control concepts

The nonlinear nature of the pulsed combustor means that traditional linear control algorithms would be less effective and less efficient than nonlinear control strategies. The combustion instabilities have been shown to result from a bifurcation in system dynamics as the equivalence ratio approaches the lean flammability limit. Near the bifurcation point, the system intermittently alternates between the stable operating mode, in which the combustion quality is similar for each cycle, and the unstable mode, in which the system alternates between good and poor quality combustion events due to the repeated consumption and restocking of the fuel inventory. Due to the nonlinear nature of the system, when a small disturbance pushes the pulsed combustor toward one of these modes of operation, it becomes entrained in that mode until another small disturbance causes the system to deviate back toward the other mode.

A modification of the control strategy employed by In *et al.* (1997) should be effective in controlling the pulsed combustor. The combustion instabilities produce a very charac-

teristic pattern in the combustor-pressure time series which allows the occurrence of the instabilities to be easily detected by monitoring the magnitude of the pressure oscillations or the peak pressure during each cycle. When a deviation toward the unstable mode is detected, a appropriately applied control action should push the system back toward the stable mode. Once there, due to the nonlinear nature of the system, the combustor should become entrained in the stable operating mode for some period of time before eventually deviating back toward the unstable mode, at which point another action would be required. In this manner, control actions are only applied when the system is observed to deviate from the stable mode.

The misfires and poor quality combustion events associated with the combustion instabilities are due to the rapid consumption and slow restocking of the fuel inventory. The most effective control perturbation would seem to be one which hastens the restocking of the fuel inventory. For this reason, supplemental fuel injections were chosen as the control perturbation in this study. A low-flow piezoelectric valve (Maxtex, model MV-112) capable of cycling at up to 250 Hz was chosen to introduce the perturbations to the pulsed combustor (see Section 3.1.4).

6.2   Occasional trajectory correction control algorithm

Figure 6.1 shows a graphical representation of the occasional trajectory correction control algorithm developed for this study. The controller monitors the combustor pressure looking for the peak pressure value for each cycle. The average cycle maximum is tallied from the peak values. A trigger level is specified by the operator as some percentage of this average cycle maximum. A control action is initiated when the peak pressure for a
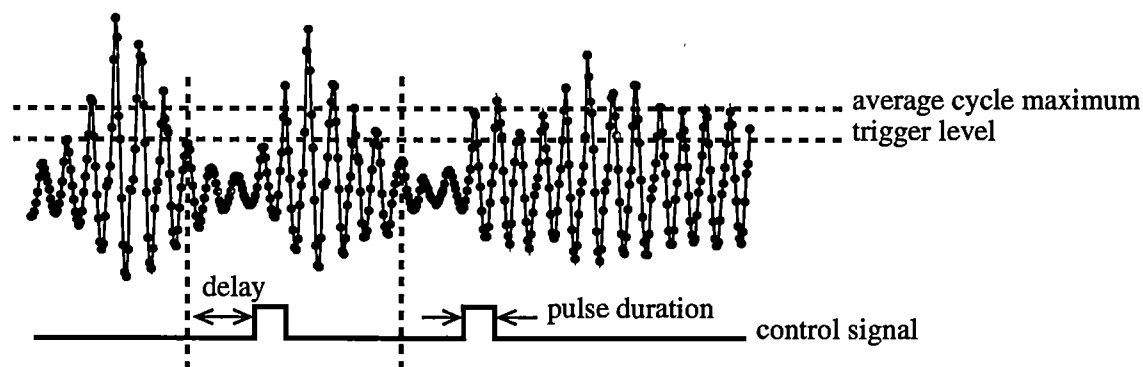
Figure 6.1: *Graphical depiction of the control algorithm. Control actions are initiated when the peak combustor pressure for a cycle falls below the trigger level.*

cycle falls below the trigger level. After a operator-specified triggering delay, a control perturbation is initiated. The control signal is sent to open the piezoelectric valve allowing a small amount of supplemental fuel to enter the mixing chamber. The amount of supplemental fuel injected with each perturbation is controlled by the pulse duration, the voltage applied to the piezoelectric valve and the supply pressure of the supplemental fuel — all variables which are selected by the operator.

In this study, the control variables were chosen by the operator through trial-and-error. The trigger level is used to determine when the system is deviating from the stable mode of operation. If the trigger level is set too high, control actions can be triggered by the stochastic variation in the magnitude of the pressure oscillations in the stable mode. However, setting the trigger level too low increases the time needed to detect the deviations from the stable mode. A trigger level of 50% of the average cycle maximum was found to provide a sufficient balance between these two concerns.

Enough fuel must be injected with each pulse to drive the system toward the desired behavior, but injecting too much is wasteful. The magnitude of the control perturbation is the most complicated variable to control as it depends upon three separate settings. The piezoelectric valve opens proportionally to the amount of voltage applied with 100 V required to fully open the valve. In this study, a 80-V power supply was used to power the valve; thus, the valve is 80% open during control perturbations. Since a pressure drop in excess of 138 kPa (20 psi) across the valve is required to insure flow, a supply pressure of 193 kPa_g (28 psig) was used throughout this study. Therefore, in this study, the magnitude of the perturbation is solely controlled by varying the pulse duration. The mass of supplemental fuel injected with each pulse is determined by the pulse duration and the throughput of the valve which, with the aforementioned settings, is approximately 121 kg/s (55 lbm/s).

The amount of supplemental fuel which must be injected to achieve control can be substantial and can significantly change the equivalence ratio of the mixture. The time-averaged mass flow rate of supplemental fuel is used to determine the effective equivalence ratio, $\bar{\phi}$, which would exist were an equivalent amount of fuel introduced at a steady rate via the primary fuel supply.

The delay between the triggering of the controller and the actual implementation of the control perturbation is one of the most crucial variables. In addition to the triggering delay set in the controller, there is an additional injection delay due to the time required for the piezoelectric valve to open and for the fuel to flow through the opened valve into the mixing chamber.

Figure 6.2 demonstrates the effect of the triggering delay upon the effectiveness of control at a particular operating condition ($\phi = 0.611$, $\tau = 50$ ms); other operating conditions
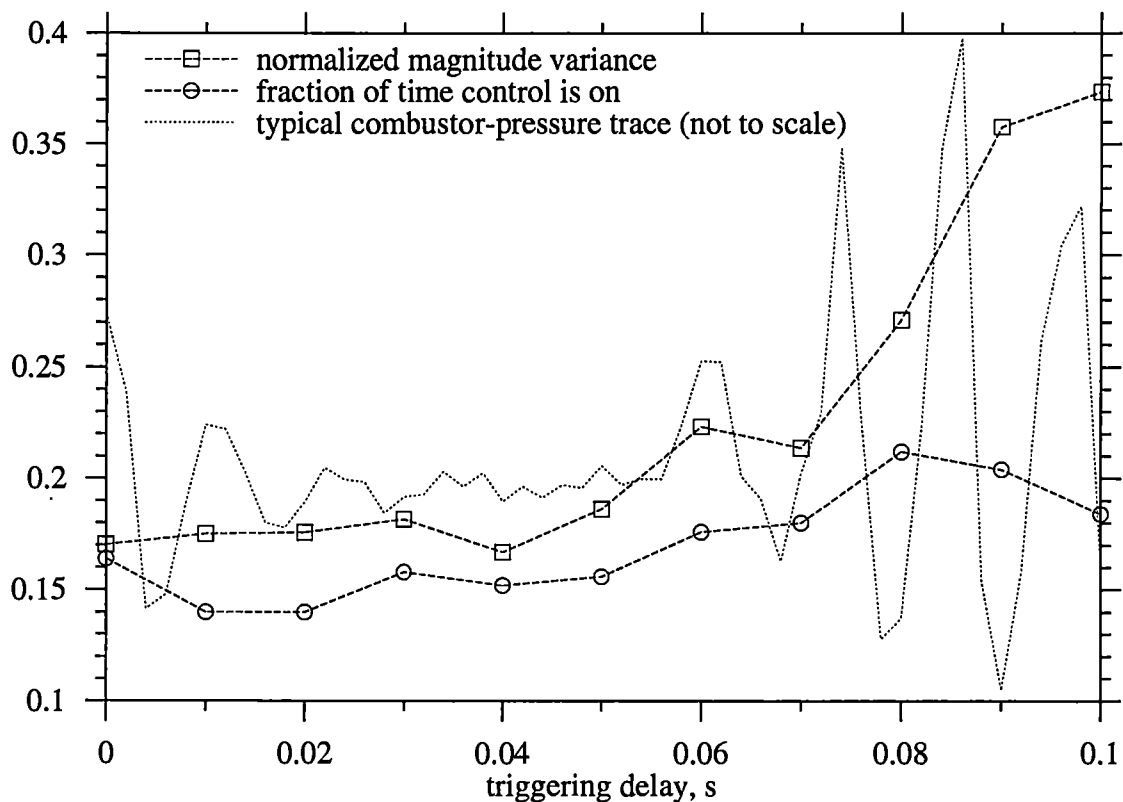
Figure 6.2: *The effect of varying triggering delay upon the effectiveness of control as quantified by the fraction of time control actions are required and the variance in the magnitude of the controlled combustor-pressure oscillations normalized with respect to the uncontrolled case. The combustor-pressure trace is included to aid in visualization of when the control action is initiated relative to a typical misfire-and-recovery event. Operating conditions: $\phi = 0.611, \tau = 50$ ms.*

exhibit roughly similar trends. The delay between the trigger and the initiation of the control action was varied from 0 to 0.1 s in 10 ms increments. The range covered corresponds to the approximate period of the combustion instabilities. Typical combustor-pressure data are included in the background to help visualize the point at which the control action is initiated. For these purposes, the effectiveness of control is quantified by the variance in the magnitude of the controlled combustor-pressure oscillations and the average fraction of time that control is active (*i.e.,* the percentage of time that the valve is open) once the

system has stabilized. The variance in cycle magnitude shown in **Figure 6.2** has been normalized with respect to the variance in cycle magnitude without control.

For short delays, control reduces the variance in the magnitude of the combustor-pressure oscillations by approximately 83%. Varying the triggering delay over the first half of the misfire-and-recovery event seems to have little effect upon the variance. There does appear to be a significant minimum at 0.04 s after which the variance begins to increase dramatically with increased triggering delay. When the initiation of control is delayed for the full extent of the misfire-and-recovery event, control is only capable of reducing the magnitude variation by approximately 62%. This reduction in the effectiveness of control for long triggering delays is believed to be due to the inability to predict the behavior of nonlinear systems far into the future.

In this example, the minimum number of control actions is required for triggering delays ranging from 0.01 to 0.02 ms with control being active approximately 14% of the time. As with the magnitude variance, varying the triggering delay over the first half of the misfire-and-recovery event seems to have little effect. Control actions are required more frequently when they are initiated during recovery with control being active approximately 21% of the time. As the triggering delay approaches the period of the misfire-and-recovery event, the fraction of time that control actions are required decreases, approaching the value required when control is initiated without delay.

The effects of triggering delay upon control effectiveness observed for this particular operating condition are roughly similar for other conditions. At most operating conditions, control appears most effective and requires the fewest perturbations when the control action is initiated during misfire when the pressure oscillations are at their weakest (*i.e.,* the triggering delay is in the range of 0.03-0.04 s). Without knowing the length of the injection

delay, it is impossible to be certain as to how control is modifying the combustor dynamics; however, it is speculated that the control perturbation enters the combustor while the fuel concentration is low, hastening the restocking process and subsequent recovery.

6.3 Effectiveness of control

The control scheme has proven to be effective in reducing the cyclic variability in the combustor-pressure magnitude caused by the combustion instabilities and lowering UHC emission levels. **Figure 6.3(a)** shows time-series segments of the combustor pressure and control signal collected while the pulsed combustor operates at an equivalence ratio of $\phi = 0.427$ and a flow time of $\tau = 75$ ms. At this operating condition, the pulsed combustor experiences frequent and severe misfire and will eventually flame out unless control is applied. The controller is turned on at time $t = 0$ with a trigger level of 50% of the average cycle maximum, a triggering delay of 42 ms and a pulse duration of 33 ms. The controller enters a brief learning period to determine the average cycle maximum before any control actions can be applied. The uncontrolled behavior is apparent in the time series in **Figure 6.3(a)** during the learning period (from $t = 0$ to $t = 1.2$ s).

The first control action is initiated at $t \approx 1.2$ s, momentarily driving the system into an erratic, low-amplitude behavior from which the combustor quickly recovers. Initially, control actions are frequent resulting in an effective equivalence ratio of $\bar{\phi} \approx 0.61$. Within 4 s, combustor performance is already improving, as evidenced by the slightly longer periods of stable operation without misfire. As the combustor becomes entrained in a more stable operating mode, the wall temperature increases, thereby further stabilizing the behavior. Control actions are required less frequently and within 90 s are only occasionally

(a) $\bar{\phi} \approx 0.45$ ($\phi = 0.427$), $\tau = 75$ ms, $T_w = 520$ K, ~ 80 ppm UHC

(b) $\phi = 0.45$, $\tau = 75$ ms, $T_w = 450$ K, ~ 1600 ppm UHC
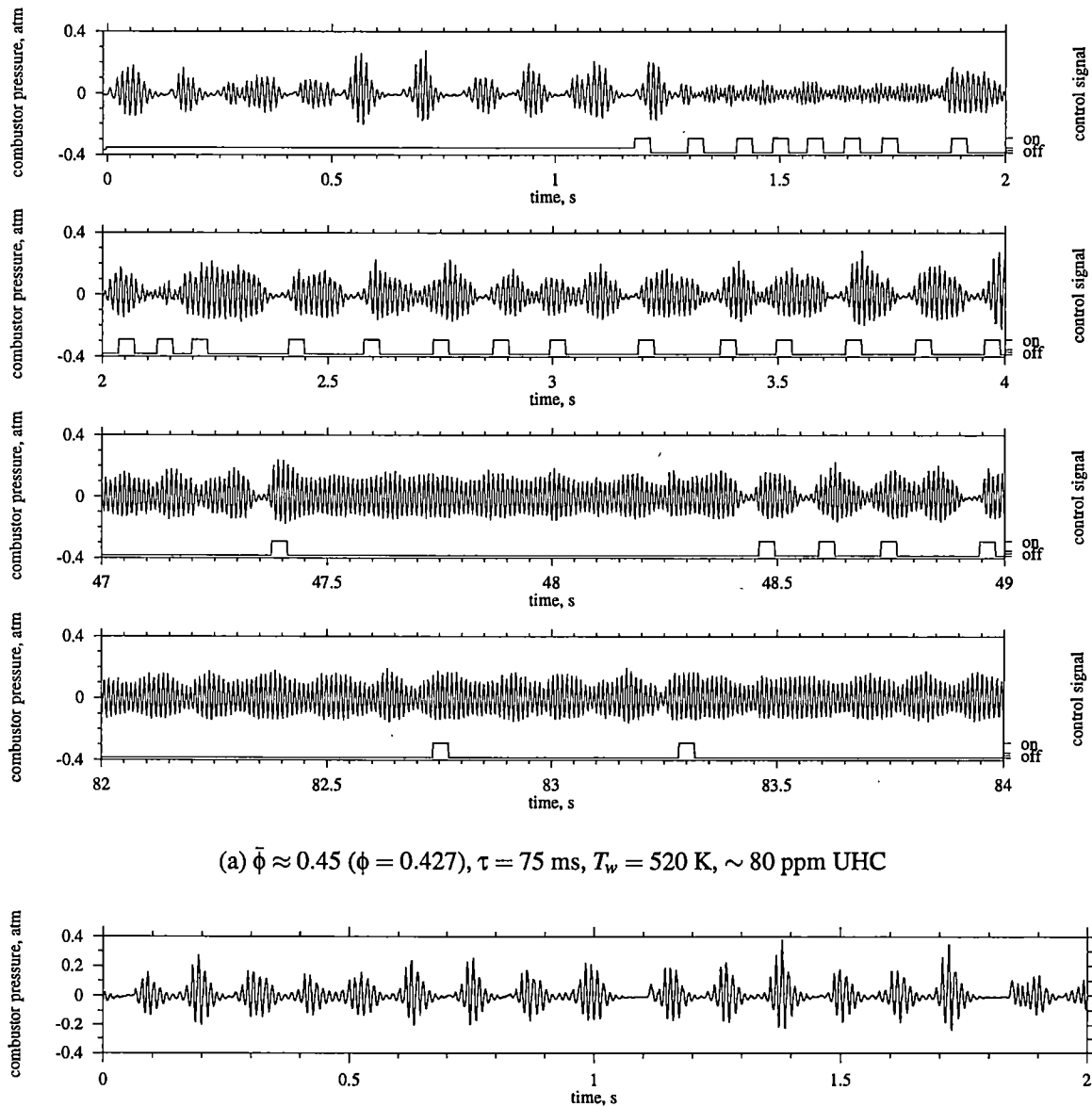
Figure 6.3: *Time-series segments of combustor pressure showing the application of control and the effect of injecting an equivalent amount of fuel via the primary-fuel supply. Control variables used in this example: trigger level = 50%; delay = 42 ms; pulse duration = 33 ms.*

necessary to keep the system entrained in the stable operating mode indefinitely. At this point, the injections of supplemental fuel result in an effective equivalence ratio of $\bar{\phi} \approx$ 0.45. There are still low-frequency fluctuations in the magnitude of the combustor pressure due to the combustion instabilities, but the magnitude of the fluctuations have been greatly reduced and misfire has been all but eliminated.

It is important to note that the behavior of the pulsed combustor is much more efficient with control than if the mass flow rate of primary fuel were increased to yield a similar equivalence ratio. **Figure 6.3(b)** shows a combustor-pressure time-series segment collected at an equivalence ratio of $\phi = 0.450$. The enhanced combustion quality with control is readily evident. At $\phi = 0.450$, the behavior of the combustor is not noticeably different than the uncontrolled behavior at an equivalence ratio of $\phi = 0.427$, and flameout still occurs. With control, the UHC emission levels are greatly reduced from 1600 ppm at $\phi = 0.450$ to approximately 80 ppm with $\bar{\phi} \approx 0.45$.

When control is terminated, the system remains entrained in the stable operating mode briefly as seen in **Figure 6.4**. At this operating condition, the combustor returns to characteristic misfire-and-recovery behavior within 4 s after control is turned off and will usually flame out within a few minutes.

Figure 6.5 demonstrates the effectiveness of the control algorithm in reducing the severity of the fluctuations in combustor-pressure magnitude at various equivalence ratios. At $\phi = 0.665$ **(Figure 6.5(a))**, the fluctuations in magnitude are greatly reduced with control; however, the system is occasionally pushed into a low-amplitude oscillation, suggesting that further optimization of the control variables is needed. After control is terminated, the system remains entrained in the stable operating mode for some time before slowly diverging. Similar results are obtained at $\phi = 0.629$ **(Figure 6.5(b))**. The reduction
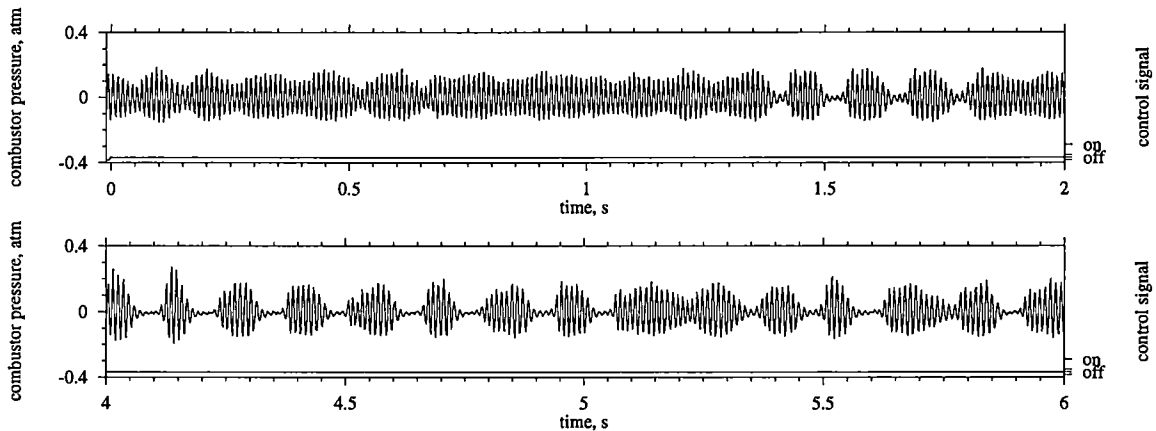
Figure 6.4: *Time-series segments of combustor pressure showing the deactivation of control at time $t = 0$ and the resultant degradation of system behavior.*

in magnitude fluctuation is slightly less, but the system is less frequently driven toward the low-amplitude oscillation. In both cases, the amount of supplemental fuel required once the system has stabilized only increases the effective equivalence ratio by approximately 1–2%. At lower equivalence ratios (**Figures 6.5(c)** and **6.5(d)**), control is less effective. Even though flameout is prevented, magnitude fluctuation is only slightly reduced, and misfires occur rather often. Furthermore, the amount of supplemental fuel injected increases the effective equivalence ratio by approximately 5–7%. Still, the behavior with control is often more efficient than if the same amount of fuel were added via the primary fuel supply. Furthermore, without control, the pulsed combustor would flame out at these conditions. This is evident in **Figures 6.5(c)** and **6.5(d)** in which the combustor quickly flames out once control is deactivated as indicated by the last few data points in those data records which fall upon the x-axis indicating that the combustor-pressure oscillation have zero amplitude (*i.e.,* , combustion is not occurring).

Table 6.1 demonstrates the effectiveness of the controller in reducing UHC emission

(a) $\phi = 0.665$, $\tau = 50$ ms

(b) $\phi = 0.629$, $\tau = 50$ ms
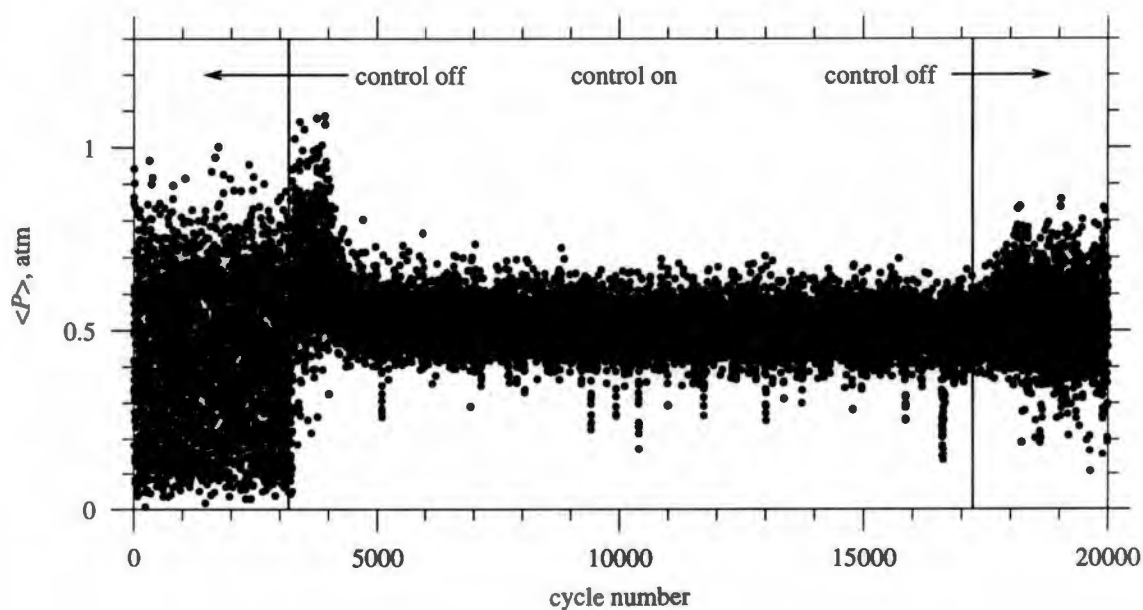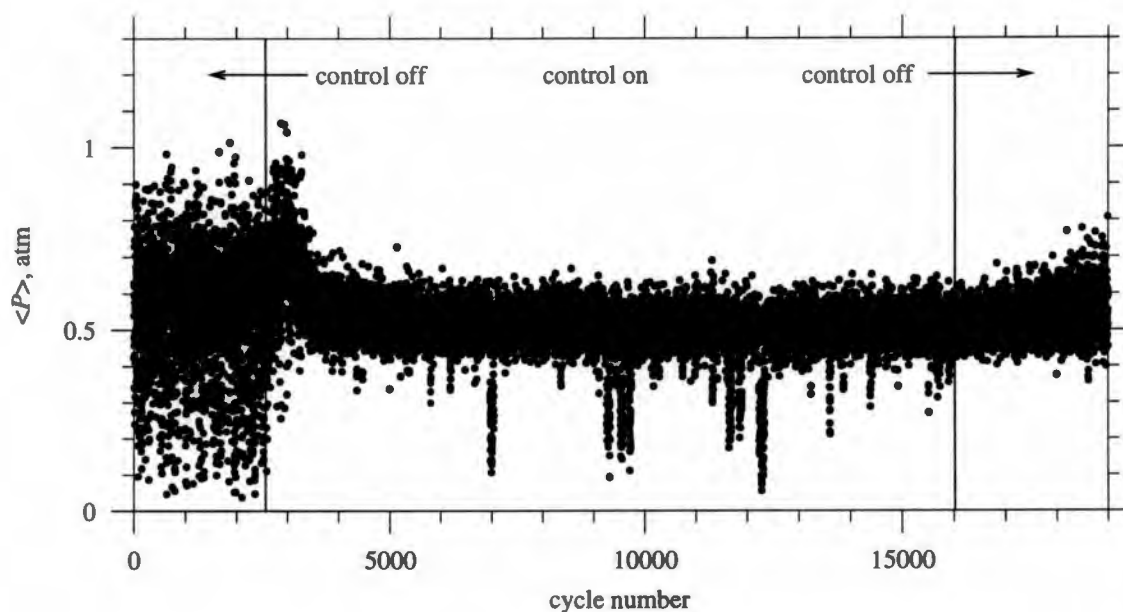
Figure 6.5: *Combustor-pressure cycle-magnitude traces showing the effectiveness of control. Control variables used in these examples: trigger level = 50%; delay = 42 ms; pulse duration = 33 ms.*

(c) $\phi = 0.593$, $\tau = 50$ ms

(d) $\phi = 0.558$, $\tau = 50$ ms
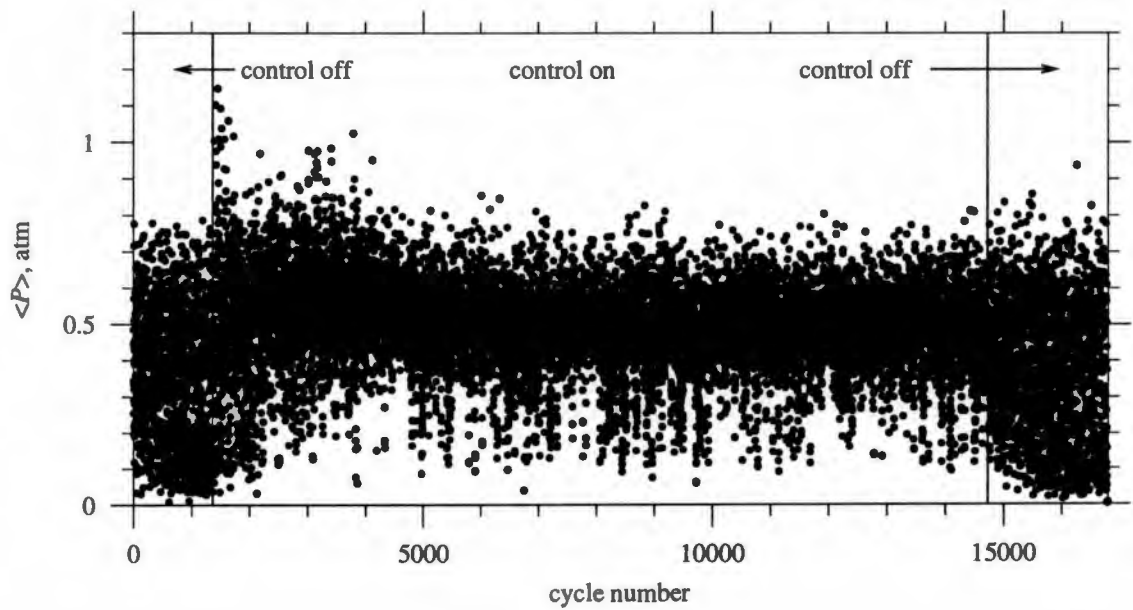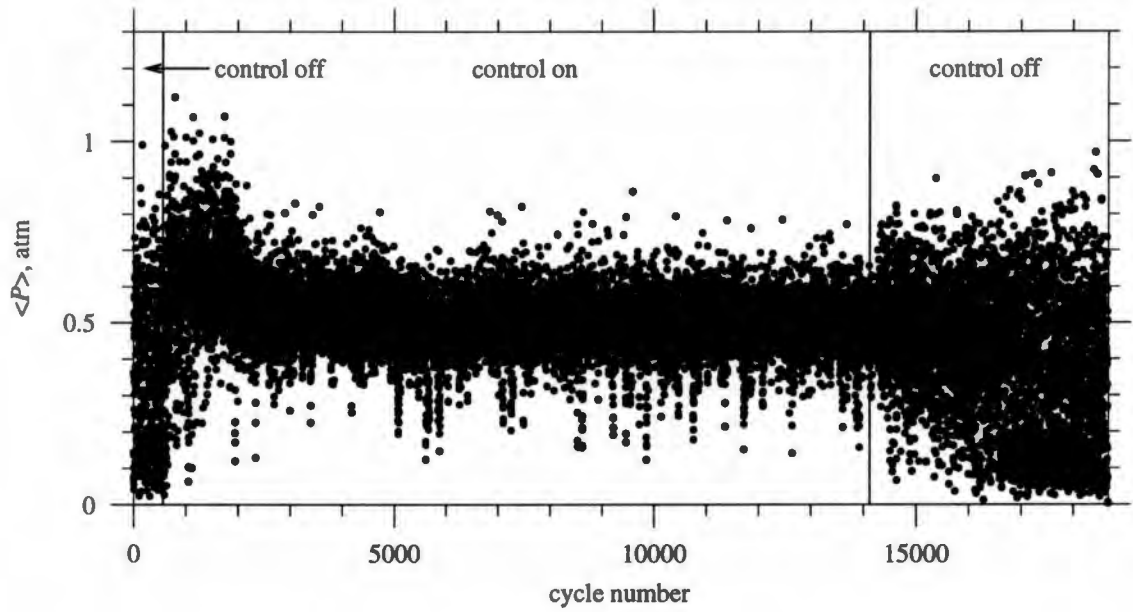
Figure 6.5: *(continued) Combustor-pressure cycle-magnitude traces showing the effectiveness of control. Control variables used in these examples: trigger level = 50%; delay = 42 ms; pulse duration = 33 ms.*

Table 6.1: UHC emission levels with and without control.

(a) $\tau = 50$ ms			
ϕ	UHC emission levels without control (ppm)	$\bar{\phi}$	UHC emission levels with control (ppm)
0.665	340±50	0.687	100±20
0.647	540±100	0.669	100±20
0.629	870±100	0.663	125±10
0.611	1150±100	0.656	130±10
0.593	1550±200	0.672	130±20
0.575	1750±200	0.688	160±30
0.558	2100±300	0.670	190±40
0.540	2300±300	0.653	220±50
0.522	—	0.635	400±150

(b) $\tau = 75$ ms			
ϕ	UHC emission levels without control (ppm)	$\bar{\phi}$	UHC emission levels with control (ppm)
0.487	105±20	0.487	60±20
0.469	980±200	0.469	60±10
0.452	1600±300	0.452	160±30
0.435	1600±300	0.450	125±25
0.418	—	0.435	250±200
0.400	—	0.430	500±200
0.382	—	0.425	700±100
0.366	—	0.410	850±100

levels at lean conditions. For a flow time of $\tau = 50$ ms, it is clear that the controller significantly reduces the UHC emission levels. For example, at an equivalence ratio of $\phi = 0.647$, the UHC emission levels are reduced from 540 ± 100 ppm without control to 100 ± 20 ppm with control while the effective equivalence ratio is only raised to $\bar{\phi} = 0.669$. Comparing this value to the UHC emission levels for the uncontrolled case for $\phi = 0.665$, it is clear that the controller provides a greater reduction in UHC emission levels than would be achieved were the same amount of fuel introduced at a steady rate through the primary fuel supply.

As the equivalence ratio is reduced further, even greater reductions in UHC levels are seen. For example, at an equivalence ratio of $\phi = 0.540$, UHC emission levels are reduced by a factor of ten with control. At this condition, control actions are required more frequently which greatly increases the effective equivalence ratio (to $\bar{\phi} = 0.653$ in this example); however, the reduction in UHC emission levels is still about twice that which would be achieved by injecting a similar amount of fuel at a steady rate through the primary fuel supply (based interpolation from data at $\phi = 0.665$ and $\phi = 0.647$).

The reductions are even more dramatic at a flow time of $\tau = 75$ ms. At an equivalence ratio of $\phi = 0.452$, the UHC emission levels are reduced by a factor of ten using control perturbations which are required so infrequently that there is no measurable increase in effective equivalence ratio. With control, the operating regime of the pulsed combustor can be extended further lean to equivalence ratios at which the system would otherwise flame out. For example, with control, the combustor will operate at an equivalence ratio of $\phi = 0.366$. While the UHC emission levels are quite high at this condition (850 ± 100 ppm), note that the combustor would flame out were an equivalent amount of fuel injected through the primary fuel supply. The effectiveness of control at low mass

flow rates, where poor mixing has been shown produce a stratified mixture, suggests that injecting the fuel in such a way as to produce a locally stratified region in the combustion chamber could prove to be a very effective technique.

Chapter 7

Conclusions

It has been shown that the behavior of the pulsed combustor is driven by two different mechanisms. Large-amplitude pressure oscillations which occur at the acoustic frequency of the system are the result of acoustic coupling with the tailpipe. These oscillations are nonlinear in nature due to interactions with the combustion reaction and turbulent mixing effects. In addition to the acoustically driven oscillations, the nonlinear nature of the combustion reaction leads to a bifurcation in system dynamics as the equivalence ratio of the fresh mixture approaches the lean flammability limit.

At near-stoichiometric and moderately lean operating conditions, the behavior of the combustor is fairly regular. The combustion quality is similar for each cycle except for small, random fluctuations due to turbulent mixing effects. The combustion quality of the current cycle seems to have no effect upon the quality of subsequent cycles.

As the equivalence ratio approaches the lean flammability limit, the system dynamics undergo a bifurcation due to the highly nonlinear behavior of the combustion reaction at very lean conditions. At these conditions, the combustion quality of the current cycle has a significant effect upon the quality of several subsequent cycles. High-quality combus-

tion events consume the available fuel inventory which must then be restocked. During the restocking process, the combustion events are of poor quality, and at extremely lean conditions, the combustor will misfire. If the restocking process is too slow, the combustor walls and ceramic flameholder will begin to cool until self-sustained combustion can no longer be maintained and the pulsed combustor flames out.

A control strategy has been developed which monitors the peak pressure of each cycle to detect when the available fuel inventory has been consumed and the pulsed combustor begins to experience poor-quality combustion events while the fuel inventory is restocked. The controller then injects a small amount of supplemental fuel to hasten the restocking process and push the system back toward the stable operating mode. The control strategy has proven to be very effective at dampening the combustion instabilities and thereby reducing the UHC emission levels and extending the operating regime of the combustor further toward the lean flammability limit.

There are several opportunities for further work with this system. Poor mixing at low mass flow rates in the current design has limited the ability to explore the effects of flow rate upon the behavior of the pulsed combustor. Redesigning the combustor so that the air and fuel are premixed should allow better determination of the effects of flow rate and should also reduce the amount of cyclic variability in the combustion quality at near-stoichiometric conditions.

It has been shown both experimentally and analytically that the rate of heat transfer from the combustor to the surroundings has a significant effect upon the performance of the pulsed combustor. This would be of great concern were the combustor to be used in an engineering application such as heating or drying. Active control of the combustor-wall temperature with a coolant flow would allow further investigation of these effects.

Changes in the behavior of the pulsed combustor can readily be detected by the human ear. Recent work (Teh 2000) suggests that an acoustic sensor could be used to make non-intrusive measurements of the performance of the pulsed combustor, thus eliminating the need for the pressure transducer and pressure tap.

The trial-and-error method used to choose the control variables in this study is far from efficient. A neural-network algorithm could be developed to improve selection of the control variables and refine control. Using this method, it is suspected that control would be more efficient near the lean flammability limit. This method would require a much faster computer than the 486-33MHz PC currently being used.

Finally, in addition to the reduction in UHC emission levels, it is suspected that control reduces emission levels of pollutants such as NO_x. Reducing the variation in the magnitude of the combustor-pressure oscillations also reduces the magnitude of temperature excursions inside the combustion chamber. Limiting the size of these temperature excursions should reduce the production rate of thermal NO_x. Access to NO_x-detection equipment would allow exhaust-gas analysis to test this theory.

Bibliography

Bibliography

Alhaddad, A. A. and G. A. Coulman (1982). Experimental and theoretical study of heat transfer in pulse-combustion heaters. *Proceedings Vol. 1: Symposium on Pulse-Combustion Applications*. Gas Research Institute, GRI-82/0009.2. March, Atlanta GA, USA.

anon. (1998). Company history and activities. Electronic hypertext document from www.dynafog.com. (See Appendix B).

anon. (1999). Lennox history: 1980-1995. Electronic hypertext document from www.davelennox.com. (See Appendix B).

Arpaci, V. S. (1986). Microscales of turbulence and heat transfer correlations. *International Journal of Heat and Mass Transfer 29*(8), 1071–1078.

Arpaci, V. S., J. E. Dec, and J. O. Keller (1991). Heat transfer in pulse combustor tailpipes. *Proceedings of the International Symposium on Pulsating Combustion, Volume 2*. Sandia National Laboratories and Gas Research Institute. Paper F-3. 5-8 August, Monterey CA, USA.

Arpaci, V. S., J. E. Dec, and J. O. Keller (1993). Heat transfer in pulse combustor tailpipes. *Combustion Science and Technology 94*(1-6), 131–146.

Arpaci, V. S. and A. Selamet (1991). Buoyancy-driven turbulent diffusion flames. *Combustion and Flame 86*, 203–215.

Cox, D. R. (1981). Statistical analysis of time series: some recent developments. *Scandinavian Journal of Statistics 8*, 93–115.

Daw, C. S., C. E. A. Finney, J. Green, M. B. Kennel, J. F. Thomas, and F. T. Connolly (1996). A simple model for cyclic variations in a spark-ignition engine. Technical report, SAE Paper No. 962086.

Daw, C. S., C. E. A. Finney, and M. B. Kennel (2000). A symbolic approach for measuring temporal irreversibility. *Physical Review E 62*(1). In press.

Daw, C. S., M. B. Kennel, C. E. A. Finney, and F. T. Connolly (1998). Observing and modeling nonlinear dynamics in an internal combustion engine. *Physical Review E 57*(3), 2811–2819.

Daw, C. S., J. F. Thomas, and G. A. Richards (1992). Modeling deterministic chaos in thermal pulse combustion. *1992 Technical Meeting of the Central States Section of the Combustion Institute*. 27-28 April.

Daw, C. S., J. F. Thomas, G. A. Richards, and L. L. Narayanaswami (1994). Experimental evidence for deterministic chaos in thermal pulse combustion. *1994 Technical Meeting of the Central States Section of the Combustion Institute*, pp. 439–444. 5-7 June, Madison WI, USA.

Daw, C. S., J. F. Thomas, G. A. Richards, and L. L. Narayanaswami (1995). Chaos in thermal pulse combustion. *Chaos 5*(4), 662–670.

Dec, J. E. and J. O. Keller (1986). High speed thermometry using two-line atomic fluorescence. *Twenty-first Symposium (International) on Combustion*, pp. 1737–1745. The Combustion Institute. 3-8 August, Munich, West Germany.

Dec, J. E. and J. O. Keller (1989). Pulse combustor tail-pipe heat-transfer dependence on frequency, amplitude, and mean flow rate. *Combustion and Flame 77*, 359–374.

Dec, J. E. and J. O. Keller (1990). Time-resolved gas temperatures in the oscillating turbulent flow of a pulse combustor tail pipe. *Combustion and Flame 80*, 358–370.

Dec, J. E., J. O. Keller, and V. S. Arpaci (1992). Heat transfer enhancement in the oscillating turbulent flow of a pulse combustor tail pipe. *International Journal of Heat and Mass Transfer 35*(9), 2311–2325.

Dec, J. E., J. O. Keller, and I. Hongo (1991). Time-resolved velocities and turbulence in the oscillating flow of a pulse combustor tail pipe. *Combustion and Flame 83*, 271–292.

Delarive, G. (1802-1803). Memoir on tubes rendered harmonius by hydrogen gas. *The Philosophical Magazine 14*, 24–31.

Diks, C., J. C. van Houwelingen, F. Takens, and J. DeGoede (1995). Reversibility as a criterion for discriminating time series. *Physics Letters A 201*, 221–228.

Edwards, K. D., C. E. A. Finney, K. Nguyen, and C. S. Daw (1997). Using symbolic dynamics for characterizing the lean-limit behavior of a chaotic thermal pulse combustor. poster presentation. Fourth Experimental Chaos Conference, 6-8 August, Boca Raton FL, USA.

Edwards, K. D., C. E. A. Finney, K. Nguyen, and C. S. Daw (1998). Use of symbol statistics to characterize combustion in a pulse combustor operating near the fuel-lean limit. *1998 Technical Meeting of the Central States Section of the Combustion Institute*, pp. 385–390. 31 May - 2 June, Lexington KY, USA.

Edwards, K. D., C. E. A. Finney, K. Nguyen, and C. S. Daw (2000). Application of nonlinear feedback control to enhance the performance of a pulsed combustor. *2000*

Technical Meeting of the Central States Section of the Combustion Institute, pp. 249–254. 16-18 April, Indianapolis IN, USA.

Figliola, R. S. and D. E. Beasley (1995). *Theory and Design for Mechanical Measurement* (2 ed.). John Wiley & Sons, Inc.

Finney, C. E. A. (2000). *Symbolization-based analysis of noisy engineering time series.* Ph. D. thesis, University of Tennessee, Knoxville.

Foa, J. V. (1960). *Elements of Flight Propulsion.* John Wiley & Sons.

Gemmen, R. S., J. O. Keller, and V. S. Arpaci (1991). Heat/mass transfer from a cylinder in the strongly oscillating flow of a pulse combustor tailpipe. *Proceedings of the International Symposium on Pulsating Combustion, Volume 2.* Sandia National Laboratories and Gas Research Institute. Paper F-5. 5-8 August, Monterey CA, USA.

Gemmen, R. S., J. O. Keller, and V. S. Arpaci (1993). Heat/mass transfer from a cylinder in the strongly oscillating flow of a pulse combustor tailpipe. *Combustion Science and Technology 94*(1-6), 103–130.

Green, J. B., C. S. Daw, J. S. Armfield, C. E. A. Finney, R. M. Wagner, J. A. Drallmeier, M. B. Kennel, and P. Durbetaki (1999). Time irreversibility and comparison of cyclic-variability models. Technical report, SAE Paper No. 1999-01-0221.

Hanby, V. I. (1969). Convective heat transfer in a gas-fired pulsating combustor. *Journal of Engineering for Power 91*, 48–52.

In, V., M. L. Spano, J. D. Neff, W. L. Ditto, C. S. Daw, K. D. Edwards, and K. Nguyen (1997). Maintenance of chaos in a computational model of a thermal pulse combustor. *Chaos 7*(4), 605–613.

Keller, J. O., T. T. Bramlette, P. K. Barr, and J. R. Alvarez (1994). NO_x and CO emissions from a pulse combustor operating in a lean premixed mode. *Combustion and Flame 99*, 460–466.

Keller, J. O. and I. Hongo (1990). Pulse combustion: The mechanisms of NO_x production. *Combustion and Flame 80*, 219–237.

Keller, J. O. and K. Saito (1987). Measurements of the combusting flow in a pulse combustor. *Combustion Science and Technology 53*, 137–163.

Lawrance, A. J. (1991). Directionality and reversibility in time series. *International Statistical Review 59*(1), 67–79.

Margolis, S. B. (1994). The nonlinear dynamic so intrinsic acoustic oscillations in a model pulse combustor. *Combustion and Flame 99*, 311–322.

McManus, K. R., T. Poinsot, and S. M. Candel (1991). A review of active control of combustion instabilities. *Proceedings of the International Symposium on Pulsating*

Combustion, Volume 2. Sandia National Laboratories and Gas Research Institute. Paper G-1. 5-8 August, Monterey CA, USA.

McManus, K. R., T. Poinsot, and S. M. Candel (1993). A review of active control of combustion instabilities. *Progress in Energy Combustion Science 19*, 1–29.

Moon, F. C. (1987). *Chaotic Vibrations*. John Wiley & Sons.

Morris, G. J., M. J. Welter, and G. A. Richards (1990). An investigation of pulse-combustor design for slurry atomization. *ASME Energy-sources Technology Conference & Exposition, Fossil Fuel Combustion Symposium*. 14-18 January, New Orleans LA, USA.

Nicholson, W. and B. Higgins (1802). On the sound produced by a current of hidrogen gas passing through a tube. with a letter from Dr. Higgins, respecting the time of its discovery. *A Journal of Natural Philosophy, Chemistry and the Arts 1*, 129–131.

Putnam, A. A., F. E. Belles, and J. A. C. Kentfield (1986). Pulse combustion. *Progress in Energy and Combustion Science 12*(1), 43–79.

Rayleigh, L. (1945). *Theory of Sound, Volume II*. Dover.

Rhode, M. A., R. W. Rollins, A. J. Markworth, K. D. Edwards, K. Nguyen, C. S. Daw, and J. F. Thomas (1995). Controlling chaos in a model of thermal pulse combustion. *Journal of Applied Physics 78*(4), 2224–2232.

Richards, G. A., G. J. Morris, D. W. Shaw, S. A. Keeley, and M. J. Welter (1991). Thermal pulse combustion. *Proceedings of the International Symposium on Pulsating Combustion, Volume 1*. Sandia National Laboratories and Gas Research Institute. Paper A-11. 5-8 August, Monterey CA, USA.

Richards, G. A., G. J. Morris, D. W. Shaw, S. A. Keeley, and M. J. Welter (1993). Thermal pulse combustion. *Combustion Science and Technology 94*(1-6), 57–85.

Stam, C. J., J. P. M. Pijn, and W. S. Pritchard (1998). Reliable detection of nonlinearity in experimental time series with strong periodic components. *Physica D 112*, 361–380.

Sterling, J. D. (1993). Nonlinear analysis and modelling of combustion instabilities in a laboratory combustor. *Combustion Science and Technology 89*, 167–179.

Sterling, J. D. and E. E. Zukoski (1991). Nonlinear dynamics of laboratory combustor pressure oscillations. *Combustion Science and Technology 77*(4-6), 225–238.

Strogatz, S. H. (1994). *Nonlinear dynamics and chaos*. Addison-Wesley Publishing Company.

Teh, T.-Y. (2000). Investigating the feasibility of monitoring dynamic behavior of a fluidized bed using piezoelectric accelerometer. Master's thesis, University of Tennessee, Knoxville.

Timmer, J., U. Schwarz, H. U. Voss, I. Wardinski, T. Belloni, G. Hasinger, M. van der Klis, and J. Kurths (1999). Linear and nonlinear time series analysis of the black hole candidate Cygnus X-1. *Physical Review E 61*(2), 1342–1352.

Turns, S. R. (1996). *An Introduction to Combustion: Concepts and Applications*. McGraw-Hill, Inc.

Wagner, R. M., J. A. Drallmeier, and C. S. Daw (1998a). Nonlinear cycle dynamics in lean spark ignition combustion. *Twenty-seventh Symposium (International) on Combustion*, pp. 2127–2133.

Wagner, R. M., J. A. Drallmeier, and C. S. Daw (1998b). Prior-cycle effects in lean spark ignition combustion: fuel/air charge considerations. Technical report, SAE Paper No. 981047.

Weiss, G. (1975). Time-reversibility of linear stochastic processes. *Journal of Applied Probability 12*, 831–836.

Zinn, B. T. (1986). *Advanced Combustion Methods*, Chapter 2. Pulsating Combustion. Academic Press, Inc.

Appendix

Appendix A

Nomenclature

Abbreviations

A/D	analog to digital
DAC	data acquisition and control
FID	flame ionization detector
GUI	graphical user interface
METC	the former Morgantown Energy Technology Center, Morgantown, WV, currently the National Energy Technology Laboratory in part
ODE	ordinary differential equation
PC	personal computer
PSD	power spectral density
RMS	root-mean-square
SA	standard air
UHC	unburned hydrocarbon(s)
UTK	The University of Tennessee, Knoxville

Variables

Roman

a	speed of sound
A'	pre-exponential term in Arrhenius rate law
A_e	cross-sectional area of the taipipe, METC model
A_s	surface area of the combustor
A_t	cross-sectional area of the tailpipe/pressure tap
AF	air-to-fuel ratio
C	variable used to simplify determination of uncertainty in flow time

117

C_p	specific heat at constant pressure
C_v	specific heat at constant volume
d	diameter of critical-flow orifice
D_{TP}	tailpipe diameter, METC model
e	internal energy
e_r	resolution error in measurement of orifice diameter
E	energy
$\dot{E}$	rate of energy exchange
E_A	activation energy
f	friction factor, METC model
f_H	acoustic frequency for a Helmholtz combustor
h	enthalpy
i	datum/cycle index
k	specific-heat ratio
L_t	length of the tailpipe/pressure tap
L_{TP}	length of the tailpipe, METC model
m	mass
M	Mach number
$\dot{m}$	mass flow rate
$\dot{m}_R$	rate of fuel consumed by the combustion reaction
N	order of Arrhenius rate law in terms of oxidizer
P	combustor pressure, *i.e.,* pressure inside the combustion chamber
$\tilde{P}$	non-dimensional pressure, METC model, P/P_o
$<P>$	peak-to-trough magnitude of the combustor-pressure oscillations
P_{crit}	supply pressure required to choke the critical-flow orifice
P_e	pressure at the entrance of the tailpipe, METC model
P_o	supply pressure (or ambient pressure, METC model)
P_{rms}	root-mean-square of the combustor pressure during one cycle
q'''	heat generated during combustion reaction
$\dot{Q}$	heat loss from combustor to surroundings
R	species-specific ideal-gas constant
R_u	universal gas constant
S_Δ	difference symbolization statistic
SG	specific gravity of the mixture
t	time
T	temperature of the mixture inside the combustion chamber
$\tilde{T}$	non-dimensional temperature, METC model, T/T_o
$\tilde{T}_a$	non-dimensional activation temperature, METC model
T_e	temperature at the entrance of the tailpipe, METC model
T_o	supply temperature (or ambient temperature, METC model)
T_w	approximate temperature of the combustor wall

T_{wall}	measured combustor-wall temperature, METC notation
T_∞	ambient temperature
u	uncertainty
u_{atm}	uncertainty in supply-pressure measurement due to fluctuations in atmospheric pressure
u_{ave}	uncertainty in diameter of critical-flow orifice due to averaging measurements of non-circular orifice
u_{pf}	uncertainty in supply-pressure measurement due to fluctuations in the supply line
u_o	overall instrument error in supply-pressure measurement
U	heat transfer coefficient
$\tilde{U}$	non-dimensional velocity at tailpipe entrance, METC model, tailpipe velocity divided by cold-flow velocity
V	internal volume of combustion chamber, METC model
V_c	internal volume of combustion chamber
Y	mass fraction
Z	ratio of mass flow rate to combustion chamber volume, METC model

Greek

ΔH_R	enthalpy of reaction
θ	non-dimensional temperature, T/T_∞
θ_A	non-dimensional activation temperature
λ	non-dimensional mass fraction of fuel, $Y_f/Y_{f,i}$
ξ	non-dimensional time, t/τ
ρ	density of mixture in combustion chamber
ρ_{SSL}	density of air at standard sea-level conditions
ρ_o	ambient density, METC model
τ	characteristic flow time; defined as the approximate time that the mixture resides in the combustion chamber
τ_A	characteristic time related to the rate of fuel consumption
τ_c	characteristic combustion time, METC model
τ_C	characteristic time related to the rate of energy release by combustion
τ_f	characteristic flow time, METC model
τ_{HT}	characteristic heat transfer time, METC model
τ_T	characteristic time related to the rate of energy transport from the combustor
ϕ	equivalence ratio based upon the mass flow rates of air and primary fuel
$\bar{\phi}$	effective equivalence ratio; defined as the equivalence ratio which would exist were an amount of fuel equivalent to that introduced by the control perturbations injected at a steady rate via the primary fuel supply

Subscripts

a	air
actual	actual operating conditions
e	exit
f	fuel
i	inlet
in	in to the control volume
o	oxidizer
out	out of the control volume
stoich	stoichiometric conditions
te	tailpipe entrance, METC model
x	dummy variable, either *a* or *f*

Appendix B

Referenced electronic hypertext documents

The Internet has developed into a rich source of information; however, at the time of this writing, those sources are still often fleeting — changing and disappearing daily. For this reason, the electronic hypertext documents referenced in this work are included in this Appendix for future reference. All material included herein is considered to be copyrighted by the relevant party and is credited as such.

B.1   Lennox

The following is a transcript of a hypertext document found at www.davelennox.com, © Copyright Lennox Industries Inc., 1999:

Lennox History:
1980-1995

A Strong Pulse

John Norris Jr. became the third-generation Norris family member to head Lennox as president and CEO on January 1, 1980, while Ray Robbins remained as chairman of the board. Lennox could look back on 85 highly successful years. They were an innovator and market leader in a highly competitive and complex industry.

When asked about the reasons for Lennox' success, John Norris Jr. once said, "Lennox is one of the few companies that can invest heavily in a research and development project over a long period before seeing any results because our shareholders are willing to commit for the long term."
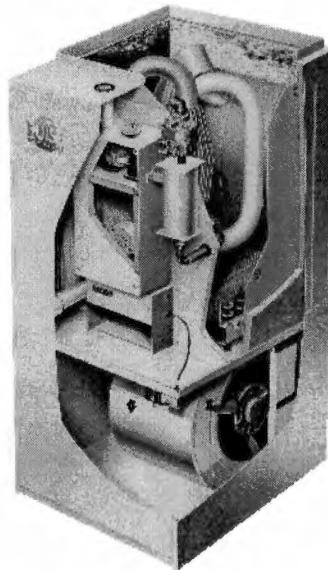
It was a formula responsible for one of Lennox' greatest achievements to date, the G14 Pulse®; furnace — the industry's first high-efficiency furnace — in 1982.

"Unquestionably The Best"

The story of the Pulse's development is in many ways a condensed version of the story of Lennox. It is a story of how strong business instincts, combined with a commitment to innovation and long-term development, worked closely together – not just to make a superior product, but to push the HVAC industry in new directions. "The Pulse," Norris commented, "demonstrates the importance Lennox places on research and development."

The Pulse had its beginnings in the mid-1970s, when studies underway at Lennox convinced management the price of natural gas would probably double or triple within the next five or six years. At about the same time, the American Gas Association (AGA) was studying the use of pulse combustion technology to improve the efficiency of forced-air furnaces from an industry average of about 58% to 96 or 97%.
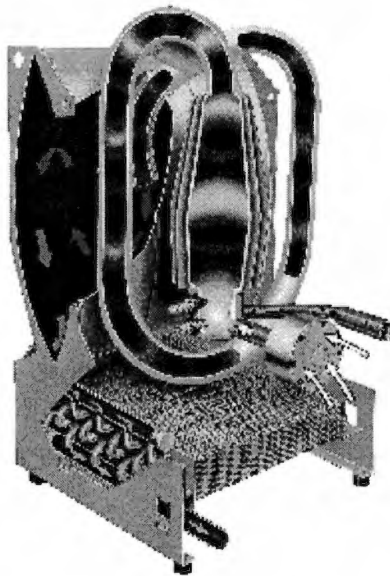
Lennox management entered into a development agreement with AGA, and later with the Gas Research Institute (GRI), to commercialize a pulse combustion furnace. Extensive laboratory and field tests over the next five years helped develop the Lennox Pulse combustion chamber and heat exchanger.

"When we started the Pulse project in 1975, we weren't even sure if the concept would work," Norris said. By the time the project was completed, Lennox had spent several million dollars — before even a single unit had been sold. "That's a long time to keep your eye on the ball unless the company is in full support of your efforts," Norris noted.
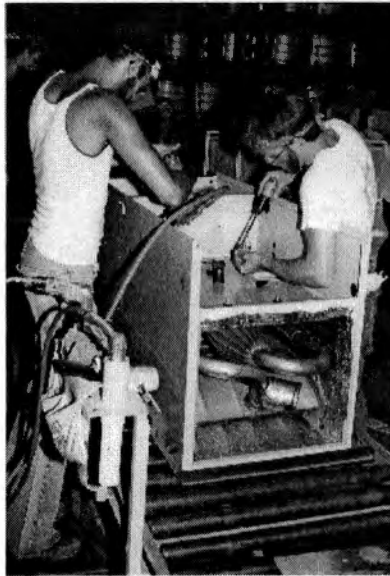
But the long-term commitment paid off. In 1982, the first year of Pulse production, orders ran far ahead of production capacity. Just as Lennox studies had predicted, the price of natural gas had nearly tripled since 1976 and the market was ripe for a high-efficiency furnace.

Throughout the 1980s the Pulse received extensive national media attention and scientific recognition, as well as numerous awards from private industry, state and federal government. "The Pulse," said Norris on the furnace's 10th anniversary in 1992, when the millionth unit rolled off the Marshalltown assembly line, "is unquestionably the best furnace built by Lennox — and, with almost no failures reported over the years, one of the best gas furnaces on the market." In 1986, Lennox became the first HVAC manufacturer to offer a limited lifetime warranty — on the Pulse furnace.

The Pulse's spectacular success led to industry-wide development of high-efficiency equipment. Lennox continued its own high-efficiency product development with the release of the HS14 PowerSaver®; in 1984, the first air conditioner to achieve a 15.0 Seasonal Energy Efficiency Ratio (SEER).

Lennox' role as an industry innovator was further enhanced in 1986 when the company was the first HVAC manufacturer to join the SMART HOUSE Development Venture, Inc., an organization working to develop high-tech appliance control systems. In 1990, Lennox received its first patents on a revolutionary thermal energy storage (TES) system for residential and light commercial installation. And in 1994, the company unveiled the CompleteHeat system — the first combination space and hot water high-efficiency system by a major HVAC producer.

....

B.2 Curtis Dyna-Fog

The following is a transcript of a hypertext document found at www.dynafog.com,

© Copyright Curtis Dyna-Fog, 1998:

COMPANY HISTORY AND ACTIVITIES

Curtis Dyna-Fog, Ltd. was founded in 1947 in Dayton, Ohio by Russell R. Curtis and his father W.H. Curtis. Originally named Curtis Automotive Devices, the company specialized in manufacturing valves for the automotive and aircraft industry. Before joining his father in business, Russell Curtis attended the University of Cincinnati where he graduated in Aeronautical Engineering and later completed a cooperative work program at Wright Airfield (now Wright Patterson Air Force Base) At the time, Wright Airfield was the center of all aircraft technology. In 1952 Curtis Automotive Devices moved to Bedford, Indiana to be closer in proximity to its major customers. The company began producing other types of components for the aircraft industry and began doing some development work using acquired Pulse-Jet Engine Technology. During Russell Curtis' employment at Wright Airfield in Dayton he was first exposed to a Pulse-Jet Engine, a unique device used to power the German VI rockets during the war. The Pulse-Jet was comprised of the basic technology that would later be the foundation for his companies future.

Russell and his father continued working on the possibilities of producing a pulse-jet fogger for use in commercial applications. One of the first pulse-jet products they produced was the Dyna-Jet "Red Head" miniature engine for use in model rocketry. Initially developed in 1945 by a long time associate of Russell Curtis, William Tenny of Aeromarine Company, the Dyna-Jet once held the American Modelers Association land speed record at 179+ MPH! A speed amazing at the time, especially when only standard grade gasoline was available.

After years of refining existing designs, by 1954 the first commercially available pulse-jet mosquito fogger (The Curtis Junior Model) was being produced. In the first year more than 500 machines were sold throughout the country. By 1956, demand grew to the point where more than 4000 machines were being produced each year. As a result of increasing demand for the pulse-jet machines, Russell Curtis moved the company in 1958 into a newly constructed

20,000 square foot facility in Westfield, Indiana. By this time the company was producing several different equipment models including the very first production "Cold Fog" sprayer. It was the machine that pioneered the way for what is known today as ULV technology.

In 1964, mainly due to no longer producing products specifically for the automotive industry, the company name was changed to Curtis Dyna-Products Corp. During the next several years many new products were developed and the facility was expanded. In 1992, the group of Curtis employees who were already managing the company purchased it and the name was changed to Curtis Dyna-Fog, Ltd.

Today, still located in Westfield, Indiana Curtis Dyna-Fog, Ltd. produces a complete line of spraying and fogging products. With the latest in manufacturing technology in its 80,000 square foot facility, Curtis is renowned as a world leader in manufacturing and distribution. Curtis supplies its products through distributors around the United States and throughout the world in over 60 different countries. All products are manufactured in the one facility in Indiana to help assure a high level of product quality that has been the cornerstone of Dyna-Fog equipment.

Curtis Dyna-Fog, Ltd. strives to identify the requirements of the market place and react quickly to market demand. Dyna-Fog's worldwide distributor network assures rapid response to all customers. All service shipments of stock items are made within 48 hours by air or sea freight. The sale of Dyna-Fog products are supported with comprehensive literature and a complete technical staff equipped with the latest laboratory testing facilities. Presentations on recent developments are continuously made to all world markets as well as the scientific community.

Some recent examples are:

- Application of deodorants in small droplets: International Conference on Air Pollution from Ag. Operations, Feb 1996, Kansas City, MO USA

- A new tool for ULV Applications. American Mosquito Control Association Meeting, March 1996, Norfolk, VA, USA.(Dyna-Fog Twister)

- The use of Thermal Fogging as a technique for the total eradication of Fire Ant colonies. USDA Imported Fire Ant Research Conference, April 1997, Gainesville, FL, USA. (Dyna-Fog Ant Bear)

Other scientific publications available:

- Newcastle Disease in Commercial Turkeys (Dyna-Fog Hurricane)

- Effects of pressure and flow rate on VMD (Dyna-Fog Cyclotronic Maxi-Pro)
- Understanding LVM (Dyna-Fog Nighthawk)
- Effect of droplet size on adulticide efficiency (Dyna-Fog Cyclotronic (Maxi-Pro)
- A summary of Ultra-Low-Volume Technology
- The Proper Application of Modern ULV Technology
- A Blueprint For The Control of Nuisance Birds in the Airport Environment
- Aerosol, Fog, and ULV: Perceptions and Realities in Maintenance Uses Curtis Dyna-Fog, Ltd. is present at many major exhibitions both in the USA and worldwide either exhibiting alone or in conjunction with local distributors.

Vita

Kevin Dean Edwards was born on a cold December morning in 1969 shortly before one of the largest snowfalls in the recorded history of Jefferson City, TN (pop. 5494, 1990 census). After twelve years in the fine Jefferson County school system, Dean enrolled at the University of Tennessee, Knoxville (UTK), for the fall semester of 1988. After a couple of years of slacking off, he got a wake-up call in Doc Hodgson's *Thermodynamics I* course. After retaking the course under Doc during the summer at the insane hour of 7:40 A.M. (and making an "A" I might add), Dean reapplied himself toward achieving a degree in aerospace engineering under the fine tutelage of Dr. Harvey Joe Wilkerson. Dean graduated with a B.S. in aerospace engineering in 1992; however, due to the poorly-timed (at least for Dean) fall of the Soviet Union, the end of the Cold War and the subsequent complete and utter lack of jobs in aerospace engineering, Dean decided to continue his education by going to graduate school along with his good friends Scott Hale and Chris Widner.

In the summer of 1992, Dean began work with Dr. Ke Nguyen at UTK studying the ignition and combustion of aluminum agglomerates by igniting them with a 100-W CO_2 laser. During this time Dean came to work for the Mechanical and Aerospace Engineering Department as a teaching assistant which he found he strangely enjoyed. It was also during this time that Dean's hobby of birding began to take on a life of its own. Formerly just

128

a way to relieve stress by getting out into the woods and away from engineering, birding quickly became an obsession. After two years, during which he remarkably failed to injure himself seriously with the infra-red, 100-W laser, Dean finished his thesis entitled *Effects of Initial Diameter and Ambient Pressure on the Ignition and Combustion of Laser-ignited Aluminum Agglomerates* in 1994 and graduated from UTK once again, this time with an M.S. in mechanical engineering.

Having found that he liked teaching, Dean decided that he might someday wish to teach at a university. So, once again, Dean ("Dino" to his friends), Scott (a.k.a. "Frank") and Chris (also a.k.a. "Frank") returned to UTK in 1994 to pursue Ph.D.s in mechanical engineering. Once again Dean worked with Dr. Ke Nguyen, this time as part of the Chaos Research Group at UTK. After spending some time playing with a pulsed-combustion hot-water heater and some horrible nightmares involving a Rijke tube, Dean finally settled upon a research project which involved designing, building, testing and controlling a pulsed combustor. After several arduous years, during which time Dean continued to teach several courses (including, ironically, *Thermodynamics I* at 7:40 A.M. in the morning — the pleonasm is intentional for emphasis) and the Big Orange won several national championships in women's basketball and one in football, Dean finally stopped birding long enough to finish his research and graduate from UTK for the third time in 2000 with a Ph.D. in mechanical engineering. Woohoo!

Dean's future has yet to be written. Whether he will join (soon to be Dr.) Scott and Dr. Chris in the "real world" or pursue a teaching career or take up alpaca wrangling with Dr. Charles Finney or emulate Kenn Kaufman by hitchhiking around the country looking for birds is uncertain. One thing is for certain, however: Dean has vowed never again to seek another degree.